Analytical and Experimental Study of the Effect of Cutting Tool Microgeometry on the Impact Resistance of Milling Tools

by

Connor G. Hopkins

A thesis submitted to the
School of Graduate and Postdoctoral Studies in partial
fulfillment of the requirements for the degree of

Master of Applied Science in Mechanical Engineering

Department of Mechanical and Manufacturing Engineering

Faculty of Engineering and Applied Science

University of Ontario Institute of Technology (Ontario Tech University)

Oshawa, Ontario, Canada

January 2021

THESIS EXAMINATION INFORMATION

Submitted by: **Connor G. Hopkins**

Master of Applied Science in **Mechanical Engineering**

Thesis title: Analytical and Experimental Study of the Effect of Cutting Tool Microgeometry on the Impact Resistance of Milling Tools

An oral defense of this thesis took place on January 20, 2021 in front of the following examining committee:

Examining Committee:

Chair of Examining Committee	Dr. Martin Agelin-Chaab
Research Supervisor	Dr. Sayyed Ali Hosseini
Examining Committee Member	Dr. Hossam Kishawy
Thesis Examiner	Dr. Ahmad Barari, University of Ontario Institute of Technology

The above committee determined that the thesis is acceptable in form and content and that a satisfactory knowledge of the field covered by the thesis was demonstrated by the candidate during an oral examination. A signed copy of the Certificate of Approval is available from the School of Graduate and Postdoctoral Studies.

ABSTRACT

This thesis conducted a two-part investigation into the ability of a milling tool cutting insert to resist the impacts that occur during the milling process, with respect to the cutting edge microgeometry. The first part of this thesis contains a mathematical model that was used to predict the cutting forces acting on the tool during milling, accounting for the edge radius. The second part reports the findings of a series of milling tests that were performed, both to verify the mathematical model and to track the wear and failure of the various milling inserts. Five different edge radii were tested and compared. It was found that altering the edge geometry of the tool does affect the cutting forces, wear behaviour, and impact resistance of the cutting inserts, with an edge radius of 35 μm proving to be the optimum choice.

Keywords: milling; indexable cutters; edge radius; impact resistance; force model

AUTHOR'S DECLARATION

I hereby declare that this thesis consists of original work of which I have authored. This is a true copy of the thesis, including any required final revisions, as accepted by my examiners.

I authorize the University of Ontario Institute of Technology (Ontario Tech University) to lend this thesis to other institutions or individuals for the purpose of scholarly research. I further authorize University of Ontario Institute of Technology (Ontario Tech University) to reproduce this thesis by photocopying or by other means, in total or in part, at the request of other institutions or individuals for the purpose of scholarly research. I understand that my thesis will be made electronically available to the public.

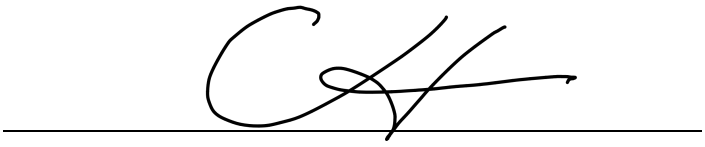

CONNOR HOPKINS

STATEMENT OF CONTRIBUTIONS

The experimental work that was performed for this thesis was conducted in the Machining Research Laboratory at the University of Ontario Institute of Technology. All milling tests were performed using the HAAS VF-2 CNC milling machine. The experiments were performed by myself, Connor Hopkins, along with Mr. Mohamd Imad, as Mr. Imad used the same set of experimental data for his own thesis. I was responsible for machine operation, G-Code creation, tool wear measurement, and cutting insert replacement.

A portion of the results that are presented in this thesis have already been published in a submission to the Canadian Society for Mechanical Engineering (CSME) International Congress 2020, under the title “An Oxley-Based Force Model for Milling of Hardened Steel Using Indexable Milling Tools”. Additionally, more information that is being compiled as a result of these experiments will be published in a future journal paper.

ACKNOWLEDGEMENTS

I would like to extend my sincerest thanks to my supervisor, Dr. Sayyed Ali Hosseini, for his guidance during the course of my graduate studies, for his support during difficulties, and for his confidence in me. I would also like to thank Mohamd Imad, who worked collaboratively with me throughout my time in the Master of Applied Science – Mechanical Engineering program. Lastly, I would like to thank every member of the Machining Research Lab, whose feedback was invaluable to my development in this program.

I would also like to extend my thanks to Sandvik-Coromant and Dr. Nima Zarif, who provided the cutting inserts with customized edge radii for use during experimentation, as well as technical support during analysis of the results.

Lastly, I would like to thank Dr. Martin Agelin-Chaab, Dr. Hossam Kishawy, and Dr. Ahmad Barari for being on my examination committee.

TABLE OF CONTENTS

LIST OF TABLES

LIST OF FIGURES

LIST OF ABBREVIATIONS AND SYMBOLS

A	Yield Strength Coefficient
B	Strain Hardening Coefficient
C	Strain Rate Sensitivity Constant
n	Strain Hardening Exponent
m	Temperature Sensitivity Exponent
FEM	Finite Element Method
CEEID	Cutting Edge Entry Impact Duration
F_x	X-Component of Measured Force
F_y	Y-Component of Measured Force
F_z	Z-Component of Measured Force
F_c	Cutting Force
θ	Tool Position
F_s	Shear Force
R	Resultant Force
ψ	Angle Between F_s and R
F_f	Friction Force Acting Along the Tool's Rake Face
N	Normal Force Acting Perpendicular to the Rake Face
n_{eq}	Modified Strain Hardening Exponent
ϕ	Shear Plane Angle
C_0	Ratio of Shear Plane Length AB to Primary Shear Zone Thickness
ζ	Ratio of Tool-Chip Interface Plastic Zone Thickness to Chip Thickness
$\dot{\varepsilon}_0$	Reference Strain Rate
t_1	Undeformed Chip Thickness
t_2	Deformed Chip Thickness
c	Chip Load
l	Shear Plane Length
V_{sh}	Shear Velocity
V_c	Cutting Speed

γ	Tool Rake Angle
ε_{AB}	Strain in the Shear Plane
$\dot{\varepsilon}_{AB}$	Strain Rate in the Shear Plane
E_T	Non-Dimensional Thermal Number
ρ	Workpiece Density
C_p	Specific Heat of the Workpiece
K	Thermal Conductivity of the Workpiece
ξ	Heat Partition Coefficient
σ_{AB}	Average Flow Stress in the Shear Plane
T_{AB}	Temperature at the Shear Plane
T_w	Temperature of the Workpiece
T_M	Melting Temperature of the Workpiece
m_{chip}	Mass of the Chip Being Removed
λ	Sensible Heat Coefficient
β	Average Friction Angle
r	Tool Edge Radius
ω	Separation Angle
υ	Deformation Angle
p	Penetration Depth
δ	Depth of Deformation
L_{int}	Length on Tool-Chip Contact Area
τ_{int}	Shear Stress Along the Tool-Chip Interface
ΔT_m	Maximum Temperature Change in the Chip
T_{int}	Temperature at the Tool-Chip Interface
Ψ	Ratio of Tool-Chip Interface Temperature Rise to the Maximum Temperature Rise of the Chip
τ_{chip}	Shear Flow Stress Along the Tool-Chip Interface
σ_N	Normal Stress Using Force
σ_N'	Normal Stress Using Boundary Conditions
κ	Normal Stress Factor

Chapter 1. Introduction

1.1 Background Information

Milling operations are among the most common and versatile machining processes currently used in various manufacturing industries, with them being especially useful in the cutting of metals. These operations can be used at almost any stage of a given part's manufacturing schedule, from cutting a rough profile to finishing a high-quality surface within tight tolerances. Given the variety of operations that can be performed on a milling machine, and the variety of materials that need to be milled, it is critical that the proper tool is selected for the job. When cutting metals, high forces are generated by the milling tool as the undesired portion of workpiece material is removed in the form of chips. These cutting forces can be controlled by a series of parameters, including:

1) The cutting speed and feed rate of the milling tool, which is controlled by the operator or the G-code executed by the machine.

2) The workpiece's mechanical properties, which are not typically variable when a certain material is selected.

3) The geometry of the cutting tool, which is controlled by the tool manufacturers.

Understanding how to control the forces that are present during metal cutting is important, since it allows the effects of these forces on different aspects of the process to be investigated. It has been observed through countless theoretical and

experimental works in the field of metal cutting that the cutting forces have a relationship with several other elements of the cutting process, including the vibration of cutting tool, workpiece material, and machine structure along with quality of the new surface being generated, the temperature at the tool-workpiece interface, and the rate of wear on the tool. In many of the most well-known mathematical machining models, the tool is represented with a perfectly sharp cutting edge. This assumption is used in order to simplify the derivations of force components and the representation of where the material undergoes transition from static workpiece to chip, referred to as the primary shear zone. While this assumption does simplify calculations and provide information that is satisfactory in some cases, it does not properly represent the reality of the interaction between cutting tool and workpiece. Instead of being perfectly sharp, every cutting edge has some additional edge preparations performed on it, such as chamfering the edge, or honing it to add a radius. This is performed in order to improve the strength of a tool, as a perfectly sharp edge would be far more susceptible to chipping, or complete breakage, before the tool has reached its expected end-of-life.

Every milling tool available on the market has needed its edge prepared, usually with a radius added in the scale of micrometers. Adding a radius to the cutting edge improves the strength and toughness of the tool, as a perfectly sharp edge would be highly susceptible to breakage. However, there is very little information available in the open literature about the process used by the tool manufacturers to determine the dimension of the radius that is added to these cutting edges. It stands to reason that a radius is chosen for a tool because some work done internally has shown that a certain

edge radius has resulted in the best tool performance, whether that be with regard to tool life, surface quality, or other factors. However, the work performed by these tool manufacturers is not available to the public, so how a certain edge radius is chosen is generally considered as the intellectual property of the tool manufacturers. With a lack of open literature involving the mathematical modelling of a cutting tool's edge radius and its effects on tool performance, there is a need to investigate this relationship.

1.2 Research Objectives

The objective of this thesis is to investigate the effects of the cutting edge microgeometry used in milling tool cutting inserts on the tool's useful life and impact resistance. This investigation will be carried out in two parts. First, a mathematical model will be developed in order to account for the tool's edge radius in the cutting force calculations, while accounting for the cutting parameters, material properties, and other geometrical features of the cutting tool. Second, a series of milling experiments will be conducted to capture the forces that are generated during the milling of AISI 4340 steel, hardened to 47±1 HRC, as well as the behaviour of wear propagation on said tools, for several different edge microgeometries. This set of experimental data will provide a baseline for the verification of the mathematical model that will be developed; if the model can accurately predict the magnitudes and trends of the force components within a reasonable margin of error, then it can be used to predict forces without the need for further experiments.

Chapter 2. Literature Review

The literature review chapter of this thesis has been divided into two parts, with each section containing relevant information to the corresponding portion of this thesis' work. In Section 2.1, important works published that pertain to the successful mathematical modeling of metal cutting operations are presented. Several aspects of these works have been adopted into the model that is presented in Chapter 3. The works that are presented in Section 2.2 explore the wear behavior and failure modes of cutting tools during their operation. Information learned while reviewing these works have guided the planning and execution of the experiments that are reported in Chapter 4.

2.1 Mathematical Models for Metal Cutting

When working in the field of modelling machining processes mathematically, the influences of the ground-breaking work published by Merchant [1, 2] are almost always present. In these two papers, Merchant explains his derivation of a set of equations that are used to describe an orthogonal cutting model in terms of known machining quantities. This set of equations consists of several geometric relationships that define the connections between the geometry of the tool, the cutting parameters of the operation, and the forces that are generated during machining. However, Merchant's work was limited by a series of assumptions that needed to be made. These equations only apply to the orthogonal cutting model, which means that the cutting edge is oriented perpendicular to the direction of cutting, and the newly generated surface is parallel to the original surface that has been removed. The model

is only valid if the chip being formed is classified as Type 2, which is continuous with no built-up edge [3]. The final assumption is that the tool is represented as a perfectly sharp edge. This assumption is consistent in many works that model various cutting operations, however it does not represent reality. A perfectly sharp tool would be weak at its tip, so all cutting tools have some type of edge preparation performed on them to increase their strength.

Oxley and Shaw [4] published a revolutionary machining model, commonly referred to as Oxley's machining theory. In their model, the thermal properties of the material are used to calculate how the material behaves during cutting by modelling flow stresses of the material. Speeds during machining operations are generally much higher than speeds in other manufacturing processes such as bulk deformation and sheet metal forming. The relatively high speed of the process causes the material to yield with a very high strain rate, and also causes large changes in the temperature at the tool-workpiece interface which in turn affect the material behavior. By accounting for these behaviours, the derivations of this set of new equations to model the machining process are closer to reality, when compared to the more simplified works [1, 2] that came before it. In total, Oxley's model can predict the stresses, temperatures, and forces acting at the tool-workpiece interface. Originally, this model was developed for analyzing orthogonal machining, just as Merchant's work had done. This model would go on to be expanded and/or altered to include considerations for oblique machining [5, 6], and more specifically the case of milling [7] with limitations placed on tool's rake and inclination angles and workpiece behaviour during machining. In this thesis, Oxley's predictive machining theory

serves as a baseline for the mathematical model that is developed considering the effects of a tool's edge radius.

One of the largest contributions to the field of machining is the constitutive material behaviour model that was developed by Johnson and Cook [8]. This model specifically describes the behaviour of metals under extreme conditions, when they are subjected to very high strains, strain rates, and temperatures, which is exactly what metals experience during machining. The model functions based on a series of empirically derived constants, referred to hereafter as Johnson-Cook parameters. The definition of each of the Johnson-Cook parameters are listed below, and the specific values for this work are discussed later in detail in Chapter 3.

1) A - Yield Strength Coefficient (MPa)
2) B - Strain Hardening Coefficient (MPa)
3) C - Strain Rate Sensitivity Constant (dimensionless)
4) n - Strain Hardening Exponent (dimensionless)
5) m - Temperature Sensitivity Exponent (dimensionless)

In order to obtain these parameters, data must be compared from a series of multiple tests, including Split-Hopkinson bar tests and torsion tests at different strain rates and temperatures. The use of this model lends itself to computational applications. It is also desirable to use because once the Johnson-Cook parameters for a certain material are known, no other experiments need to be performed. However, the model cannot be used if those constants are unknown or unavailable in open literature. Other well-known machining models that rely on empirical constants are only valid for the workpiece and tool combination being tested, such as mechanistic models [9-13] or

unified cutting force models [14], but the Johnson-Cook model describes workpiece material behaviour completely independent of the cutting tool.

Lalwani et al. [15] proposed an alteration to Oxley's predictive machining theory that allows it to accept Johnson-Cook parameters as inputs, defining the material behaviour during machining. This development greatly improves the usability of Oxley's model, as this alteration allows the workpiece material to be better defined. The Johnson-Cook constitutive model is merged with Oxley's predictive machining model by replacing the strain hardening exponent n with a new exponent n_{eq}, which itself is based on the other Johnson-Cook parameters for the workpiece material. The validity of the altered model was determined by comparing the predicted values to experimental data in the literature for 0.38% carbon steel [16] and AISI 1045 steel [17].

Another significant contribution specific to the field of milling comes from Altintas and Engin [18], who proposed a generalized method for mathematically modeling the cutting edges of helical end mills and milling tools that accept cutting inserts. In this work, the edges are represented by curves that are plotted parametrically about an axis of origin, which represents the milling tool's center of rotation. This methodology allows for tools that are commonly used in industrial settings to be modeled for the purpose of other researches involving those tools. While this method is useful for analyzing the full three-dimensional geometry of an end mill, the present work chose to analyze the problem as a series of two-dimensional representations, similar to the model developed by Pang et al [19].

Pang et al. [19] presented a modified version of Oxley's predictive machining theory for analyzing helical end mills. In this method, the cutting edge(s) are divided into differential elements, where each element is treated as a single cutting edge performing oblique cutting. This way, the total forces acting on the tool at any given time are obtained by taking the sum of the forces acting on all the differential elements. By approaching the problem in this manner, the authors were able to represent a complex, three-dimensional cutting operation as a series of multiple two-dimensional cutting problems, where factors such as the rotational position of the tool, the engagement length of the cutting edge, and the chip load are changing between each two-dimensional representation. Three series of milling tests were performed on AISI 1045, Al 7075, and Ti6Al4V. Comparisons between the calculated cutting force values of this model and published experimental data for these materials showed good agreement, validating the approach taken by the authors.

Manjunathiah and Endres [20] have published a work which details the development of a new cutting force model for the orthogonal machining process that includes the edge radius as a consideration of the tool's geometry. This work is significant, as it removes one of the critical assumptions that is typically used when modelling the orthogonal cutting process, however the assumption of no built-up edge is kept. By accounting for the tool's edge radius, a few new considerations must be made. In addition of the deformation of the material that is removed, the deformation of the material at the tertiary cutting zone is considered. At the tool-workpiece interface, the edge radius causes an average rake angle to form that is

different from the nominal rake angle of the tool. By adopting the considerations of [20], it is possible to combine them with aspects of other orthogonal machining models to develop a single, more comprehensive model.

2.2 Cutting Tool Wear and Failure Modes

A tool is considered "failed" when its ability to cut the workpiece material properly is compromised. There are two major categories of failure that can be used to sort tool failures. A tool can fail due to wear, which results from the tool gradually performing worse until it is unacceptable. This is the most common and more desirable type of tool failure in industrial applications, as this mechanism has been well-studied and it is fairly predictable. Wear on the tool can be caused by numerous factors, including abrasion, diffusion, oxidation, or a combination of these factors. It is common for the tool to be worn by the chip passing over the tool, and in certain conditions, small portions of workpiece material can adhere to the surface of the cutting tool, and when cutting forces remove those portions, wear is created on the tool. These mechanisms are called abrasive wear and adhesive wear, respectively. Diffusion wear is caused by atoms of the cutting tool diffusing into the chip, which is then removed by the machining operation. This type of wear becomes more significant when there are high temperatures at the tool-workpiece interface. These high temperatures can also instigate oxidation of the tool, which is a form of corrosive wear.

Aforementioned wear mechanisms cause the tool to gradually loose its bulk and become weaker. Gradual loss of tool material can occur on the flank or rake face of

the cutting tool. The former is called flank wear while the latter is referred to as crater wear. A diagram showing these types of wear is presented in Figure 2-1.

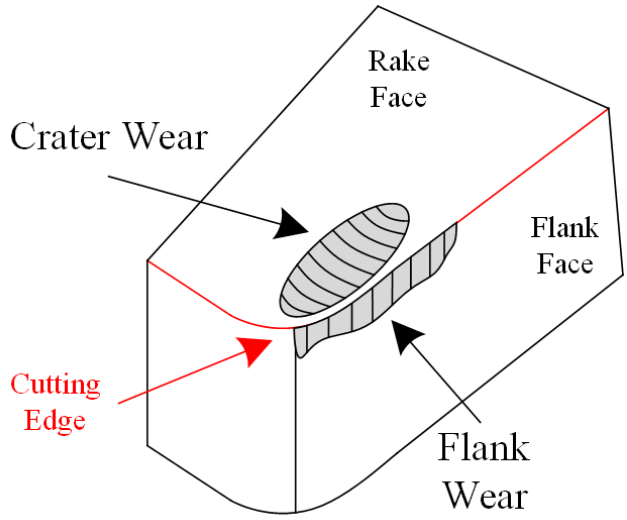

Figure 2-1: Diagram showing crater and flank wear

Flank wear is measured from the cutting edge down the flank face, also known as the clearance face. This type of wear is the most common, and detrimental to the performance of the cutting tool. As the level of flank wear increases, the total amount of tool material present at or near the cutting edge is reduced. This can dull the tool's cutting edge over time, thus increasing the amount of cutting force necessary to continue machining the workpiece material. This also weakens the tool over time, and makes to the tool more susceptible to chipping or catastrophic failure.

Crater wear is another type of induced wear that is caused by the same fundamental wear mechanisms as flank wear, however the wear appears on the rake face instead of the flank face. In this case, crater wear is caused by the chip moving over the surface of the tool, and eroding a portion of the rake face near the cutting edge into a crater shape. The crater is typically located where the chip begins to separate from

the tool, coinciding with the axial depth of cut. This is detrimental to cutting because more friction between the chip and the tool is created. Cutting tool inserts frequently have a protective coating that improves the friction characteristics of this interaction, but as crater wear forms, this coating is removed, and the contact area between the chip and the tool increasing. These factors working in tandem can weaken the tool, although crater wear is not considered as influential as flank wear in this particular case.

Usually, cutting conditions are chosen so that the likelihood of sudden failure is minimized, and the worn-out tool is replaced with a new one before any breakage occurs. However, wear will still occur during cutting with harsher conditions, so it is not possible to ignore it. For the set of experiments performed for this thesis, it was decided that flank wear will be measured. As the amount of flank wear increases, the cutting edge will become thinner, having less material to support it. By measuring this wear, it is possible to see if a tool will chip only after a certain amount of wear is present. After five runs in each cutting test, the inserts are removed from the tool holder and the flank wear is measured under the microscope. This wear is recorded and plotted to yield the wear behaviour of the tool over time, for that particular cutting test.

The other category is sudden, unexpected failure. This type of failure occurs when the tool fractures, rendering the cutting edge completely unusable. While these categories are considered separate, they are related. The propagation of wear on a cutting tool affects the cutting edge, increasing the cutting forces and reducing the strength of the tool. Fracture is significantly more likely to occur in interrupted

cutting processes, as the repetitive impacts cause large, sudden loading or unloading of the cutting tool. Smaller, localized fractures are named “tool chipping”, while larger fractures are referred to as “catastrophic failure”. This is the type of failure that the experiments performed for this thesis are designed to cause on purpose.

Özel [21] investigated the different effects that the edge preparation of cutting tools had on tool life, cutting forces, and temperature levels. Two types of edge preparations were chosen: honed and chamfered. A combination of Finite Element Method (FEM) and turning tests performed on AISI H-13 tool steel, hardened to 55 HRC, yielded many observations. It was found that honed tools typically resulted in lower measured cutting forces, meaning the workpiece material would yield more easily than compared to chamfered tools. However, the honed tools also generated higher temperatures on the tool’s rake face. It was also found that temperatures at the tool-workpiece interface would increase as the cutting speed increases. These elevated temperatures contribute to the acceleration of flank wear, as well as undesirable crater wear on the tool’s rake face. Chamfered tools tended to trap some of the workpiece material underneath the chamfer, which results in the higher forces that were observed. Özel notes that this does not prevent adequate cutting from occurring, as the material would form an effective rake angle relative to the cutting tool, which allows the chip to continue to flow over the tool and away from the workpiece.

An additional factor that plays a massive role in determining tool life is whether a machining operation is continuous or interrupted. A continuous machining process will have little or no interruptions in its chip formation, so the tool is experiencing a

near constant force for the duration of the operations. When recurrent, significant interruptions are introduced, the tool experiences sudden and repeated loading and unloading. These impacts can result in the tool failing before its predicted end-of-life is reached. A continuous load on the cutting tool results in the tool wearing out over time, while impacts have a higher likelihood to cause chipping or catastrophic failure comparatively. In addition to the repeated loads, the tool will also experience cyclic heating (when the tool is engaged with the workpiece) and cooling (when the tool is disengaged from the workpiece) throughout the operation. Pekelharing [22] conducted an investigation into cutting tool damage during interrupted cutting, and found that the small windows of when the tool enters and exits the workpiece have a higher risk of chipping occurring on the tool's cutting edge. This work was conducted experimentally, before the modern, more sophisticated cutting models were developed. The author made a note that the edge preparation of the cutting tool is a significant factor in improving the toughness of cutting tools.

Interrupted cutting is more prone to tool failure due to chipping and cracking when compared to continuous cutting, because of the cyclical load placed on the tool that has been previously described. Chipping that occurs before a tool's expected end-of-life is detrimental to the productivity of an operation, so identifying the key factors that can cause early or unexpected tool failure is of great importance. Work done by Zhou et al. [23, 24] identifies two areas of interest that are used to predict chipping or premature failure. These areas of interest are the profile of the stress load that is placed on the tool, and the workpiece material behaviour.

As a cutting operation is performed, the cutting tool is subject to vibration. Although vibration is an inherent nature of each machining process, it becomes more dominant when some factor of the cutting operation is not set correctly, such as the cutting parameter values being too high or low, or improper tool selection given the workpiece material. These vibrations can contribute to early tool failure, as detailed by Ma and Wang [25]. It was found that exposing cutting tools to ultrasonic vibrations could simulate the effects of cyclical loading found in interrupted cutting processes. When examining the tools, it was seen that there are three distinct phases of damage that can be observed. First, micro-cracks are generated near the area of the cutting tool that contacts the workpiece. Next, the micro-cracks grow in number and begin to propagate throughout the structure of the cutting tool. Finally, the presence of these micro-cracks weakens the structural integrity of the tool to the point where brittle failure occurs, in the form of either chipping or complete fracture. Tools naturally experience fatigue failure over time, and the presence of detrimental vibrations in machining can reduce the amount of time it takes for catastrophic failure to occur. However, with the proper selection of cutting parameters, the likelihood of premature failure due to fracture can be drastically reduced.

When investigating the useful life of cutting tools, more emphasis is typically placed on the wear behaviour of the tool, since most processes will avoid interrupted cutting if possible. However, interrupted cutting is sometimes necessary, so research into the strength and toughness of cutting tools in this context is important. Bouzakis et al. [26] investigated the fatigue behaviour of both coated and uncoated cutting edges when subjected to repeated impacts. In order to conduct these tests, the cutting

inserts were repeatedly loaded in an impact tester. While testing this way does provide valuable information about the properties of the cutting tools, it does not accurately simulate the impacts that the tool would be experiencing while in a cutting process. It lacks the thermal loading that the cutting tool undergoes, as well as removing the sustained load that typically follows the impact when a tool engages a workpiece. Furthermore, a cutting tool will wear as it being used, even in interrupted cutting. This wear will alter the strength and toughness of the tool as the wear levels increase, which is also a significant factor that is missed by conducting out-of-process impact testing.

Another work published by Bouzakis et al. [27] examined the period that a milling tool's cutting edge first engages with the workpiece during a cut. It has been well-established that milling tools are suddenly loaded when they engage a workpiece, but the duration of this impact can be controlled by the cutting parameters and kinematics. In up milling, the tool engages the workpiece with a near-zero chip load, which becomes larger as the tool rotates and cuts further into the workpiece. The opposite case is down milling, where the tool suddenly engages with a large chip load, which becomes smaller as the tool rotates. The authors conclude that a long cutting edge entry impact duration (CEEID), which is achieved by utilizing up milling, improves the tool life by reducing the effects of the tool's impact with the workpiece. Conversely, down milling results in a much shorter CEEID, which increases the likelihood of failure due to chipping or fracture.

Songmene et al [28] investigated the effects of lubrication on the machinability of tool steels, as well as the wear behaviour of the cutting tools being used. When

conducting dry machining, which means without lubrication, the flank wear on the tool progressed relatively evenly over time. However, when lubrication was introduced, the presence of thermal cracking in the tool inserts was present. As previously discussed, milling is an interrupted cutting process, so the tool's force and thermal load is cyclical. With the presence of lubrication, the insert was heating and cooling at a faster rate, so the propagation of thermal cracks increased. The number of cracks observed also increased as the cutting speed increased, as a higher cutting speed results in a higher temperature generated at the tool-workpiece interface. It was also found that softer workpiece materials resulted in a better tool life when compared to hardened materials.

After reviewing works that are relevant to this project, the objectives of present thesis can be defined as follows: Developing a modified version of Oxley's predictive machining model accounting for the edge radius. The model must be able to predict the cutting force for any edge radius and workpiece materials as long as the cutting conditions and Johnson-Cook parameters for the workpiece material are known.

- Aforementioned objective can be achieved by representing the milling process as a series of two-dimensional problems, edge radius considerations can be applied.
- Cutting tool impact resistance testing should be performed in-process, so that important factors, like temperature, are not excluded.

Chapter 3. Mathematical Model

This chapter presents the derivation of a mathematical model that can accurately predict the cutting forces generated during the milling process, that accounts for the effects of the tool's cutting edge microgeometry. This work uses Oxley's predictive machining theory as a starting point. By doing this, it is possible to maintain several assumptions that allows the cutting process to be represented by an orthogonal cutting model. Oxley's model allows for considerations such as the temperature change to be included as well, resulting in a more comprehensive cutting force model. Milling operations are considered three-dimensional cutting processes, so they are frequently simulated using oblique cutting models. However, it is possible to simulate milling as a series of finite two-dimensional elements that can be assumed orthogonal. The orthogonal calculations will be repeated for each angular position of cutting tool as the tool rotates. The presented model can be applied to other machining processes with a few minor alterations, so long as the use of the orthogonal cutting model is appropriate for that process.

3.1 Mechanics of Milling

Milling is a machining process that uses a rotating cutting tool to remove excess material, referred to hereafter as chips, from a workpiece to produce a desired part. By controlling the movement of the cutting tool relative to the workpiece in three-dimensional space, a wide variety of shapes and profiles can be created in many manners of workpieces. This versatility has resulted in milling becoming one of the most common machining processes used in manufacturing industries globally.

This work analyzes the face milling process. Face milling is used to create flat surfaces relative to the machine's axes. In this operation, the cutting tool is fed horizontally, parallel to the XY plane of the milling machine, and the end of the cutting tool is the portion that is actively used for cutting. This process is defined having a much larger radial depth of cut compared to the axial depth of cut. A diagram of face milling can be seen in Figure 3-1.

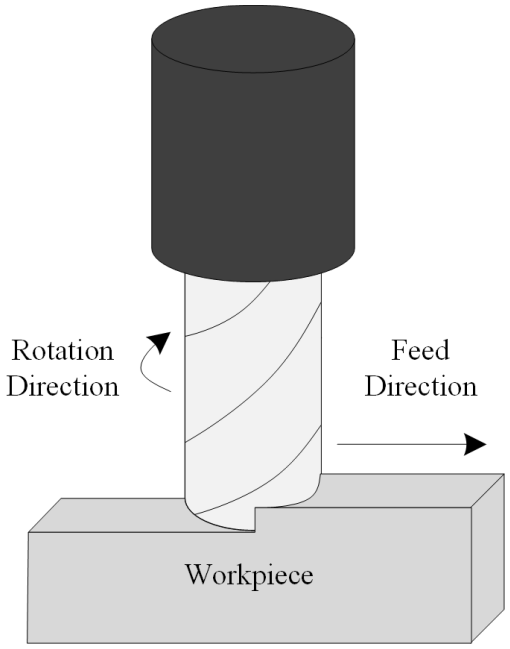

Figure 3-1: Illustration of face milling

Several parameters are needed to define a milling process, and changing these parameters will affect the mechanics of the operation, as well as the performance of the tool and quality of the part that is produced. The first of these factors is cutting speed, which is controlled by the angular speed of spindle and the diameter of the cutter. The second factor is feed rate, which is the rate at which the tool and the workpiece are moving relative to each other. Another factor is the number of cutting

edges on a cutting tool, as using a tool with more cutting edges will result in less material being removed per cutting edge. The combination of these cutting parameters determines the magnitude of the chip load, which is the area of the chip that is in contact with the tool as cutting occurs, and is found by multiplying the chip thickness with the chip width. This parameter is critical in determining the forces that are acting on the tool.

In continuous cutting operations, the chip load is a constant value, but this is not the case for milling, which is considered to be an interrupted cutting process. In this case, the chip load is changing as the tool rotates. This variable chip thickness is one of the reasons why modelling and analyzing milling operations is more complex than those with almost constant chip load. Milling also causes the cutting edges to disengage with the workpiece cyclically, which occurs when the chip is removed and before that edge re-engages with the workpiece material after completing a revolution. When the cutting tool is suddenly engaged (loaded) or disengaged (unloaded), an impact acting on the cutting tool occurs. It is possible to set up a milling process in which impact occurs during the small window of time beginning when the tool first contacts the workpiece, and ending once a steady cutting state begins. The magnitude of this impact is related to the size of the chip load during impact, as a larger chip load is related to larger forces that are generated during cutting.

It is possible to change this initial chip load by using different cutting kinematics. There are two cutting kinematics that are used for the milling operation: up milling and down milling. In up milling, the cutting edge is oriented so that the initial chip

load has a near-zero magnitude, and the chip load increases as the tool rotates, with the maximum chip load occurring near or at the end of the cut. Down milling in the opposite case, where the initial chip load on the tool is the largest, and the chip load is reduced as the tool rotates to complete the cut. Figure 3-2 illustrates the difference between up milling and down milling. In order to explore the impact behaviours of cutting tools, a large impact is desirable, so down milling was chosen for this work.

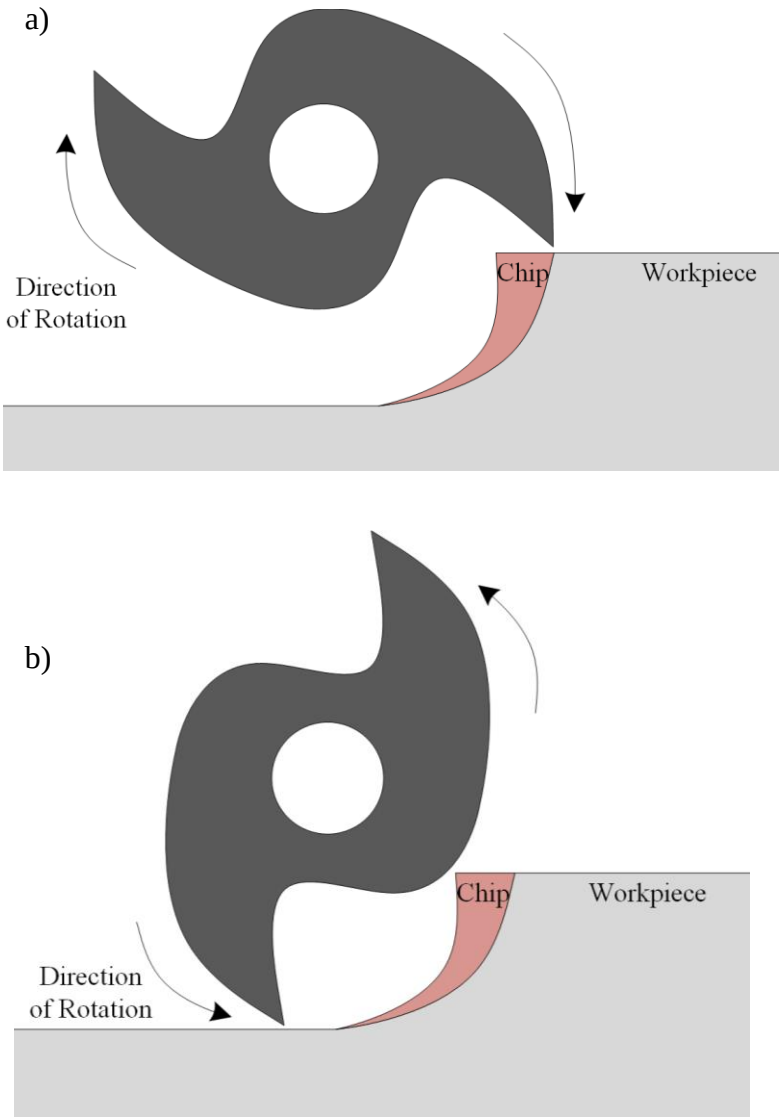

Figure 3-2: Illustration of a) down milling and b) up milling

3.2 Forces in Milling

There are several forces that are acting on a cutting tool while it is cutting. Each of these components contribute to the proper function of a milling tool. This section will define each of the force components that are modelled, describe their behaviour, and their importance to the mathematical model. The direction of each of these forces is shown in Figure 3-3.

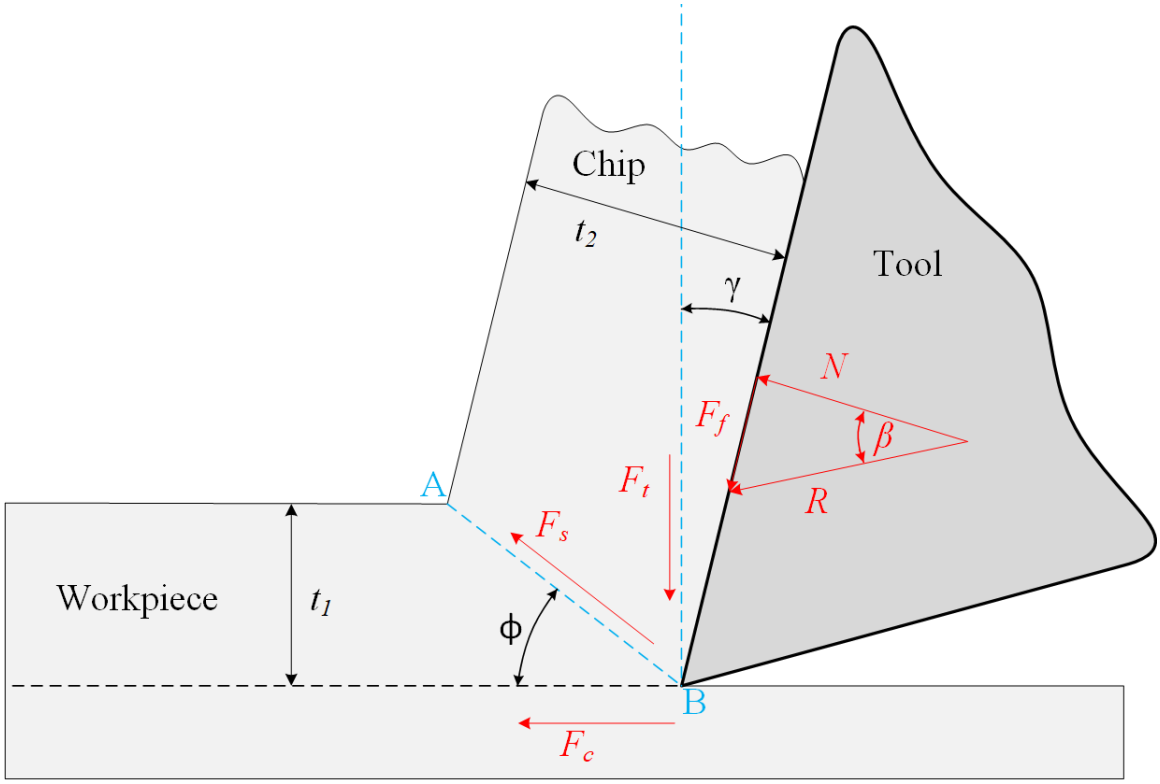

Figure 3-3: Orientation of force components in orthogonal cutting

The most important force in this model is the cutting force F_c, which is also known as the tangential force. This is the force component that is directly responsible for powering the cutting tool, and is related to the shear force F_s, which directs the workpiece material to flow along the tool's rake face, forming the chip. This

component is directly affected by the inclusion of the edge radius in this model. This force's direction is constantly changing, as it always acts perpendicular to the radius of the cutting tool. During experimentation, forces are measured in three triaxial components: F_x, F_y, and F_z. A combination of both F_x and F_y are required to determine F_c at any given point. See Figure 3-4 for the relationship between these components.

$$F_x = F_c \sin(\theta) \tag{3-1}$$

$$F_y = F_c \cos(\theta) \tag{3-2}$$

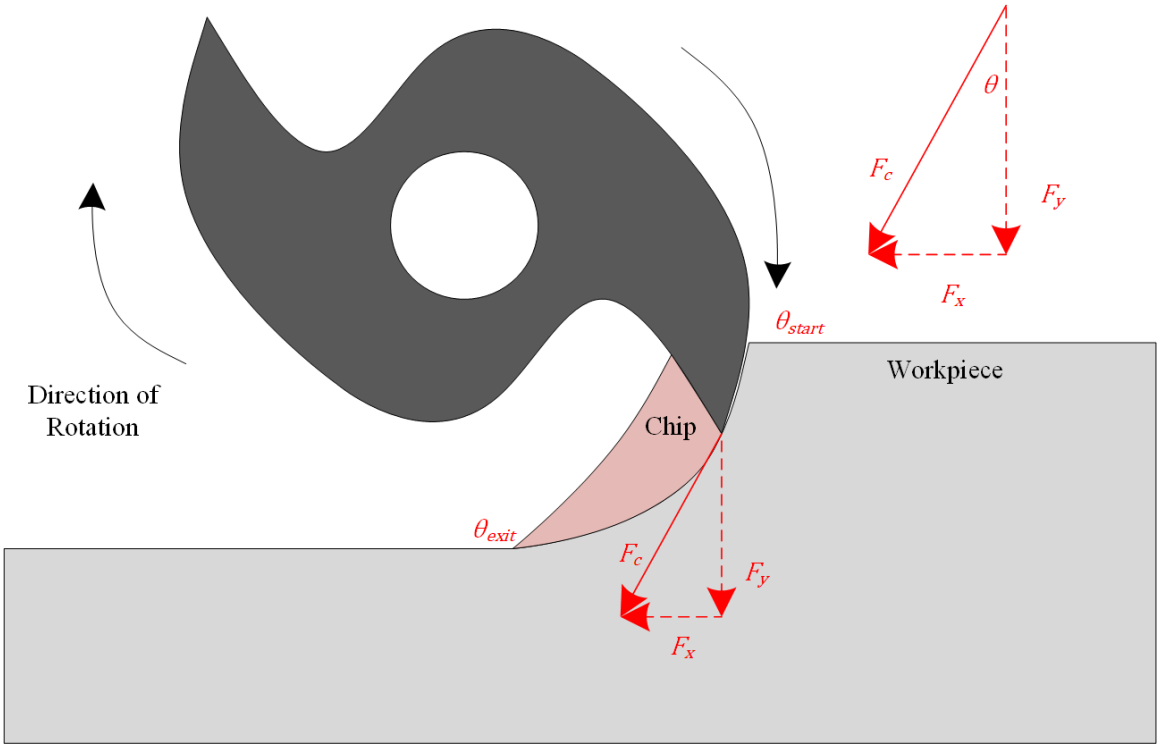

Figure 3-4: Relationship between cutting force and measured force components

Acting perpendicular to the cutting force is the thrust force F_t, or axial force. This force acts along the center axis of the cutting tool. This component counters the force of the chip acting on the cutting tool that pushes the tool away from the workpiece.

In milling, this force tends to vary less than other components. During experimentation, this force is equal to the force measured in the Z-direction, F_z.

The next important force component is the shear force F_s. This force acts in the same direction as the shear plane that is formed in the transitional zone between uncut chip thickness and chip thickness. Please note that in reality, this zone has a non-zero thickness, but it is represented as a plane to simplify the model. In Oxley's predictive machining theory, this force changes as the temperature at the tool-workpiece interface changes, and these changes are carried on through iterative loops. A resultant force R is calculated using F_s and the angle between them ψ.

As the chip flows along the tool's rake face, there is a friction force generated that opposed its motion. This friction force is represented as F_f. A coefficient of friction between the workpiece material and the cutting tool is not usually known, so this force is found through trigonometry using the resultant force R. The same relationship can be used to find the normal force N, that acts between the chip and the tool's rake face. These relationships are given in equations (3-21) and (3-22).

3.3 Force Modelling

There are several different models that currently exist regarding milling processes. Each of these models offer benefits and drawbacks, so the appropriate model choice is dependent on the application of the model. In this section, the common cutting force model types will be discussed in greater detail.

Mechanistic machining models is the term used for methods that require the acquisition of empirically-determined constants [10, 11]. These constants are

referred to as cutting coefficients, and are used in equations (3-3) to (3-5) to determine the magnitudes of the force components in the tangential, radial, and axial directions.

$$dF_t = \Delta a(K_{tc}h + K_{te}) \quad (3\text{-}3)$$

$$dF_r = \Delta a(K_{rc}h + K_{re}) \quad (3\text{-}4)$$

$$dF_a = \Delta a(K_{ac}h + K_{ae}) \quad (3\text{-}5)$$

Since these coefficients are found by analyzing experimental data for each combination of cutting tool material and geometry along with the workpiece material, this type of model tends to be very accurate when modelling the same process. However, mechanistic models have two major drawbacks. First, the cutting coefficients are only accurate for modelling the same process (same tool material and geometry and same workpiece material) that was conducted experimentally. This means that changing the workpiece material or tool in any way will render these coefficients inaccurate. The second drawback is that experiments are required if the coefficients for a specific tool-workpiece combination are unknown, which can be time-consuming to conduct. Therefore, mechanistic models can only be considered predictive models if the same tool and workpiece material are used for different cutting conditions.

A unified cutting force model refers to a model framework that can be applied to multiple metal cutting processes, such as milling, turning, or drilling [14]. This type of model works by first modelling the geometry and position of the cutting edge locally. Once the edge is defined, one or more cutting edges are positioned in a coordinate system that represents the edge's position in the tool holder. This

positioning is achieved by using transformation matrices to find the location of each cutting edge, using the edge angle κ_e, radial rake angle γ_r, and axial rake angle γ_a.

$$R_{DR} = \begin{bmatrix} \cos\kappa_e & 0 & \sin\kappa_e \\ 0 & 1 & 0 \\ -\sin\kappa_e & 0 & \cos\kappa_e \end{bmatrix} \begin{bmatrix} 1 & 0 & 0 \\ 0 & \cos\gamma_r & -\sin\gamma_r \\ 0 & \sin\gamma_r & \cos\gamma_r \end{bmatrix} \begin{bmatrix} \cos\gamma_a & -\sin\gamma_a & 0 \\ \sin\gamma_a & \cos\gamma_a & 0 \\ 0 & 0 & 1 \end{bmatrix}$$

The orientations of forces are also transformed in a similar way, so that the force components acting on each cutting edge, in the case of more than one cutting edge being used, can be analyzed separately. This model excels in its versatility, as the same model can be applied to multiple cutting processes with only a few changes between each process. However, the mathematics used for this model is more complex than other common models, and this model does not consider the high strain rates and temperatures that occur during machining, which affects the mechanical properties of the workpiece.

This thesis uses a modified version of Oxley's predictive machining theory as the basis for the force prediction model. Oxley's model works by modelling the flow stress behaviour and thermal changes of the workpiece material under high strain rate conditions [16]. Oxley's model is also capable of accommodating the presence of strain hardening, which is a phenomenon that causes a change in a material's mechanical properties when material dislocations move due to an applied strain. The introduction of the modified strain hardening exponent n_{eq} allows Oxley's model to accept Johnson-Cook material properties as inputs, resulting in a more comprehensive machining model that includes material properties, thermal conditions, tool geometry, and cutting parameters in its analysis. One major assumption that is kept in Oxley's model is the assumption of a perfectly sharp

cutting tool. In reality, all cutting tools have some form of preparation performed on them to ensure the tool is not perfectly sharp, such as honing or chamfering. Illustrations of these edge preparations can be seen in Figure 3-5.

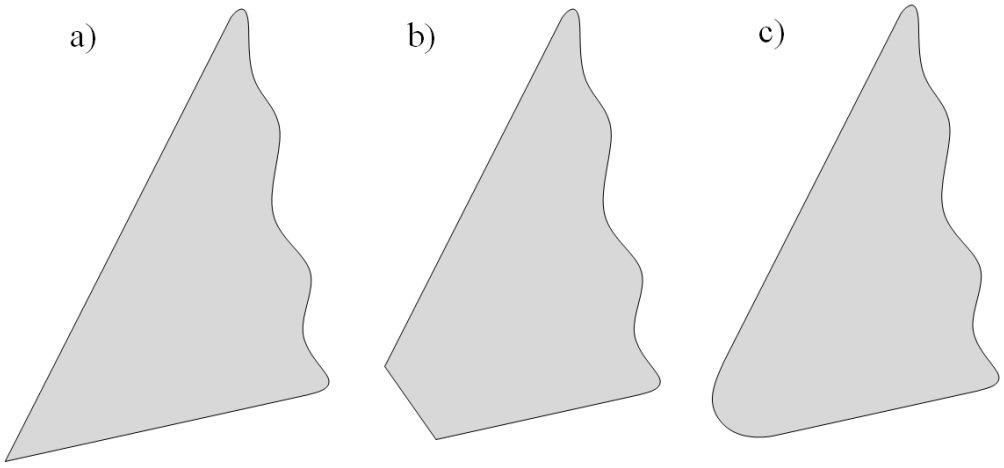

Figure 3-5: Diagrams of tools with a) no edge preparation b) chamfering and c) honing

This edge preparation increases the strength of the tool, and reduces its susceptibility to breakage. Manjunathiah and Endres derived an altered orthogonal cutting model that did include the effects of cutting edge radius in its force calculations, but the other assumptions of orthogonal cutting still apply [20]. A new consideration that is added is the deformation of material that occurs at the newly-generated surface. The edge radius of the tool causes the majority of the material that is yielding to flow away from the workpiece along the cutting tool. However, some of the material instead flows under this radius, and it compressed to form the new surface. This behaviour is illustrated in Figure 3-6. Please note that dimensions and scale have been altered for illustrative purposes.

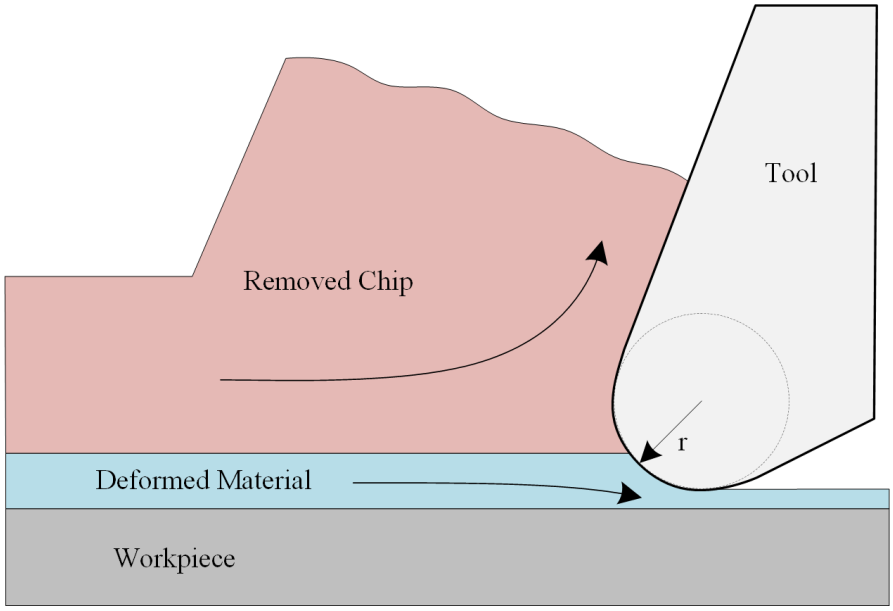

Figure 3-6: Effect of tool edge radius on material flow

The consistency between the two previous models means that it is possible to use these models together to analyze cutting forces, but only for orthogonal cutting operations. By considering each position of the milling tool as a new instance of orthogonal cutting, it is possible to merge the edge radius considerations with Oxley's model, while also accounting for the constantly-changing chip load acting on the tool. This approach provides one model that can accept the Johnson-Cook material properties of a workpiece, the tool geometry including the edge radius, and the cutting conditions of the operation as inputs, and output a prediction of the force components acting on that tool, while maintaining the ease of use provided by the orthogonal cutting model.

3.4 Calculation of Cutting Forces

To begin, the orthogonal cutting model including the edge radius of the tool is drawn. Please note that conventions and notations will follow those previously

established in this work. Figure 3-7 shows the new orthogonal cutting model that included considerations from Oxley's predictive machining model and the work done by Manjunathiah and Endres.

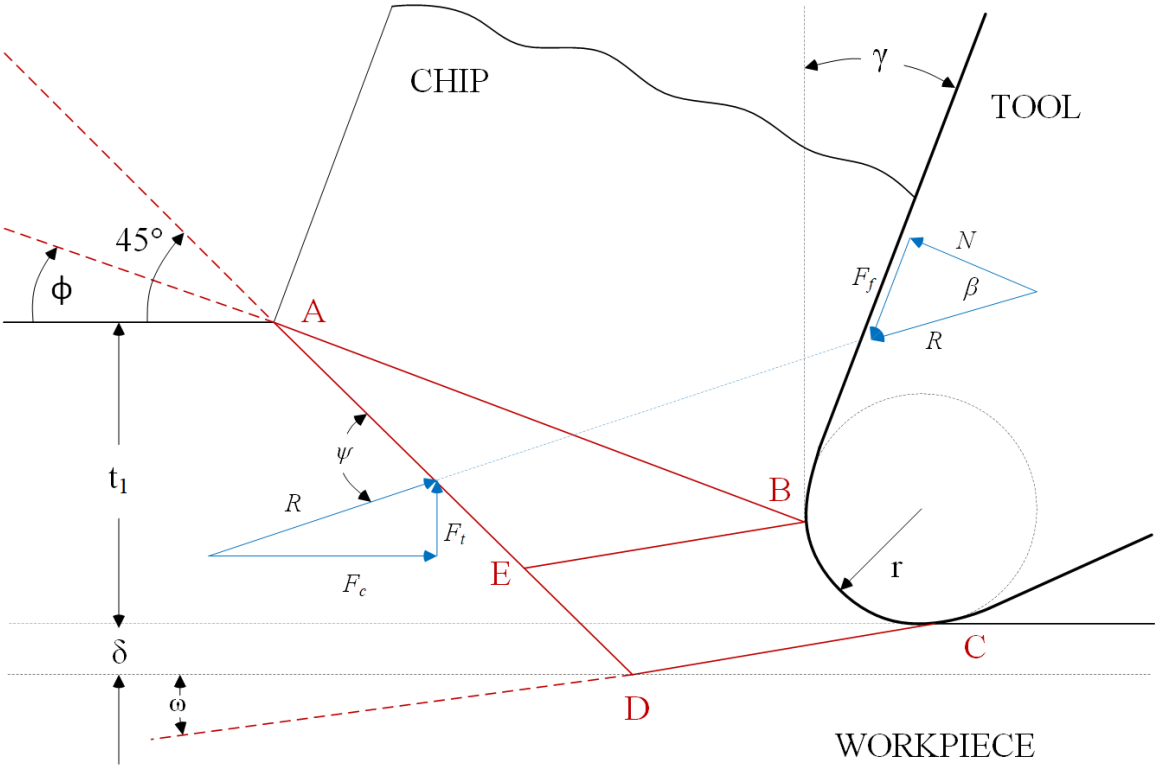

Figure 3-7: Representation of orthogonal cutting that includes edge radius

In this model, the line *AB* represents the shear plane. After material is deformed and flows past this area, the material becomes the chip that is being removed. The line *AD* represents a slip plane, which is oriented at 45°, since that is when a slip plane meets an unstressed surface. The line *BE* forms the boundary of material separation, where material above the line is removed as a chip, and material below the line is compressed into the newly generated surface. It is assumed that no built-up edge is occurring, and there is no chip flow stagnation point. The line *CD* illustrates the

deformation of the workpiece material that occurs below the newly generated surface, and is inclined by the separation angle ω. This value is determined by observing deformation via experimentation, but this work assumes the value to be 30°. Please note that the point locations and dimensions have been exaggerated for illustrative purpose, and are not to scale.

Three parameters that cannot be exactly calculated for this model are the shear plane angle ϕ, the ratio of shear plane length AB to primary shear zone thickness C_0, and the ratio of tool-chip interface plastic zone thickness to chip thickness ζ. Oxley's model states that these values will change and orient themselves so that the cutting force acting on the tool is minimized. Therefore, a range of possible values for each of these variables is defined. These ranges can be set to any value, but there are combinations that create infeasible solutions. For example, ϕ cannot be less than zero, as there is no material to cut in that region. It also cannot be greater than 45°, as that is the orientation of an unstressed slip plane. Other works based on Oxley's model [4-6, 29] has found the ranges that include feasible solutions for machining of metals. The ranges for each of these variables are displayed in Table 3-1. These ranges are chosen to ensure that all solutions are found within a feasible space, meaning that cutting would be occurring. At the beginning of the analysis, all variables are set to their minimum value.

Table 3-1: List of control variables and their ranges

Variable	**Range**
ϕ	$10° - 45°$
C_0	$2 - 8$
ζ	$0.01 - 0.4$

Table 3-2: Johnson-Cook parameters

Johnson-Cook Parameter	**Value for hardened AISI 4340 [30]**
A	950 MPa
B	725 MPa
C	0.015
n	0.375
m	0.625
$\dot{\varepsilon}_0$	3500 $\frac{1}{s}$

In all milling processes, the uncut or undeformed chip thickness t_1 changes as the milling tool rotates. Thus, t_1 is equal to the instantaneous chip thickness at a certain tool position. In milling operations, this chip thickness can be calculated using equation (3-6).

$$t_1 = c \sin\theta \tag{3-6}$$

Where c is the feed per tooth of the milling operation. The link between the Johnson-Cook constitutive equation and Oxley's extended machining model is a modified strain hardening exponent n_{eq}, as previously discussed in the literature review section of this thesis [15]. This modified exponent can be calculated using the known Johnson-Cook parameters, shown in equation (3-7) [30]. The parameters for hardened AISI 4340 are listed in Table 3-2.

$$n_{eq} = \frac{nB\varepsilon_{AB}^{n}}{A + B\varepsilon_{AB}^{n}} \tag{3-7}$$

Where A is the yield stress of the material, B is the hardening stress, and n is the strain-rate hardening exponent. All of these values are determined through a series of experiments. In this work, the values for the workpiece material has been obtained from the literature. With the inputs completely defined, the length of the shear plane

l and shear velocity V_{sh}, which acts along the line AB, can be calculated using equations (3-8) and (3-9).

$$l = \frac{t_1}{\sin\phi} \tag{3-8}$$

$$V_{sh} = \frac{V_c \cos\gamma}{\cos(\phi - \gamma)} \tag{3-9}$$

By utilizing von Mises criteria, the equivalent plane strain and strain rate occurring at the shear zone of the material, which is defined by the line AB, are found by equations (3-10) and (3-11) [29]. In reality, the shear zone that forms during cutting is a zone with a measurable thickness, but representing it with a single line is sufficient for the purposes of force prediction.

$$\varepsilon_{AB} = \frac{\eta_{AB}}{\sqrt{3}} = \frac{1}{2\sqrt{3}} \frac{\cos\gamma}{\sin\phi \cos(\phi - \gamma)} \tag{3-10}$$

$$\dot{\varepsilon}_{AB} = \frac{\dot{\eta}_{AB}}{\sqrt{3}} = \frac{1}{\sqrt{3}} \frac{C_0 V_{sh}}{l} \tag{3-11}$$

As previously stated, Oxley's machining theory accounting for changes in temperature during the operation. First, a non-dimensional thermal number E_T is determined using equation (3-12) [4, 29].

$$E_T = \frac{\rho C_p V_c t_1}{K} \tag{3-12}$$

Where ρ is the workpiece density (kg/m^3), C_p is the specific heat of the workpiece (J/kgK), and K is the thermal conductivity of the workpiece (W/mK). With E_T known, the heat partition coefficient ξ can be calculated using either equation (3-13)

or equation (3-14) [4, 29]. A combination of the shear plane angle and the non-dimensional thermal number determine which equation is chosen.

$$if\ 0.04 \leq E_T \tan\phi \leq 10 \rightarrow \xi = 0.5 - 0.35\log(E_T \tan\phi) \tag{3-13}$$

$$if\ E_T \tan\phi \geq 10 \rightarrow \xi = 0.3 - 0.15\log(E_T \tan\phi) \tag{3-14}$$

In order to determine the shear force acting in the shear plane, the shear stress determined by the Johnson-Cook constitutive equation is multiplied by the area of the shear plane, shown in equation (3-15).

$$F_{sh} = \sigma_{AB} l t_1 \tag{3-15}$$

Considering the plastic work being done in the primary shear zone, the average temperature at the shear zone T_{AB} can be found using equation (3-16). In this paper, it is assumed that the value of the sensible heat coefficient λ is 0.9. This value is chosen to follow the assumption that that sensible heat to latent heat ratio is 90% in favour of sensible heat, as experiments performed on a similar steel have determined to be reasonable [29].

$$T_{AB} = T_w + \lambda \frac{(1-\xi) F_{sh} V_{sh}}{m_{chip} C_p} \tag{3-16}$$

Where m_{chip} is the mass of the chip being removed during the current tool rotation. Using the average temperature at the primary shear zone, the average flow stress in the primary shear zone σ_{AB} can found using the Johnson-Cook constitutive equation (3-17).

$$\sigma_{AB} = (A + B\varepsilon_{AB}^{n})\left(1 + C\ln\left(\frac{\dot{\varepsilon_{AB}}}{\dot{\varepsilon}_0}\right)\right)\left(1 - \left(\frac{T_{AB} - T_w}{T_M - T_w}\right)^{m}\right) \quad (3\text{-}17)$$

Where m is the thermal softening coefficient, and $\dot{\varepsilon}_0$ is the reference strain rate. These parameters are also determined with same set of experiments that determined the values of other Johnson-Cook parameters. With the average flow stress now known, the angle between the shear plane and the resultant force (ψ) can be determined using equation (3-18).

$$\tan\psi = 1 + 2\left(\frac{\pi}{4} - \phi\right) - C_0 n_{eq} \quad (3\text{-}18)$$

The average friction angle between the tool and the chip being removed β can be calculated using equation (3-19).

$$\beta = \psi - \phi + \gamma \quad (3\text{-}19)$$

Using these angles, the various force components acting between the tool and the chip can be calculated at any instance of the cut using equations (3-20) - (3-23).

$$R = \frac{F_{sh}}{\cos\psi} \quad (3\text{-}20)$$

$$F_f = R\sin\beta \quad (3\text{-}21)$$

$$N = R\cos\beta \quad (3\text{-}22)$$

$$F_t = R\sin(\beta - \gamma) \quad (3\text{-}23)$$

At this point, the effects of the edge radius r can begin to be calculated. It is here that the model will differ from the Oxley model to incorporate the edge radius in the force calculations. While the Oxley model does not consider the edge radius, its

inclusion in this work shows that is not negligible. This consideration is based on the work done by Manjunathiah and Endres [20]. First, two new constants are defined: the separation angle ω and deformation angle υ. The value of the separation angle is chosen based on previous experiments that have investigated this parameter [31, 32]. These works have predicted the value of ω to be 30° for most cutting conditions, and it was found that adjusting the value of ω has a negligible effect on the cutting forces. As for υ, the same experiments predict this value to be 20°, and show that adjusting the value only marginally affects the shear stresses, but also by a negligible amount. Therefore, the current work will consider these two values as constants with values of ω = 30° and υ = 20°. The penetration depth p and depth of deformation δ can be calculated using equations (3-24) and (3-25).

$$p = r(1 - \cos\omega) \tag{3-24}$$

$$\delta = \frac{(t_1 - p)cot\phi + r\sin\omega - h}{1 + \cot\upsilon} \tag{3-25}$$

At this point, other factors need to be calculated using the Oxley model. The effects of the edge radius will be further explored later in this analysis. The next step is calculating the deformed chip thickness, which can be found using equation (3-26).

$$t_2 = \frac{t_1 \sin\psi}{\cos(\phi - \gamma)} \tag{3-26}$$

In order to determine if these force values are accepted for the given inputs, various stresses must be calculated. To begin this section, the length of the contact area between the tool and the chip L_{int} can be calculated using equation (3-27).

$$L_{int} = \frac{t_1 \sin\psi}{\cos\beta \sin\psi}\left(1 + \left(\frac{C_0 n_{eq}}{3\left(1 + 2\left(\frac{\pi}{4} - \phi\right) - C_0 n_{eq}\right)}\right)\right) \tag{3-27}$$

The shear stress along the tool-chip interface (τ_{int}) is calculated using equation (3-28).

$$\tau_{int} = \frac{F_f}{L_{int} w} \tag{3-28}$$

Next, the maximum shear strain and the shear strain rate at this interface must be determined using equations (3-29) and (3-30).

$$\varepsilon_{int} = \frac{\eta_{int}}{\sqrt{3}} = \frac{1}{\sqrt{3}}\left(2\eta_{AB} + \frac{0.5 L_{int}}{\zeta t_2}\right) \tag{3-29}$$

$$\dot{\varepsilon}_{int} = \frac{\dot{\eta}_{int}}{\sqrt{3}} = \frac{1}{\sqrt{3}}\left(\frac{V_{chip}}{\zeta t_2}\right) \tag{3-30}$$

Where η_{AB} can be calculated by rearranging equation (3-10). The maximum temperature change in the chip during cutting ΔT_m can be calculated using equations (3-31) and (3-32).

$$\log\left(\frac{\Delta T_m}{\Delta T_c}\right) = 0.06 - 0.195\xi\sqrt{\frac{E_t t_2}{t_1}} + 0.5\log\left(\frac{E_T t_2}{L_{int}}\right) \tag{3-31}$$

$$\Delta T_c = \frac{F_f V_{chip}}{m_{chip} C_p} \tag{3-32}$$

The temperature at the tool-chip interface T_{int} can be calculated using equation (3-33).

$$T_{int} = T_w + \frac{(1-\xi)F_{sh}V_{sh}}{m_{chip}C_p} + \Psi \Delta T_M \tag{3-33}$$

Where Ψ is the ratio of tool-chip interface temperature rise to the maximum temperature rise of the chip [19]. For the purposes of this analysis, this value was assumed to be 0.9. Using these temperatures, the Johnson-Cook constitutive equation is used again to determine the shear flow stress along the tool-chip interface, using equation (3-34).

$$\tau_{chip} = \frac{1}{\sqrt{3}}(A + B\varepsilon_{int}^{n})\left(1 + C\ln\left(\frac{\dot{\varepsilon}_{int}}{\dot{\varepsilon}_0}\right)\right)\left(1 - \left(\frac{T_{int} - T_w}{T_M - T_w}\right)^{m}\right) \tag{3-34}$$

At this point, the values of τ_{int} and τ_{chip} are compared. After running these calculations for every value of ϕ, the final value of ϕ is chosen such that the difference between τ_{int} and τ_{chip} is minimized. For the next check, the normal stress at the tool-chip interface is calculated. This is done with two methods: one using the normal force (σ_N), and the other using stress boundary conditions at point B (σ'_N). These are given in equations (3-35) and (3-36).

$$\sigma_N = \frac{N}{L_{int}w} \tag{3-35}$$

$$\sigma'_N = \sigma_{AB}\left(1 + \frac{\pi}{2} - 2\gamma - 2C_0 n_{eq}\right) \tag{3-36}$$

Similar to the determination of the value for ϕ, the values of σ_N and σ'_N are compared, and the value of C_0 is chosen such that the difference between them in minimized. It is now possible to finish calculating the total cutting force, while

considering the tool's edge radius. The last factor needed is called the normal stress factor κ, and it is found using equation (3-37).

$$\kappa = \frac{\sigma_N}{\sigma_N'} \tag{3-37}$$

With every variable known, it is now possible to calculate the cutting force acting on the tool using equation (3-38).

$$F_{cut} = \sigma_N' \delta((t_1 - p)\cot\phi + t_1 + r\sin\omega - (\kappa - 1)) \tag{3-38}$$

The final determination that is needed is the value of ζ. As previously mentioned, all possible values of F_{cut} are compared. The value of ζ is chosen corresponding to the minimum value of F_{cut}. At this point, the three variables discussed at the beginning of this analysis are determined (ϕ, C_0, and ζ), and the forces are known. However, this is only the solution for this position of the tool. To continue, the cutting force prediction is stored, the angle of the milling tool θ is incremented up, and the entire process repeats. A visualization of the model's logic is shown in Figure 3-8.

The model described in this chapter can be used to predict the forces acting on a cutting tool during the milling process. It should be noted that predicted forces are estimated values, as the model uses a somewhat simplified representation of milling. In reality, the cutting tool will wear over time, and the tool's efficacy will change. This model does not account for the effects of tool wear directly, so for verification purposes, experimental forces will be taken from runs with minimal tool wear.

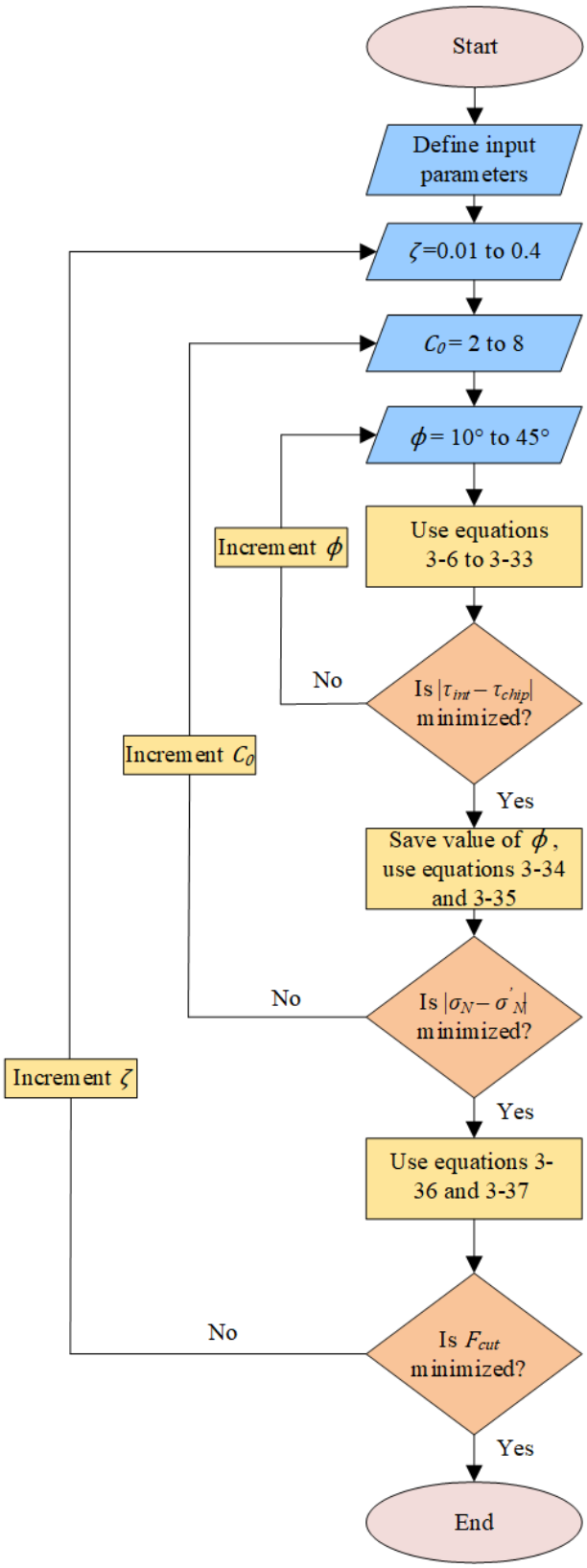

Figure 3-8: Flowchart representing the logic of the model

Chapter 4. Experimentation

This chapter describes the background and purpose of the series of milling experiments that were performed to prove the validity of the mathematical model previously presented. This proof is done by comparing the cutting force values predicted by the model to a set of measured cutting forces taken from a series of machining tests, while the tests themselves were purposefully designed to instigate tool failure due to chipping to study the effects of tool microgeometry on the impact resistance of milling tools. The machining operation used to gather the experimental data is down face milling. A total of six cutting tests are performed using five different tool edge radii, resulting in a total of 30 cutting tests. Each test consists of a maximum of 45 runs in order to capture the wear behaviour of the cutting inserts and its effects on the measured forces.

4.1 Tool Selection

As the purpose of this thesis is the investigation of the effect of cutting tool edge microgeometry on the impact resistance of the milling tools, using an appropriate cutting tool for the experiments is critical. Between different tests, it is known that the tool edge microgeometry must change, but other parameters, such as the tool's material, number of cutting edges, and others geometrical parameters must be kept constant. This is done to ensure that these other factors do not affect the results that are gathered during experimentation. The tools must also be able to have their flank wear measured under a microscope. After considering all of these factors, it was decided that a tool holder with cutting inserts would be the best choice for use in this

project as it allows for easy removal of the cutting insert for wear measurements. Five sets of custom-made cutting inserts (ISO: R390-020A20-11L), along with a compatible tool holder, were provided by this project's industry partner, Sandvik-Coromant. Each set of inserts was prepared with a different edge radius on the cutting edge. The values of these radii range from 25 - 45 μm, with an increment of 5 μm between each set. Images of an insert and the tool holder can be seen in Figure 4-1. Side-by-side comparisons of the different edge radii can be seen in Figure 4-2. Dimensional values for the inserts can be seen in Table 4-1. Several benefits are offered by using this type of tool, opposed to a traditional end mill. Inserts can be secured to and removed from the tool holder quickly, without disrupting and dismantling the experimental set-up. Cutting inserts are easier to manipulate in the field-of-view of the microscope that was used to measure flank wear. It was noted that this type of cutting insert is commercially available, with a nominal edge radius of 35 μm, which provides optimal performance according to the tool manufacturers. However, the company has not explicitly published its methodology, so this set of experiments will also provide some insight into why 35 μm is the commercially available one.

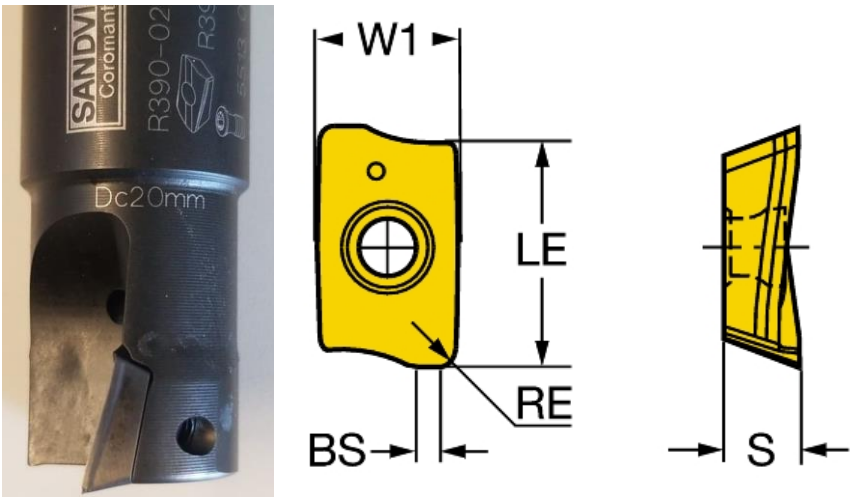

Figure 4-1: Images of the tool holder and cutting insert [33]

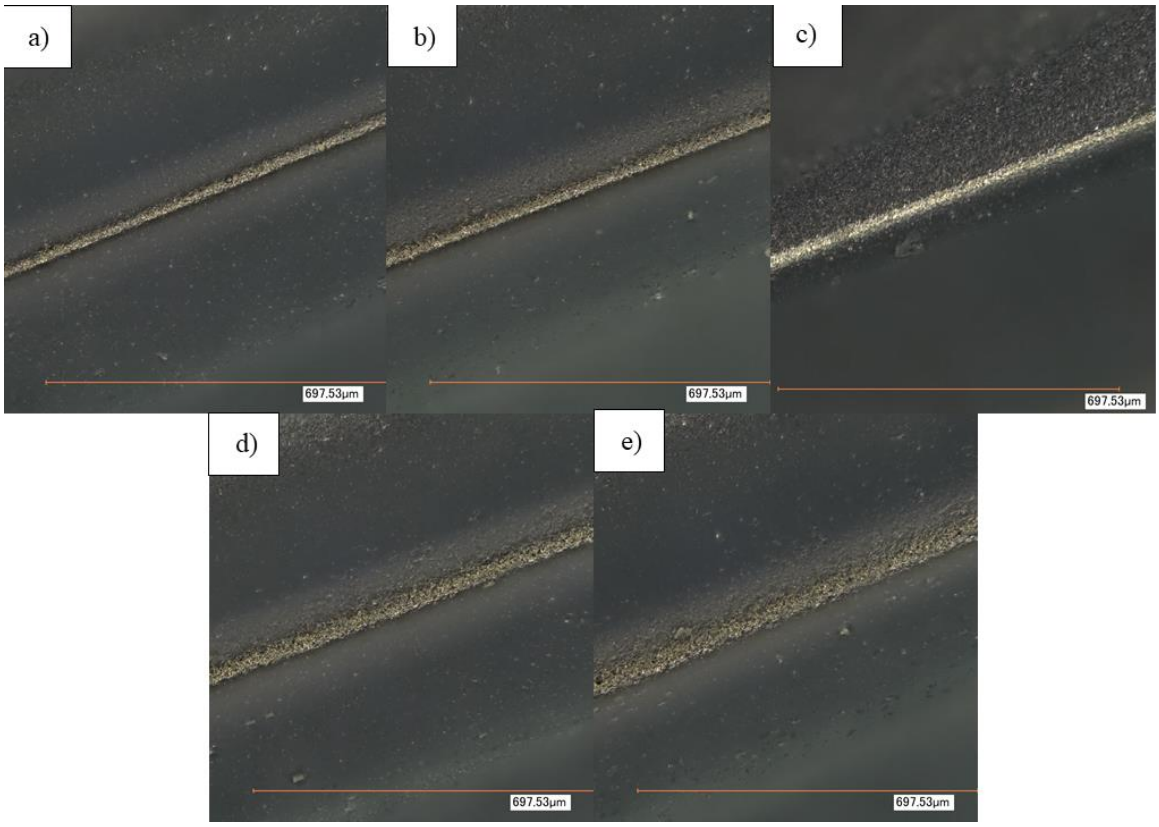

Figure 4-2: Images of the edge radii: a) 25 µm b) 30 µm c) 35 µm d) 40 µm e) 45 µm

Table 4-1: Dimensions of the cutting insert

Parameter	Value
Insert Width (W1)	6.8 mm
Cutting Edge Effective Length (LE)	10 mm
Corner Radius (RE)	0.4 mm
Wiper Edge Length (BS)	0.9 mm
Insert Thickness (S)	3.59 mm

4.2 Design of Experiment

The selection of proper cutting parameters is necessary for the experiments to yield useful results. The tool to be used for the experiments was previously decided, with the only variable relating to the tool is the different edge radii of the cutting inserts. The remaining aspects of the experiments to be determined was the workpiece material that will be used, and the cutting conditions for each test.

It was decided that a hardened steel would be the material type for the workpiece. Hardened steels are more likely to instigate cracking or chipping as the failure mode in cutting tools instead of failure due to wear, which was desirable for this project [34]. When deciding exactly what type of steel should be used, AISI 4340 alloy steel was chosen. The workpieces were hardened to 47±1 HRC. Other difficult-to-cut materials, such as titanium alloys, were briefly considered, however cost was a large inhibiting factor, as several pieces would be required. Another large consideration made was the availability of Johnson-Cook material parameters. Since one of the benefits of the mathematical model is the inclusion of the Johnson-Cook material parameters, a material with its parameters available in the literature is required. For this case, it is possible to find the J-C parameters for AISI 4340 hardened alloy steel

thanks to the work published by Ng et al. [30]. These parameters are listed in the mathematical model section of this thesis.

With the tool and workpiece material chosen, all that remains is the cutting conditions that will be used. It was determined earlier that half-immersion down milling will result in the highest instantaneous chip load, which corresponds to a large, sudden force acting on the tool as it engages the workpiece. This impact increases the likelihood of cracking and chipping in the cutting inserts. The parameters left to determine are the cutting speed, feed rate, and axial depth of cut.

The axial depth of cut was set constant at 1 mm. This was done for multiple reasons. First, the nose radius of the cutting inserts is 0.4 mm, so having a depth of cut larger than that value will allow more of the cutting edge to engage the cut. An illustration of this is shown in Figure 4-3. Second, a 1 mm axial depth of cut allows many cuts to be made on the same piece, resulting in less waste generated. Lastly, axial depth of cut is a major factor in determining the stability of the milling process. If this value is too high, then undesirable vibrations and/or chatter can occur, resulting in inaccurate force data and possible damage to the cutting tool and workpiece.

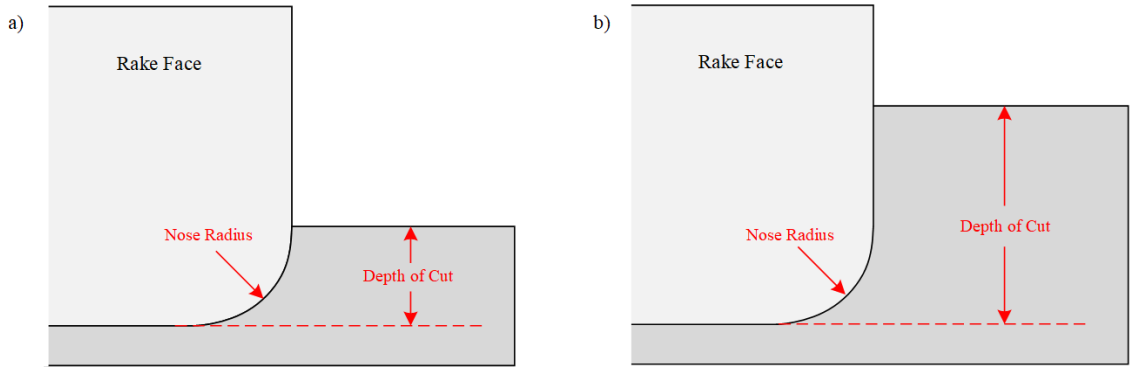

Figure 4-3: Depth of cut a) matching nose radius and b) exceeding nose radius

The final parameters to determine are the cutting speeds and feed rates to use for the experiments. The manufacturer included a set of recommended cutting parameters to maximize the tool's performance. The given recommended parameters are a cutting speed of 280 $\frac{m}{min}$ and a feed rate of 890 $\frac{mm}{min}$. It must be noted that the recommended cutting parameters provided by the manufacturer aims for longest tool life while yielding an industrially acceptable metal removal rate. However, these experiments are interested in a set of cutting conditions that will favour failure, so the recommended parameters became a basis for a series of "dry runs" to determine the best parameters for the purpose of this project. Increasing and decreasing the cutting speed and feed rate independently and investigating the condition of the tool is how the final experimental parameters were determined. By increasing the cutting speed, the tool would wear out faster due to higher temperatures, and would fail due to wear before any cracking occurs, while decreasing it would slow the wear drastically. It was found that a combination of increasing the feed rate and decreasing the cutting speed past the recommended levels increases the chip load acting on the inserts. The very lower limit of these parameters is chosen to be a cutting speed of 75 $\frac{m}{min}$ and a feed rate of 1000 $\frac{mm}{min}$. If the chip load is further increased, the insert tended to fail instantly. After many trials, the final combinations were decided with three different cutting speeds and two feed rates. These parameters can be found in Table 4-2. The results are reported using the shorthand Test 1, Test 2, etc. to refer to the corresponding combination. Table 4-3 summarizes the tool features and cutting conditions that are being kept constant throughout all tests.

Table 4-2: Finalized cutting condition combinations

Test No.	Cutting Speed ($\frac{m}{min}$)	Feed Rate ($\frac{mm}{min}$)
1	125	800
2	100	800
3	75	800
4	125	1000
5	100	1000
6	75	1000

Table 4-3: Constant values across all tests

Parameter	Value
Rake Angle (γ)	5°
Axial Depth of Cut (t_1)	1 mm
Entry Angle, Down Milling (θ_{start})	90°
Exit Angle, Down Milling (θ_{exit})	180°
Number of Cutting Edges (N)	2
Tool Diameter (N)	20 mm

4.3 Experimental Set-Up

All milling tests were performed using a HAAS VF-2YT milling machine. G-code was used to control the machine to ensure the cutting conditions were correct and repeatable. An image of the machine used can be seen in Figure 4-4.

Figure 4-4: Image of HAAS VF-2YT milling machine

The milling machine alone cannot capture the cutting forces produced during a machining operation. A Kistler dynamometer was mounted to the work table of the milling machine for this purpose. This dynamometer is capable of measuring the forces acting on the workpiece in the three triaxial directions at very high rates. For these experiments, a sampling rate of 7000 Hz is chosen. An image of the dynamometer and workpiece in the machine can be seen in Figure 4-5.

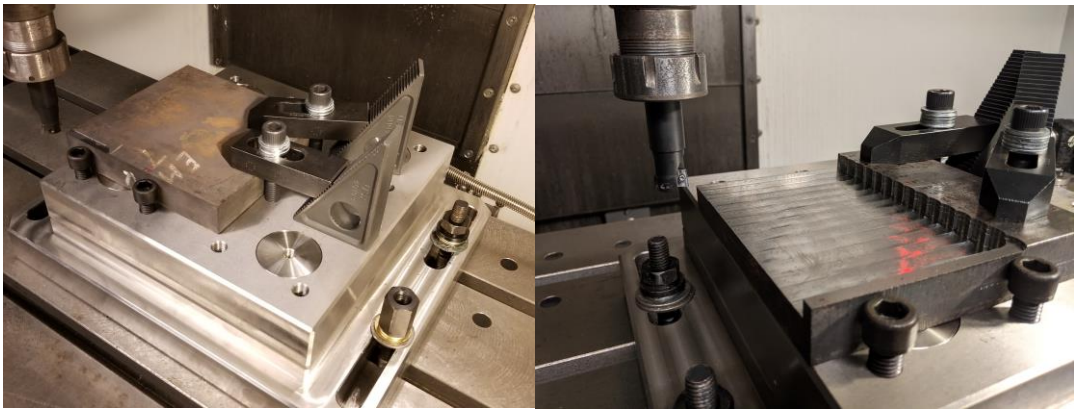

Figure 4-5: Images of Kistler dynamometer and workpiece mounted

The dynamometer uses internal piezoelectric sensors in order to convert applied forces into pulses of electric charge. However, these charges are too small to be recorded by a typical computer, so three charge amplifiers are used to increase the magnitude of the charges by a known amount. These larger charges are then received by a National Instruments Data Acquisition Card USB-9350, which is compatible with a PC. LabView is used to gather this data, tabulate it, and plot the charge values related to the three triaxial forces with respect to time. The tables are then exported to readable Excel spreadsheets.

This recording process must be started manually in LabView, and should coincide with the execution of the G-code at the milling machine to minimize the number of excess data points recorded. Due to the high data capture rate, it is possible for LabView to crash if the number of data points becomes too large, resulting in a potential loss of data for the current experiment.

After an experiment is recorded, the result is a large Excel spreadsheet which pairs the charge corresponding to a force paired with the time it was recorded. The recorded charge values must be converted into a force value in order to compare the experimental results with the mathematical model. This is done with Equation (32),

$$Force = \frac{A * B}{C} * Voltage \tag{32}$$

where A is the first charge amplifier internal conversion ($\frac{pC}{MU}$), B is the second charge amplifier internal conversion ($\frac{MU}{V}$), and C is the calibration constant of the dynamometer ($\frac{pC}{N}$). The values used for these experiments are listed in

Table 4-4.

Table 4-4: Parameters used for charge-to-force conversion

Parameter	Value	Unit
A	8.04	$\frac{pC}{MU}$
B	200	$\frac{MU}{V}$
C	3.885	$\frac{pC}{N}$

Chapter 5. Results and Discussion

In this chapter, the results of the milling tests are reported. In each test, the three triaxial force components were captured and recorded during down milling, using the cutting conditions corresponding to the test number, as presented in Chapter 4. These components acting together comprise the resultant force acting on the cutting tool. These forces are compared to the predicted forces that are generated by the mathematical model presented in Chapter 3, for the same cutting conditions. Following the results of the experiments, all patterns and behaviours that emerge from the cutting force data, as well as observations from the tests themselves, are discussed. It is in this chapter that the effects of the cutting tool's edge radius can be directly seen on various aspects of the milling tool's performance.

5.1 Cutting Force Results

In order to validate the forces that are predicted by the mathematical model presented in this thesis, milling tests needed to be performed and the forces acting on the tool needed to be captured and recorded. These measured forces indicate what is happening in reality when down milling of hardened steel is performed, which provides expectations for the values generated by the model. By plotting the measured forces and the calculated forces together in the same relative position of the tool during the cut, the accuracy of the model can be determined. For down milling, the start of the cut begins at 0°, and the tool is engaged with the workpiece for a period of 90°. After this, the tool is not engaged with the workpiece, and thus not cutting, until the next cutting edge engages with the workpiece at the position of

180°, and then the cycle repeats. One complete tool revolution is plotted for each test. It is important to note that the mathematical model does not account for the effects of wear of the tool, so for validation purposes, the measured forces are examined from runs that happened at the beginning of the cutting tests. Three triaxial forces (F_x, F_y, and F_z) are measured by the dynamometer, so at each point, the combination of the three components result in the total force acting on the tool. In order to get the resultant force from the experimental data, equation (5-1) is used.

$$F_{resultant} = \sqrt{F_x^2 + F_y^2 + F_z^2} \tag{5-1}$$

This resultant force obtained from the experiment is plotted against the resultant force R calculated by the mathematical model. It was previously stated that there are six different cutting conditions that were used. The chip loads experienced by the cutting insert for each cutting condition are listed in Table 5-1. These test conditions, combined with the five tool edge radii, resulted in a total of 30 tests that needed to be conducted. The force comparisons for Test 6 are shown in this chapter, in Figure 5-1 to Figure 5-5. Test 6 was chosen because these cutting conditions result in the highest chip load. The complete set of force comparison graphs for all cutting conditions can be found in the Appendix A1.

Table 5-1: Milling test cutting conditions

Test No.	**Cutting Speed ($\frac{m}{min}$)**	**Feed Rate ($\frac{mm}{min}$)**	**Chip Load**
1	125	800	0.201
2	100	800	0.251
3	75	800	0.335
4	125	1000	0.252
5	100	1000	0.314
6	75	1000	0.419

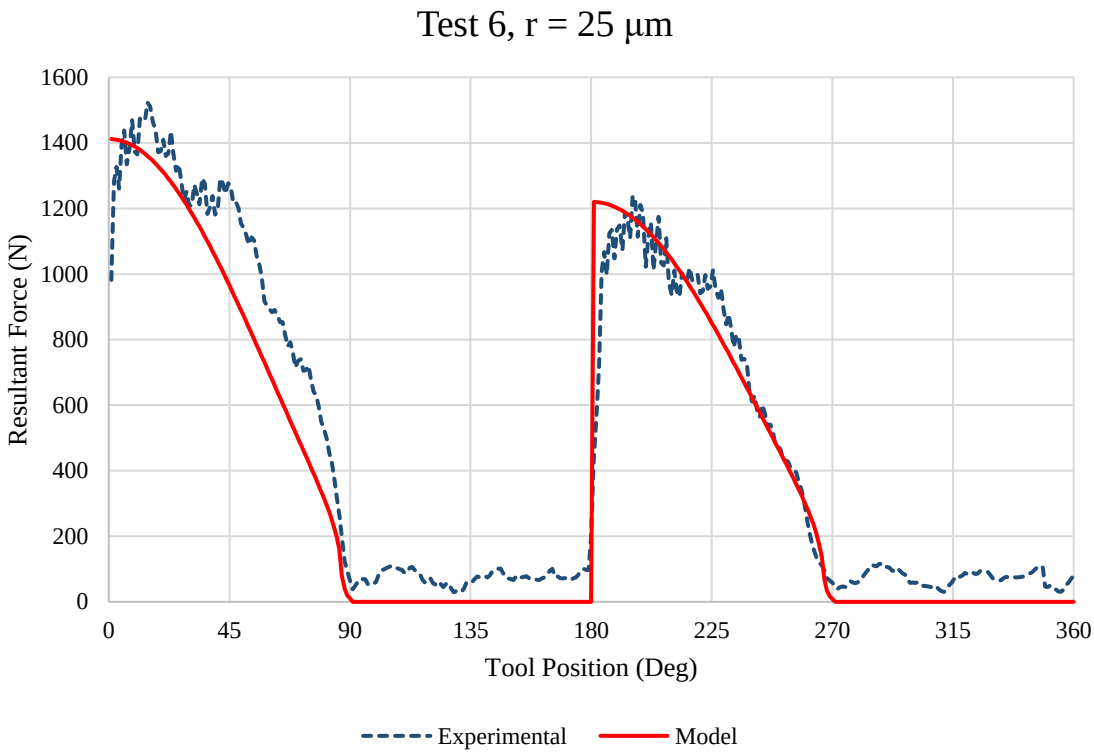

Figure 5-1: Force comparison for Test 6, r = 25 µm

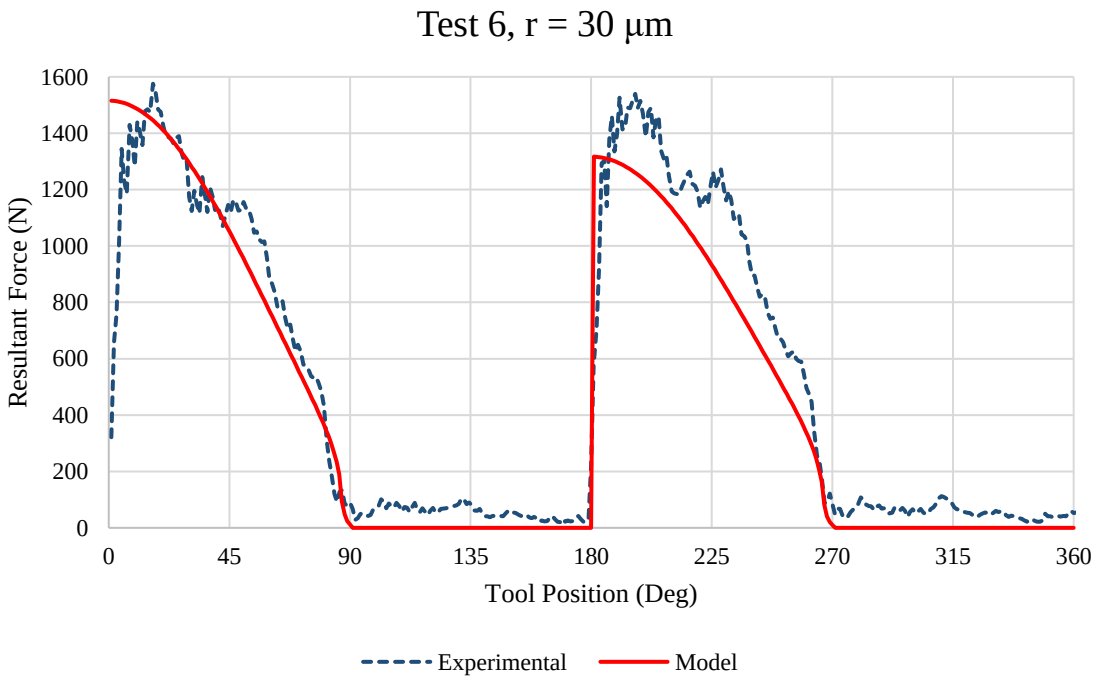

Figure 5-2: Force comparison for Test 6, r = 30 µm

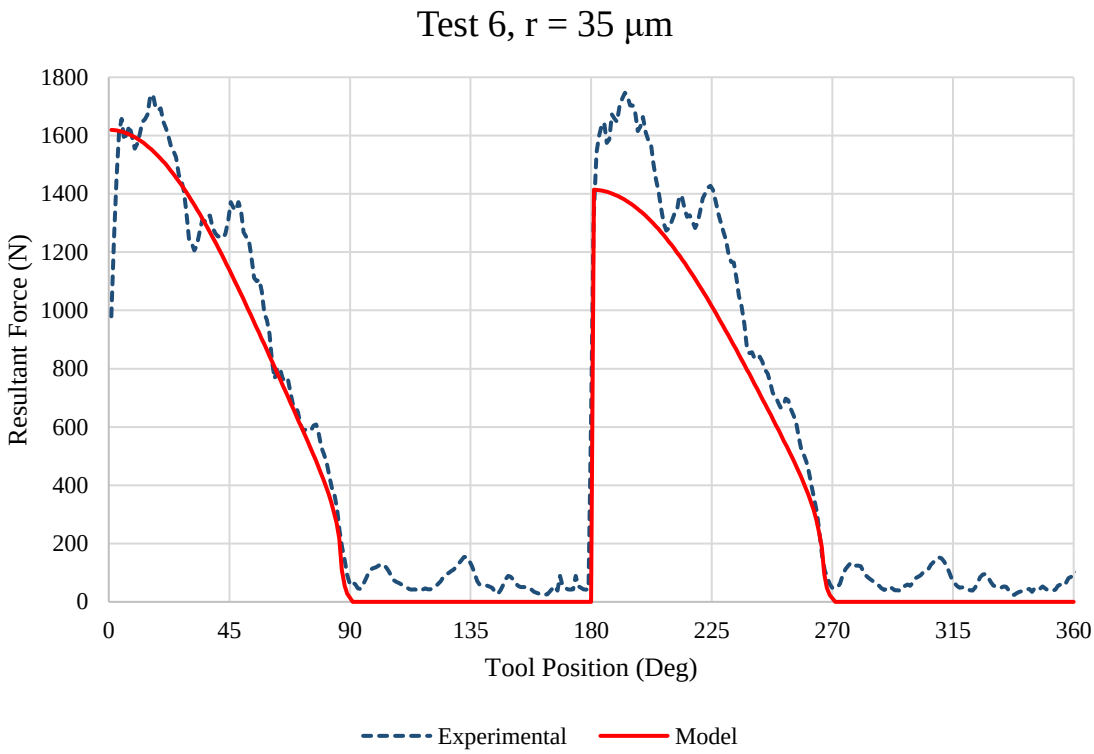

Figure 5-3: Force comparison for Test 6, r = 35 µm

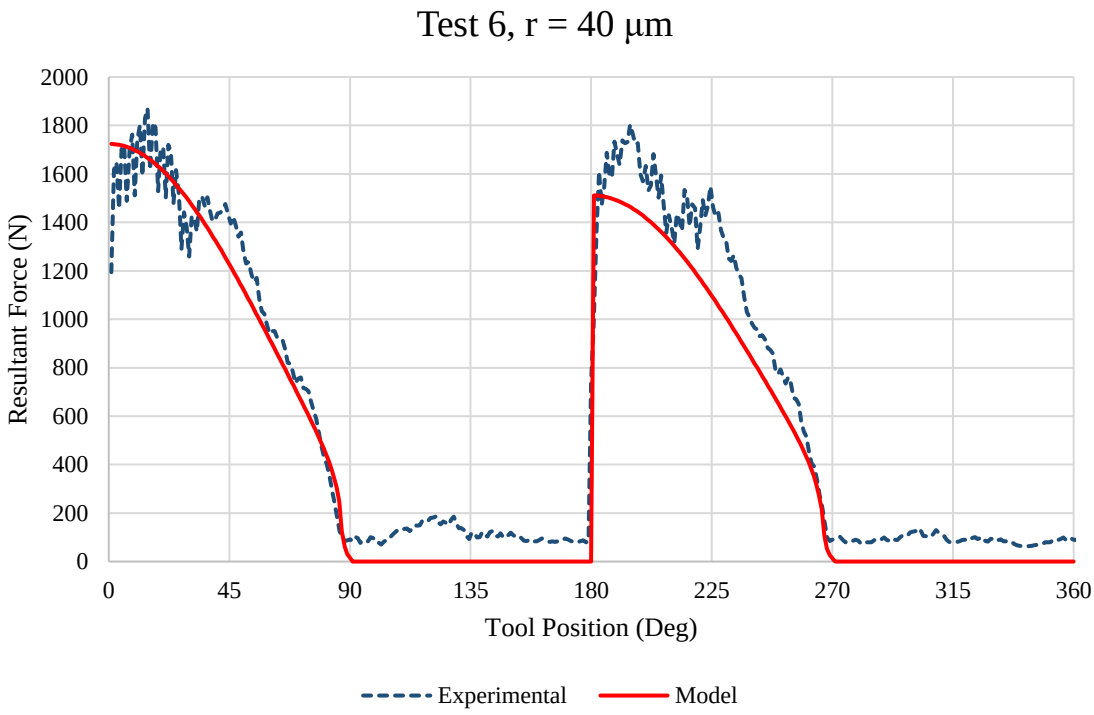

Figure 5-4: Force comparison for Test 6, r = 40 µm

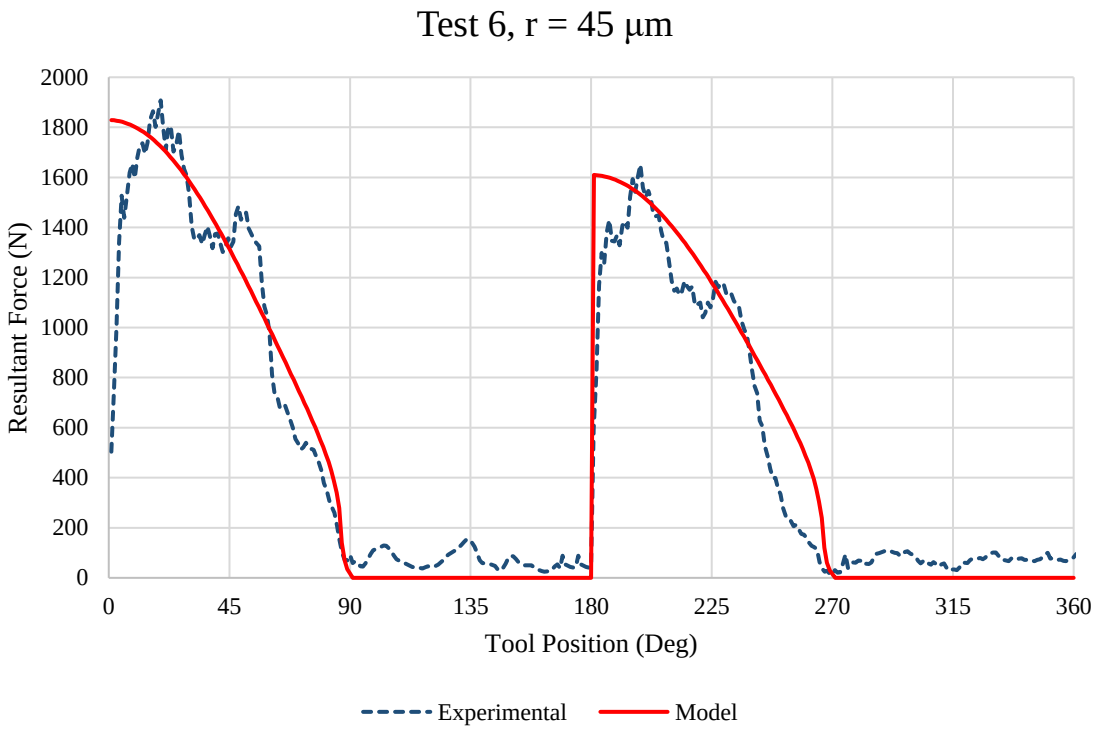

Figure 5-5: Force comparison for Test 6, r = 45 µm

For every run, numerous revolutions are recorded during the stable cutting portion of the test. In order to properly visualize the data, a section of each test was examined, and one revolution is taken for plotting. The milling tool has two cutting edges, so per one revolution, the tool engages with the workpiece twice. In each graph, these engagements are seen between 0°-90° for the roughing edge, and 180°-270° for the finishing edge. The rest of the graph shows the positions where no cutting edge is engaged. The model shows these areas as having no force whatsoever, while the experimental forces show a non-zero value for each of these positions. This is due to the movement of the milling machine table being detected by the dynamometer, which had to be set to a high sensitivity in order to capture a high number of samples for each test. The most important areas of the graphs are the large jumps in the force

magnitude that occurs at 0° and 180°. This area is the time when the edge experiences impact against the workpiece, before the workpiece material begins to yield and cutting occurs. After this, the magnitude of the forces trend downward as the tool rotates and approached the disengagement points at 90° and 270°.

In general, good agreement is seen between the experimental force acting on the tool and the force predicted by the mathematical model. As previously stated, the most important force values are those that are measured and predicted at the moment the cutting tool impacted the workpiece. The percentage difference between the measured force and the predicted force at the peak of the roughing edge impact can be seen in Table 5-2.

Table 5-2: Force value differences

Edge Radius (μm)	**Force Value Difference (%)**
25	14.1
30	11.2
35	14.9
40	13.5
45	10.7

Good agreement between these values is important when examining the impact that the tool experiences as it contacts the workpiece. The best agreement happens during the test with the 25 μm inserts. By having the ability to predict these forces within an acceptable margin of error, it is possible to analyze the impact and predict its effects on the cutting tool without the need for gathering experimental data. This model can accept several inputs, including the workpiece material's Johnson-Cook parameters, cutting conditions, and tool geometry, including the edge radius, and predict the magnitude of the force acting on the cutting tool during milling.

It can also be seen that the model is capable of predicting the force acting on the roughing edge and finishing edge of the tool separately. The roughing edge is expected to experience a larger load compared to the finishing edge, since a larger amount of material is being removed by the roughing edge. This larger load is reflected in both the measured and predicted forces, however the severity of this difference is not consistent in all tests. Good agreement in this regard is seen in the 25 μm and the 45 μm inserts, while the other tests show the difference between the two edges is smaller in the measured forces. These differences in the measured forces can be attributed to a changing chip load acting on the cutting edges. A changing chip load is likely due to vibrations that are acting on the tool. During the dry runs at the beginning of the experimentation design phase, it was ensured that the chosen cutting conditions would not result in chatter, which would be detrimental to the results of the experiments. However, some vibration in milling will always be present. Since this particular cutting tool has two cutting edges, and the cutting tests are performing half-immersion down milling, only one cutting edge is in contact with the workpiece at the time. This can cause some larger vibrations to be detected, when compared to tools with more cutting edges. A filtering algorithm was applied to the measured data to eliminate most of the noise in the signal, but larger vibrations could not be removed without altering the meaning of the results.

In the previous figures, one rotation of the tool is modelled, and then compared to one rotation of measured force data taken from the respective cutting test. Milling is a complex machining process, so every revolution, and the corresponding measured forces, will not be perfectly identical to the previous one. It would not be feasible to

plot the hundreds of revolutions that the tool undergoes for a single cutting test, but it would be helpful to see how the model compares to an entire test's worth of data. In order to illustrate this, the average peak force of the tests is plotted. This value is determined by finding the peak force reading for each revolution, and finding the average of this set of values. The values are compared to the model, for every test and for each tool geometry. These plots can be seen from Figure 5-6 to Figure 5-11.

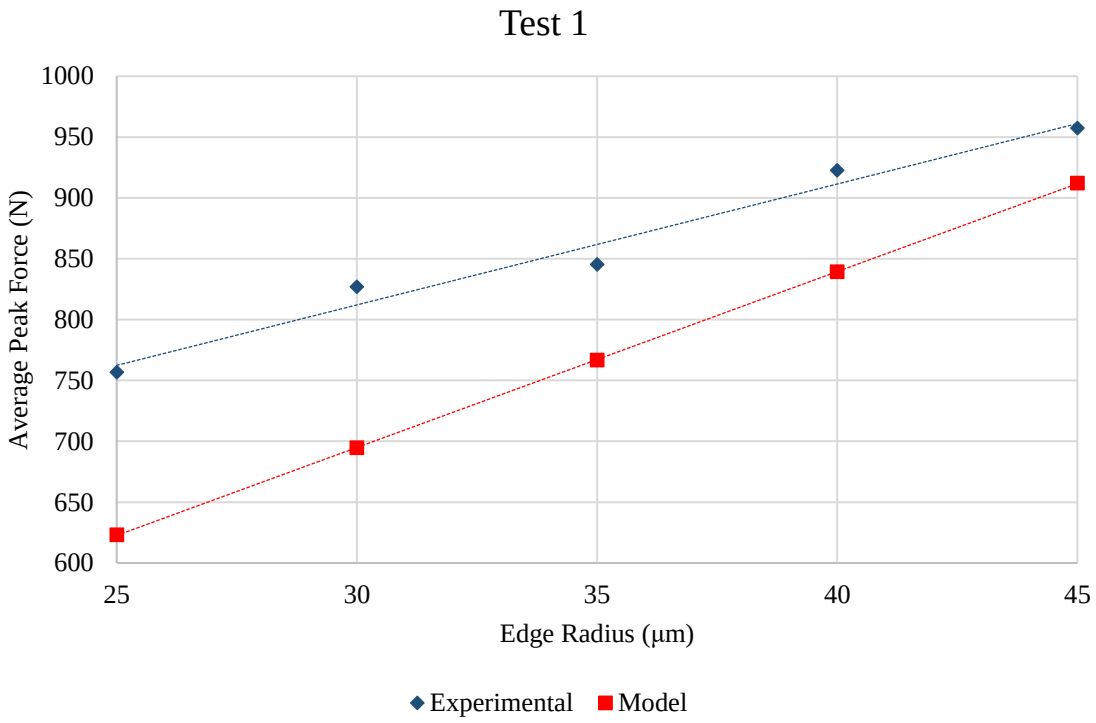

Figure 5-6: Average peak resultant force for Test 1, for all edge radii

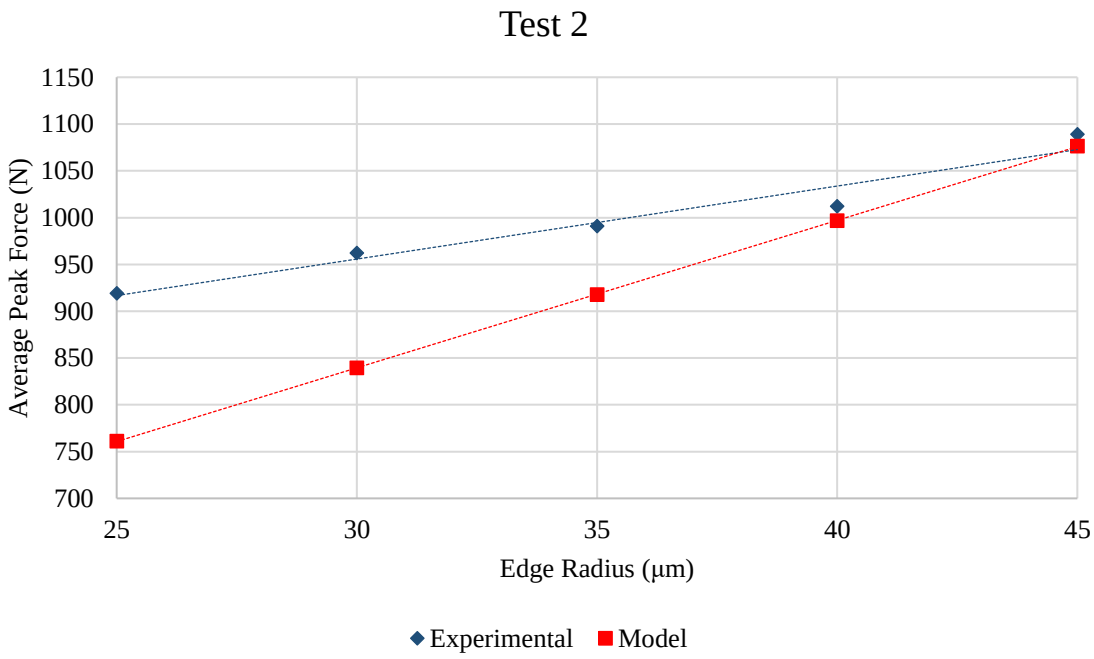

Figure 5-7: Average peak resultant force for Test 2, for all edge radii

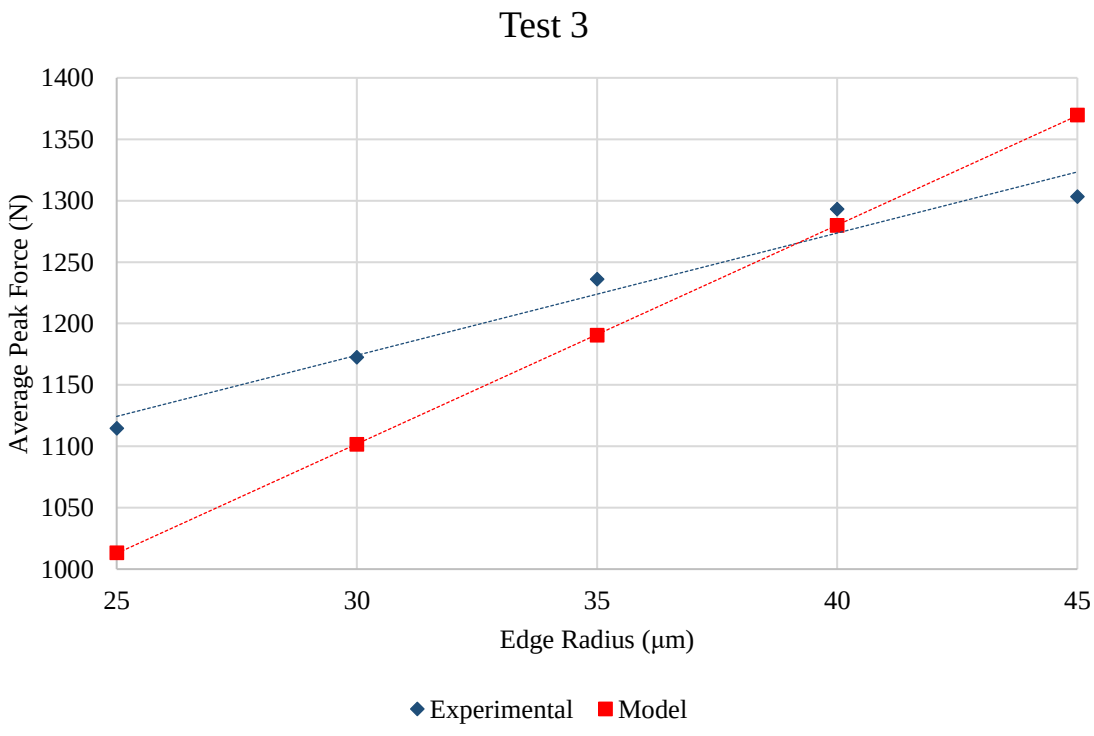

Figure 5-8: Average peak resultant force for Test 3, for all edge radii

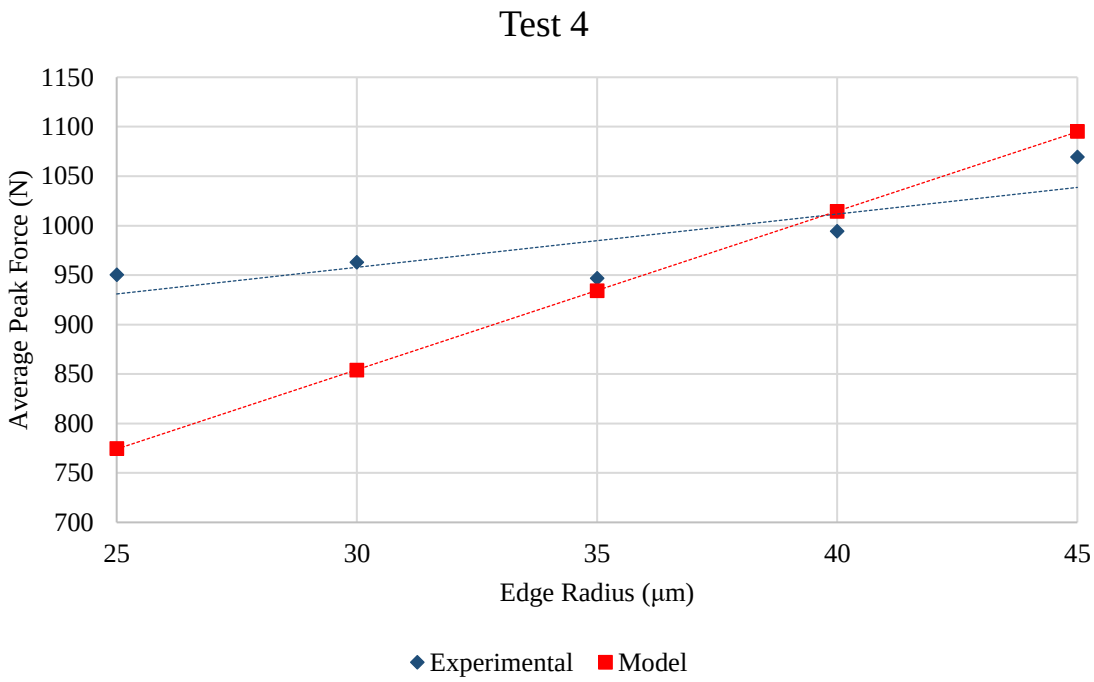

Figure 5-9: Average peak resultant force for Test 4, for all edge radii

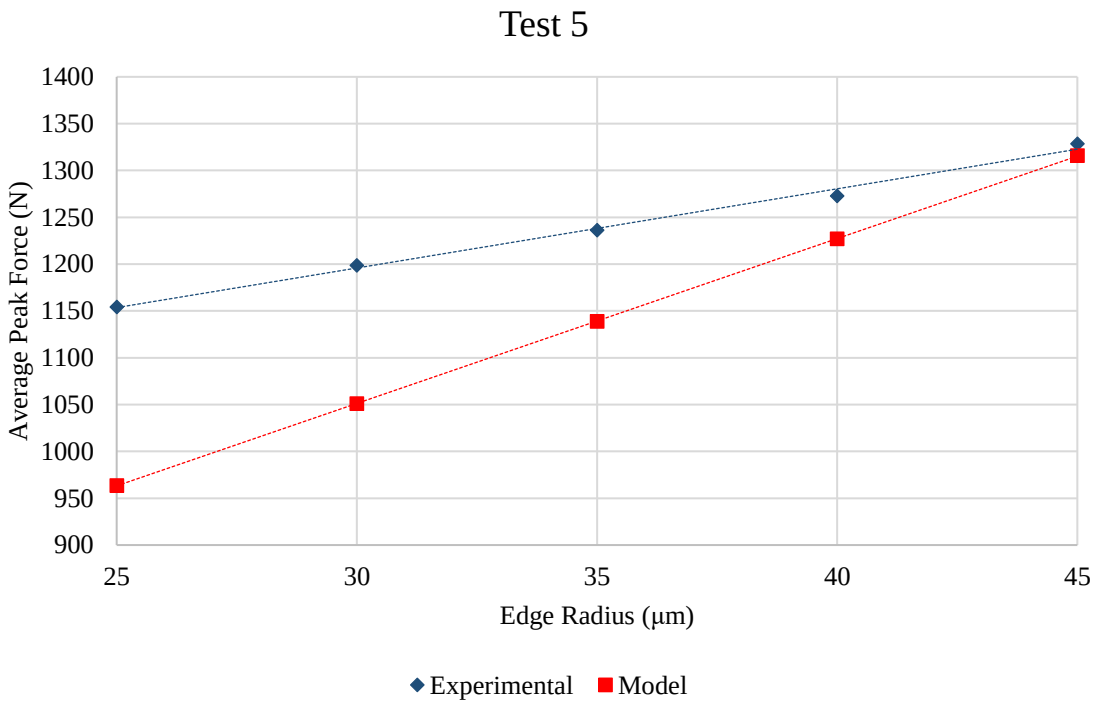

Figure 5-10: Average peak resultant force for Test 5, for all edge radii

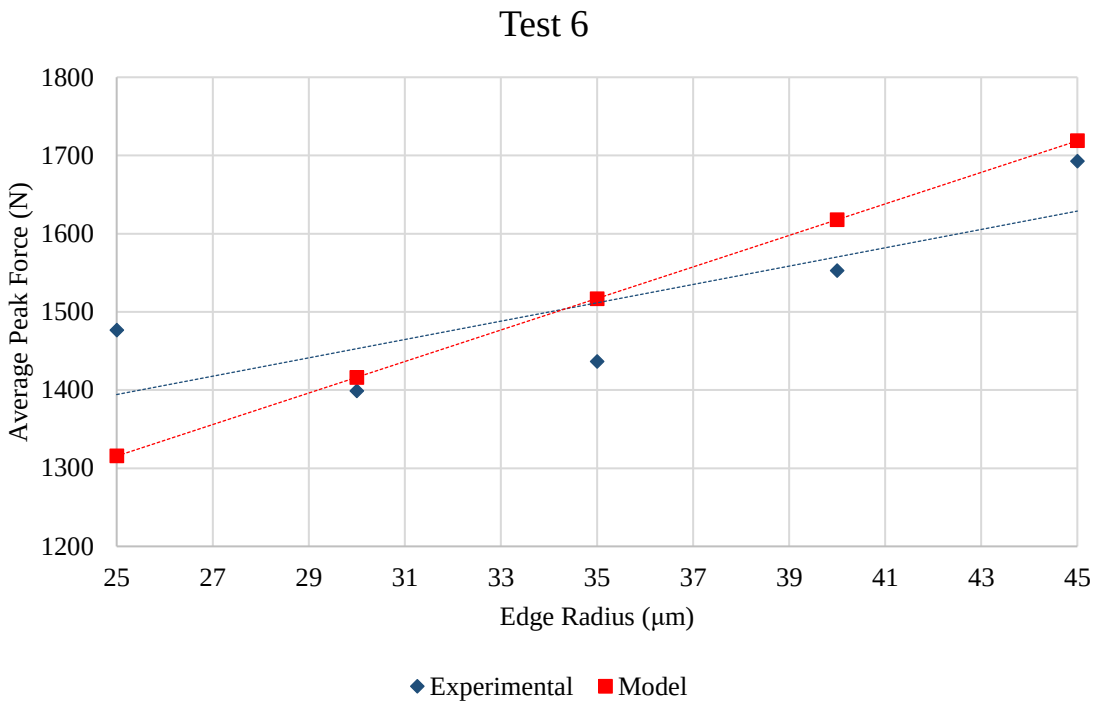

Figure 5-11: Average peak resultant force for Test 6, for all edge radii

It is immediately obvious that the average peak force from the experimental data closely approximates a linear increase that corresponds with an increase in the tool's edge radius. The greatest differences that are seen between the model and the experimental forces occur when the 25 μm tools are used. This behaviour can be seen in all six tests. When comparing the trendlines of the experimental and model forces, every test shows that the model's trendline has a slightly steeper slope. Test 1 shows the smallest difference in slope between the two trendlines, while Test 5 shows the largest difference. Overall, the plots of the average peak force for these tests show that the model detailed in this thesis is able to capture the effects of the tool's edge radius. It is worth mentioning that the inserts with a 25 μm edge radius were unable to withstand the forces generated by Tests 3, 4, 5, and 6, which is further detailed in

the next section of this chapter. In Tests 3 and 6 especially, very few runs could be completed using the 25 μm inserts, as they would fail very quickly when compared to the other edge geometries. Therefore, there was less experimental data available for these particular runs compared to the others where the tools did not fail.

In Tests 3, 4, and 6, the trendlines for the model's forces intersect with the trendlines for the experimental data. The earliest intersection occurs in Test 6, since the intersection occurs around the 35 μm mark. This test has the largest chip load of all the tests, so it was known that the forces would be higher, and tools would be the most likely to fail under these conditions. These predictions were based on the information found during the literature review portion of this thesis and observed behaviour from the dry runs conducted during the experimental design phase. This is why the agreement between the model and the experimental forces for this test shows the success of the model. By examining the plot in Figure 5-11, it can be seen that the tests conducted with the 25 μm and 35 μm inserts experiences the greatest disparity between the experimental forces and the predicted forces. Another interesting behaviour is that the 35 μm tools exhibited a noticeably lower average peak force than the trendlines predicted. This behaviour is observed in Tests 1, 4, and 6. This shows that the tools with an edge radius of 35 μm consistently improves the ability of the insert to cut the workpiece material, while other geometries do not perform as well. This trend, combined with the wear and failure performance of this tool discussed in the next section, is likely the reason that this edge geometry is chosen for commercially available inserts.

The model predicts that the average peak forces acting on the tool will increase proportionally as the edge radius of the tool increases. A perfectly linear relationship is not representative of reality, as the experimental data shows that variation can occur between different tests. The model predicts this type of behaviour due to the numerous assumptions needed to fully define it. The model also does not account for inconsistencies that are common in milling processes, such as vibrations or localized changes in the workpiece's mechanical properties, such as hardness. A more complex model that can accommodate these parameters will likely decrease the difference between the measured experimental forces and the forces predicted by said model.

It is also seen that the model usually predicts a lower average peak force when compared to the experimental data. This is due to several factors, in both the mathematical model and the experimental data. First, the model works on the assumption that the parameters ϕ, C_0, and ζ will be determined such that the cutting force acting on the tool is minimized. While this assumption does allow the model to be solved, real material will not always behave in this manner, and so the forces would be higher in those cases. Another reason for the model predicting a lower average force can be seen by examining the force comparisons for a single revolution. In many cases, the model predicts significantly lower forces acting on the finishing edge of the tool, while experiments show that certain cases have similar forces on both cutting edges. Since the model will always predict lower forces on the finishing edge, and the experiments do not always capture that effect, it is logical that the average peak force predicted by the model will be lower than the value determined via experiments.

5.2 Tool Performance

As the milling tests are performed, the inserts will experience propagation of wear, which affects their performance. As mentioned earlier in this thesis, a tool that has wear will not typically perform as well as a brand-new tool. A worn tool will generate different cutting forces, cause changes in the temperature at the tool-workpiece interface, and become more prone to fracture. For each cutting test, the behaviour of wear propagation on the cutting insert was tracked. Every cutting test was divided into a series of passes across the workpiece, referred to as “runs”. After five runs, the machine was stopped, the inserts were removed from the tool holder, and the flank wear was measured using a microscope and recorded. Flank wear was measured because it was the dominant form of wear present on the inserts, and has a more direct effect of the cutting edge microgeometry. Crater wear was never observed to be significant in any of the tests, as the cutting speed was set lower than the manufacturer’s recommended conditions. Each set began with Test 6, as this combination of cutting conditions is the most likely to fail due to chipping. Once the tool fails, the number of runs that resulted in that failure is used as the maximum number of runs for the remainder of tests in that set. This was done to prevent any single test from taking too much time, as the amount of time to complete all the experiments was limited. The wear behaviour for each edge radius is plotted for each test. These plots can be seen in Figure 5-12 to Figure 5-17.

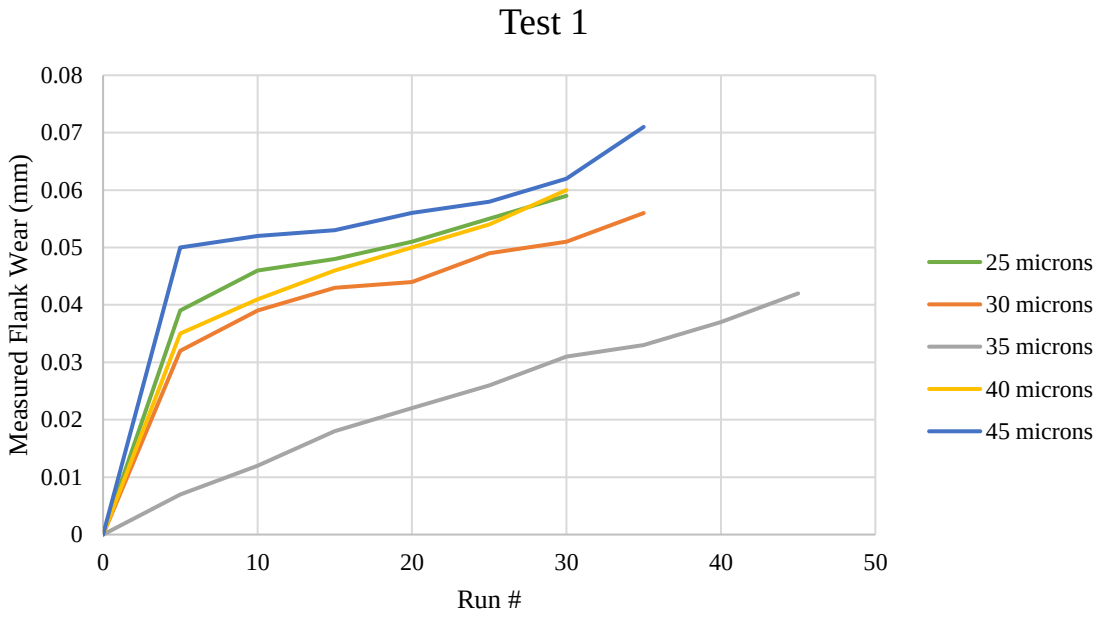

Figure 5-12: Wear propagation for all tool geometries during Test 1

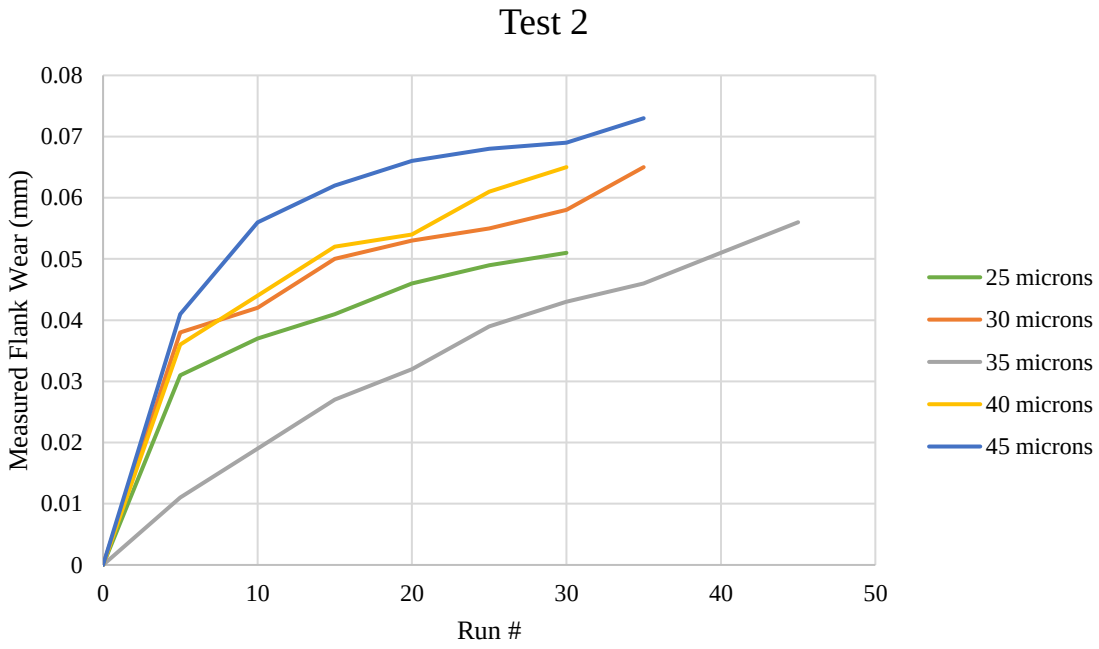

Figure 5-13: Wear propagation for all tool geometries during Test 2

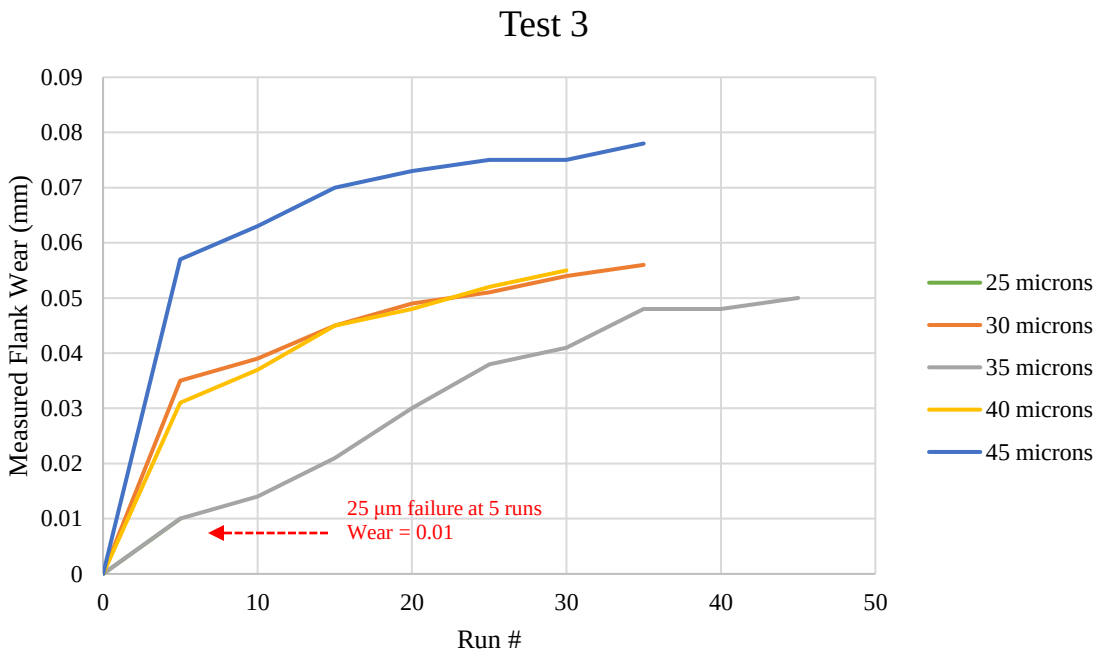

Figure 5-14: Wear propagation for all tool geometries during Test 3

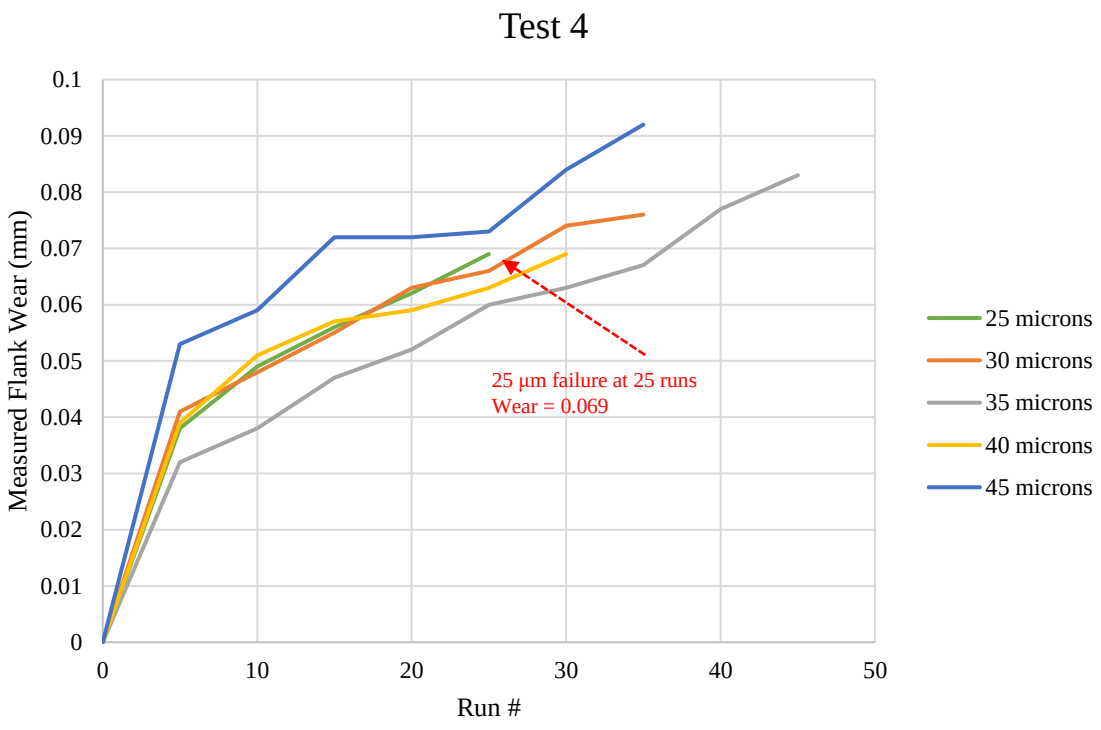

Figure 5-15: Wear propagation for all tool geometries during Test 4

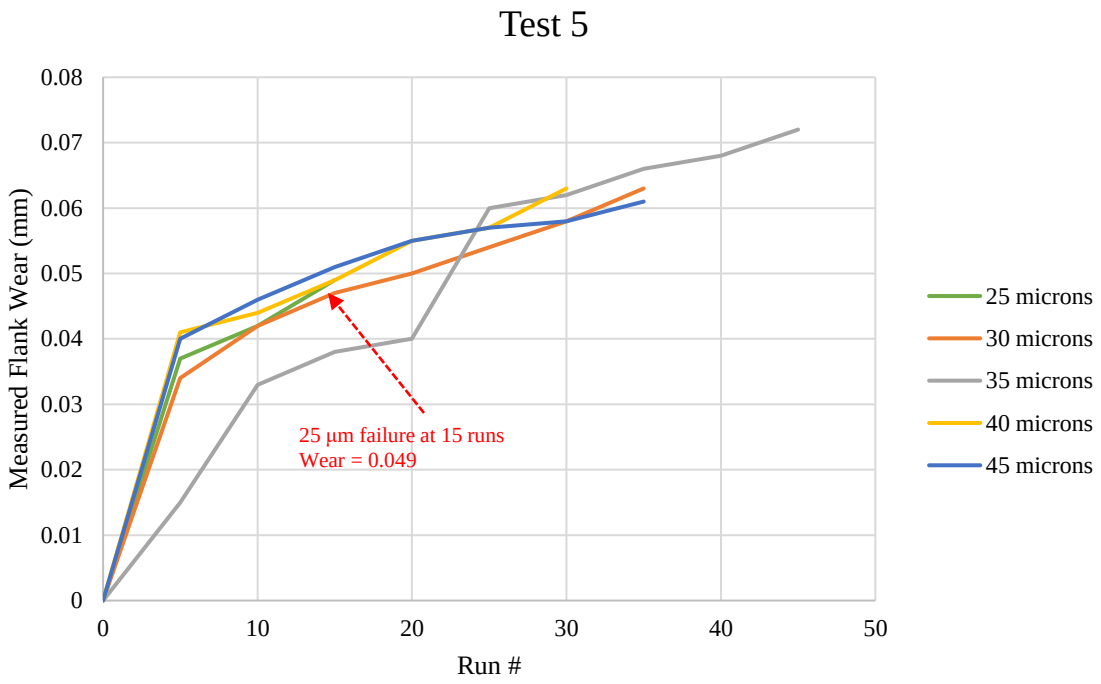

Figure 5-16: Wear propagation for all tool geometries during Test 5

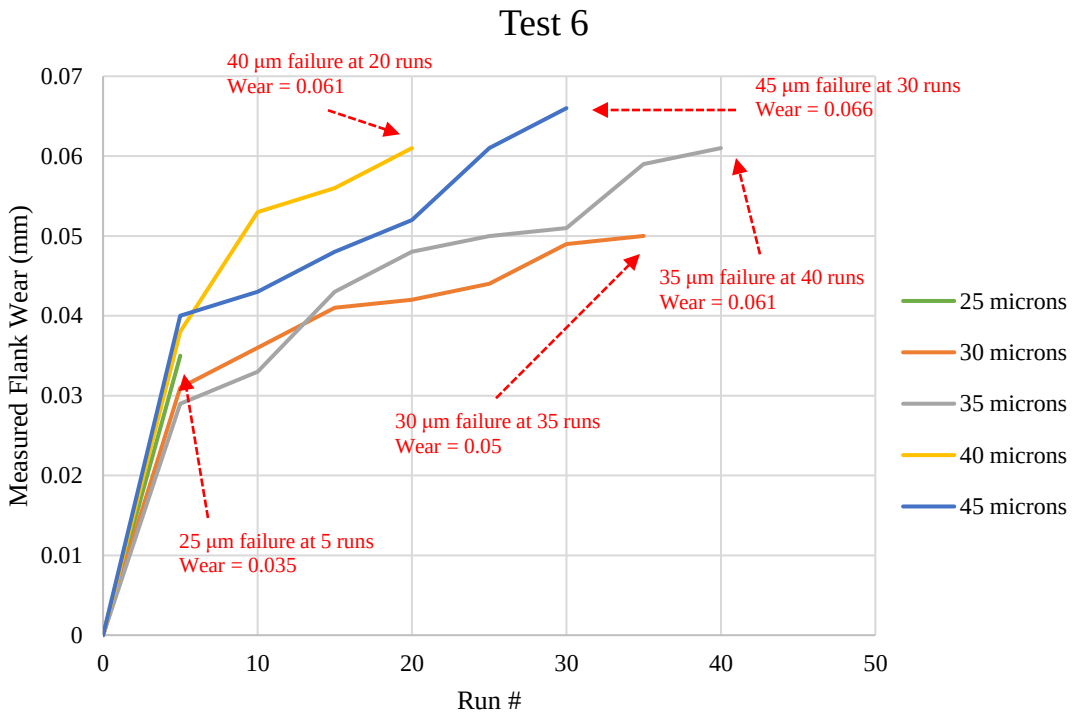

Figure 5-17: Wear propagation for all tool geometries during Test 6

A noticeable pattern that has emerged when examining the wear behaviour of all geometries across all tests in that the rate of wear propagation between sets of runs does not significantly change in most cases. Aside from the initial spike from a brand-new cutting edge to the first wear reading, the rates of wear propagation are similar. What does change between the tests is the total amount of wear that is measured at each point. In Tests 1-5, the inserts with an edge radius of 35 μm experienced the least amount of total wear over time. This can be extrapolated to show that these inserts would have the longest usable tool life before failure due to wear occurs. This pattern, in conjunction with the relatively low cutting forces that have been measured in the same tests, show experimentally why this tool geometry is the best choice for general use in machining. The only exception to this pattern occurred in Test 6, where the 30 μm showed a slower rate of wear compared to the 35 μm tool.

The inserts with an edge radius of 45 μm experienced the highest level of wear in all tests with the exception of Test 5. This corresponds with the trend of higher cutting forces acting on these tools. As the edge radius increases, the ability of the chip to flow over the rake face of the cutting tool is negatively affected, as the stagnation point changes. More material is compressed to form the newly generated surface left behind by the cutting tool compared to tools with a sharper edge radius. The total amount of wear that every tool in these tests experiences is low, as a typical cutting insert is considered failed when the measured flank wear reaches 0.3 mm. However, these tests were purposefully designed to not replicate typical tool usage. These tests were conducted to increase the chance of failure by chipping, using cutting speeds that are lower than the manufacturer's recommended value.

Regarding failure to due to chipping or catastrophic failure, the inserts with an edge radius of 25 μm failed the most often. In Tests 3, 5, and 6, the 25 μm inserts failed before 30 runs could be completed. In Tests 3 and 6 specifically, the tools would fail completely after very few runs, when compared to the other geometries. These tests were repeated to ensure these failures were repeatable, and not a random failure. It was expected that the tools with smaller edge radii would be more prone to failure due to chipping, as the sharper edge corresponds to less material in the inserts to absorb the repetitive impacts that occur during milling. It should also be noted that in every test, it was the insert loaded into the roughing edge of the tool holder that would chip, in the event that only insert chipped. In Tests 3 and 6 for the 25 μm inserts, both the roughing and finishing inserts would chip during the same run.

5.3 Conclusions

In this section, the work accomplished by this thesis is summarized. The project began by identifying a gap in the literature regarding milling tools. Tool performance investigations regarding the ability of a tool to resist impacts are far less common than those studying end-of-life due to wear. It was decided that the impact resistance of milling tool inserts would be investigated in two parts: a mathematical model that could predict cutting forces while accounting for the cutting edge radius, and a series of milling tests to verify the model, as well as monitor tool failure. A vast majority of works assume a perfectly sharp tool for simplification purposes, but in reality, all cutting tools possess some form of edge preparation to improve the performance of the cutting tool. It was decided that by examining works related to Oxley's predictive machining theory [4, 5, 15] and the work of Manjunathiah and Endres [20], it would

be possible to combine aspects of their models to create a more comprehensive method of estimating the cutting forces acting on a milling tool.

A detailed explanation of the mathematical model was given, including a flowchart illustrating the logic used for the purpose of recreation by the reader. A series of six milling tests were designed to instigate tool failure due to chipping, and they were conducted using AISI 4340, hardened to 47±1 HRC, as the workpiece material. It was found that the predicted resultant forces had good agreement with the measured forces acting on the tool, in many cases. The inserts with an edge radius of 25 μm were unable to withstand the cutting conditions of the majority of tests, proving that geometry negatively affected the impact resistance of the tool. Inserts with an edge radius of 35 μm frequently showed the best wear behaviour, by having less flank wear when compared to the other geometries for the same cutting distance. This geometry also resulted in relatively low cutting forces, considering that the cutting tests were purposefully designed to be detrimental to the tool's performance. These factors are likely why this geometry is chosen by the tool manufacturers for commercially available cutting inserts. Ultimately, this thesis successfully investigated the cutting forces and the impact resistance of the five milling insert edge geometries that were provided.

REFERENCES

[1] M. E. Merchant, "Mechanics of the metal cutting process. I. Orthogonal cutting and a type 2 chip," *Journal of applied physics,* vol. 16, no. 5, pp. 267-275, 1945.

[2] M. E. Merchant, "Mechanics of the metal cutting process. II. Plasticity conditions in orthogonal cutting," *Journal of applied physics,* vol. 16, no. 6, pp. 318-324, 1945.

[3] H. Ernst, *Physics of metal cutting*. Cincinnati Milling Machine and Cincinnati Grinders, 1939.

[4] P. L. B. Oxley and M. C. Shaw, "Mechanics of machining: an analytical approach to assessing machinability," 1990.

[5] J. Arsecularatne and P. Mathew, "The Oxley modeling approach, its applications and future directions," *Machining Science and Technology,* vol. 4, no. 3, pp. 363-397, 2000.

[6] H. Young, P. Mathew, and P. Oxley, "Allowing for nose radius effects in predicting the chip flow direction and cutting forces in bar turning," *Proceedings of the Institution of Mechanical Engineers, Part C: Journal of Mechanical Engineering Science,* vol. 201, no. 3, pp. 213-226, 1987.

[7] H.-T. Young, P. Mathew, and P. Oxley, "Predicting cutting forces in face milling," *International Journal of Machine Tools and Manufacture,* vol. 34, no. 6, pp. 771-783, 1994.

[8] G. R. Johnson and W. H. Cook, "A constitutive model and data for metals subjected to large strains, high strain rates and high temperatures," in *Proceedings of the 7th International Symposium on Ballistics*, 1983, vol. 21, no. 1: The Netherlands, pp. 541-547.

[9] G. Yücesan and Y. Altintaş, "Improved modelling of cutting force coefficients in peripheral milling," *International journal of machine tools and manufacture,* vol. 34, no. 4, pp. 473-487, 1994.

[10] O. Gonzalo, J. Beristain, H. Jauregi, and C. Sanz, "A method for the identification of the specific force coefficients for mechanistic milling simulation," *International Journal of Machine Tools and Manufacture,* vol. 50, no. 9, pp. 765-774, 2010.

[11] H.-J. Fu, R. DeVor, and S. G. Kapoor, "A mechanistic model for the prediction of the force system in face milling operations," 1984.

[12] A. Hosseini, B. Moetakef-Imani, and H. Kishawy, "Mechanistic modelling for cutting with serrated end mills–a parametric representation approach," *Proceedings of the Institution of Mechanical Engineers, Part B: Journal of Engineering Manufacture,* vol. 225, no. 7, pp. 1019-1032, 2011.

[13] H. A. Kishawy, T. DesRoches, A. Hosseini, T. El-Wardany, and C. Guo, "Generic method to determine coefficients of mechanistic milling force model," *International Journal of Manufacturing Research,* vol. 8, no. 1, pp. 43-63, 2013.

[14] M. Kaymakci, Z. Kilic, and Y. Altintas, "Unified cutting force model for turning, boring, drilling and milling operations," *International Journal of Machine Tools and Manufacture,* vol. 54, pp. 34-45, 2012.

[15] D. Lalwani, N. Mehta, and P. Jain, "Extension of Oxley's predictive machining theory for Johnson and Cook flow stress model," *Journal of materials processing technology,* vol. 209, no. 12-13, pp. 5305-5312, 2009.

[16] P. L. B. Oxley, *The mechanics of machining: an analytical approach to assesing machinability*. Ellis Horwood, 1989.
[17] R. W. Ivester *et al.*, "Assessment of machining models: progress report," *Machining science and technology,* vol. 4, no. 3, pp. 511-538, 2000.
[18] Y. Altintas and S. Engin, "Generalized modeling of mechanics and dynamics of milling cutters," *CIRP Annals,* vol. 50, no. 1, pp. 25-30, 2001.
[19] L. Pang, A. Hosseini, H. Hussein, I. Deiab, and H. Kishawy, "Application of a new thick zone model to the cutting mechanics during end-milling," *International Journal of Mechanical Sciences,* vol. 96, pp. 91-100, 2015.
[20] J. Manjunathaiah and W. J. Endres, "A new model and analysis of orthogonal machining with an edge-radiused tool," *J. Manuf. Sci. Eng.,* vol. 122, no. 3, pp. 384-390, 2000.
[21] T. Özel, "Modeling of hard part machining: effect of insert edge preparation in CBN cutting tools," *Journal of materials processing technology,* vol. 141, no. 2, pp. 284-293, 2003.
[22] A. Pekelharing, "Cutting tool damage in interrupted cutting," *Wear,* vol. 62, no. 1, pp. 37-48, 1980.
[23] J. Zhou, M. Andersson, and J.-E. Ståhl, "Cutting tool fracture prediction and strength evaluation by stress identification, part I: stress model," *International Journal of Machine Tools and Manufacture,* vol. 37, no. 12, pp. 1691-1714, 1997.
[24] J. Zhou, M. Andersson, and J.-E. Ståhl, "Cutting Tool Fracture Prediction and Strength Evaluation by Stress Identification, Part II: Experimental Studies," *International Journal of Machine Tools & Manufacture,* 1997.
[25] C. Ma and Z. Wang, "Experimental and numerical investigation of the breakage of a cutting tool with ultrasonic vibration," *Precision Engineering,* vol. 51, pp. 393-402, 2018.
[26] K.-D. Bouzakis, M. Batsiolas, G. Skordaris, F. Stergioudi, and N. Michailidis, "Repetitive impact test near uncoated and coated cutting edges for assessing their fatigue behavior," *CIRP Journal of Manufacturing Science and Technology,* vol. 8, pp. 63-69, 2015.
[27] K.-D. Bouzakis *et al.*, "Coated tools' wear description in down and up milling based on the cutting edge entry impact duration," *CIRP annals,* vol. 61, no. 1, pp. 115-118, 2012.
[28] V. Songmene, I. Zaghbani, and G. Kientzy, "Machining and machinability of tool steels: Effects of lubrication and machining conditions on tool wear and tool life data," *Procedia CIRP,* vol. 77, pp. 505-508, 2018.
[29] C. K. Sagar, T. Kumar, A. Priyadarshini, and A. K. Gupta, "Prediction and optimization of machining forces using oxley's predictive theory and RSM approach during machining of WHAs," *Defence Technology,* 2019.
[30] E.-G. Ng, T. I. El-Wardany, M. Dumitrescu, and M. A. Elbestawi, "Physics-based simulation of high speed machining," *Machining science and technology,* vol. 6, no. 3, pp. 301-329, 2002.
[31] I. Kragelskii, "Friction and wear, 1965," ed: Butterworths, London.
[32] P. Basuray, B. Misra, and G. Lal, "Transition from ploughing to cutting during machining with blunt tools," *Wear,* vol. 43, no. 3, pp. 341-349, 1977.
[33] Sandvik-Coromant. "R390-020A20-11L." (accessed.

[34] H. A. Kishawy and A. Hosseini, "Machining difficult-to-cut materials," *Mater. Form. Mach. Tribol*, 2019.

Appendices

A1. Complete set of force comparison graphs

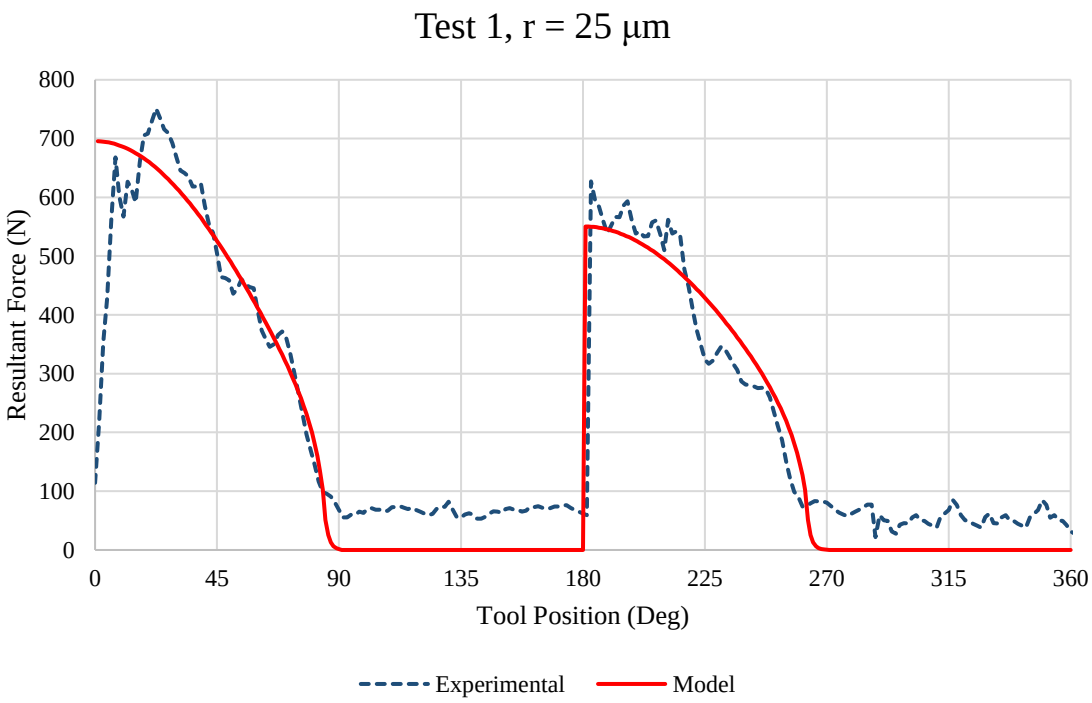

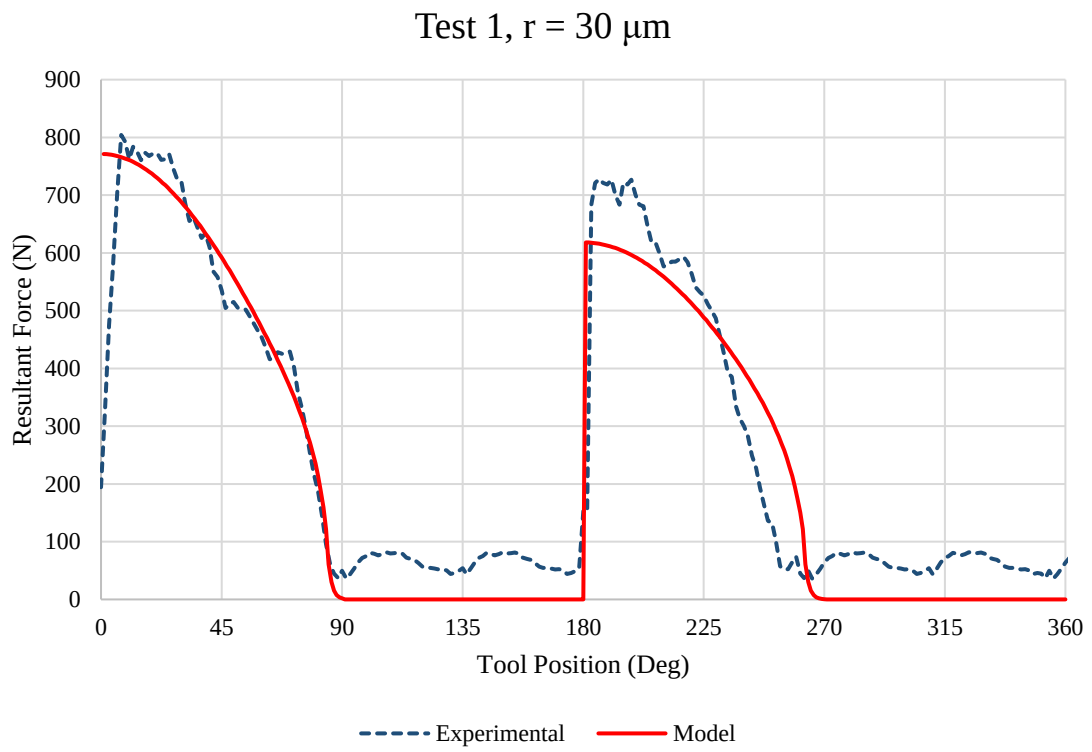

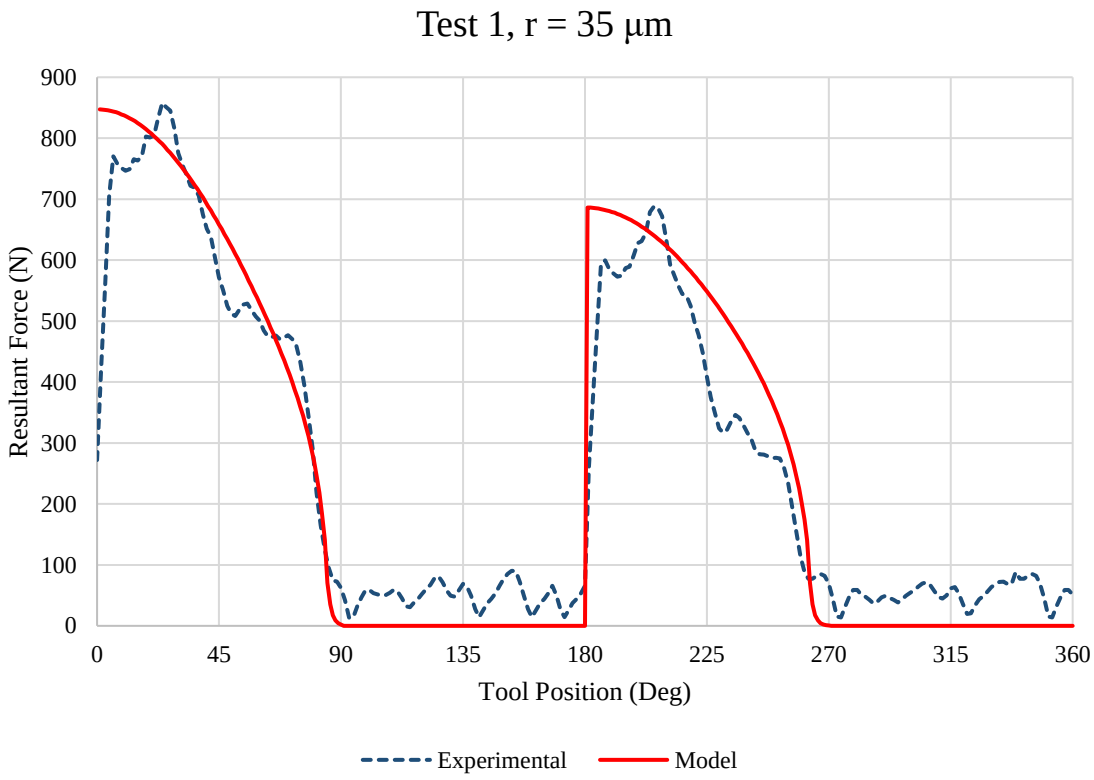
Test 1, r = 35 µm
Resultant Force (N)
900
800
700
600
500
400
300
200
100
0
0
45
90
135
180
225
270
315
360
Tool Position (Deg)
Experimental
Model

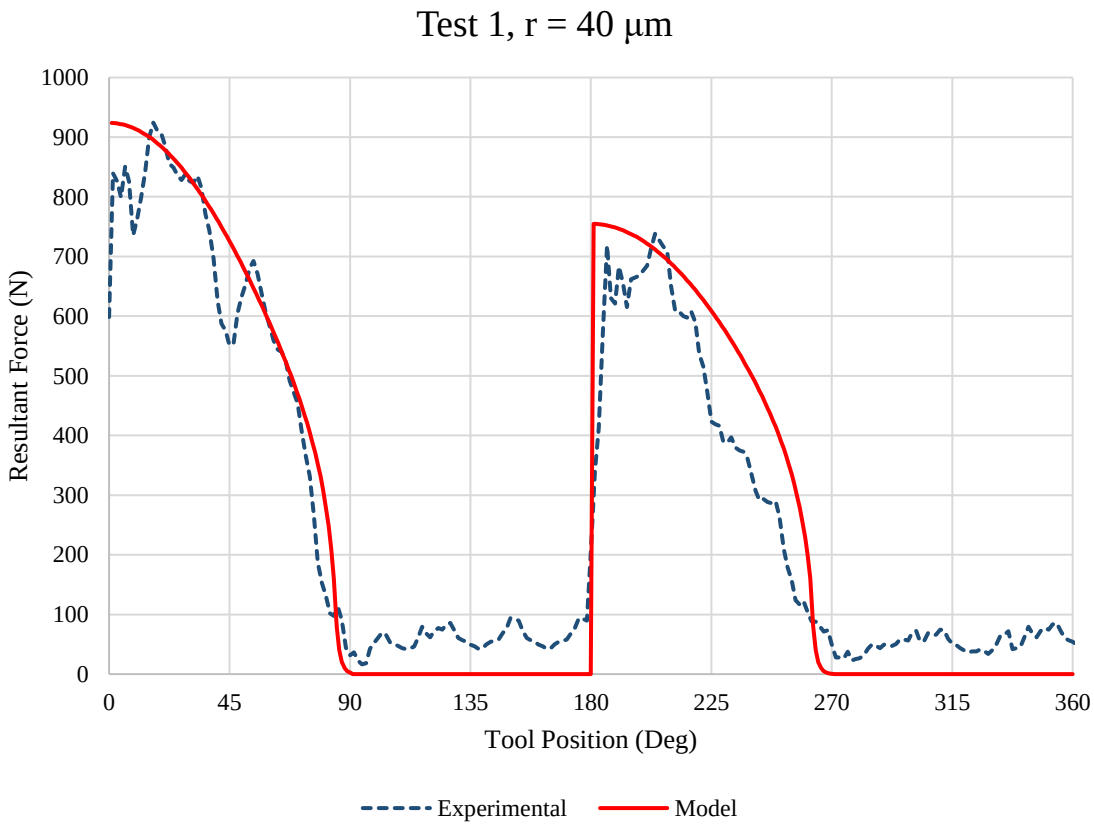
Test 1, r = 40 µm
Resultant Force (N)
1000
900
800
700
600
500
400
300
200
100
0
0
45
90
135
180
225
270
315
360
Tool Position (Deg)
Experimental
Model

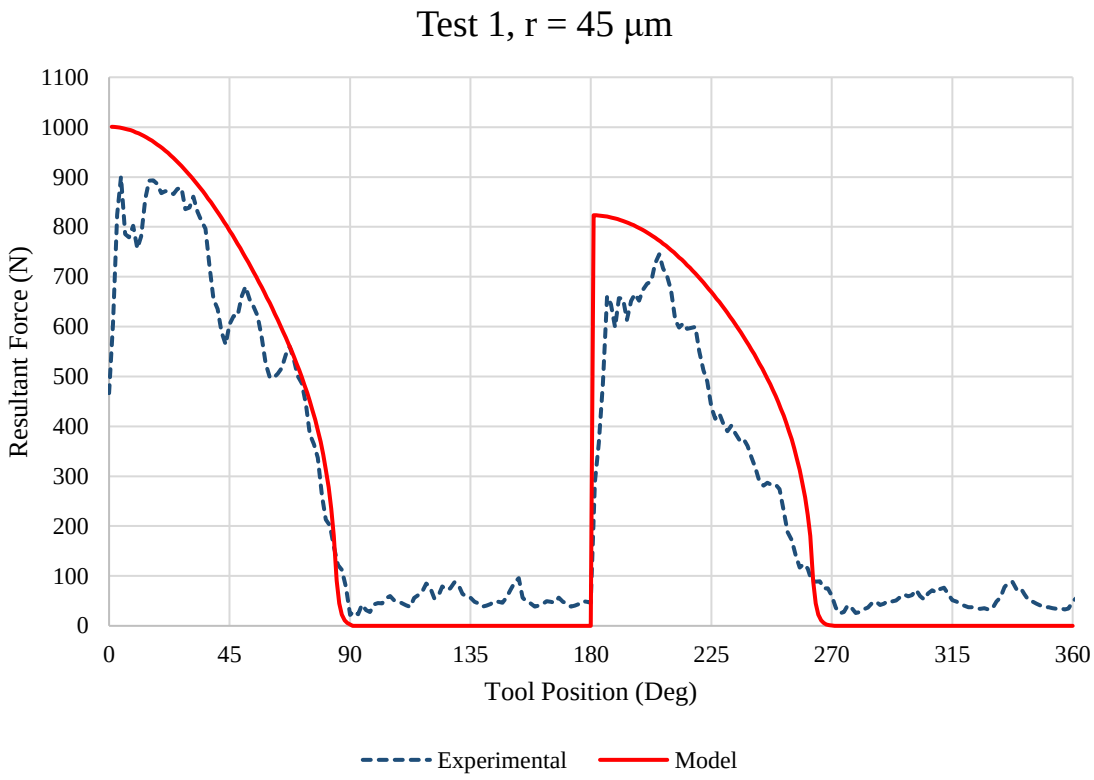
Test 1, r = 45 μm
Resultant Force (N)
1100
1000
900
800
700
600
500
400
300
200
100
0
0
45
90
135
180
225
270
315
360
Tool Position (Deg)
Experimental
Model

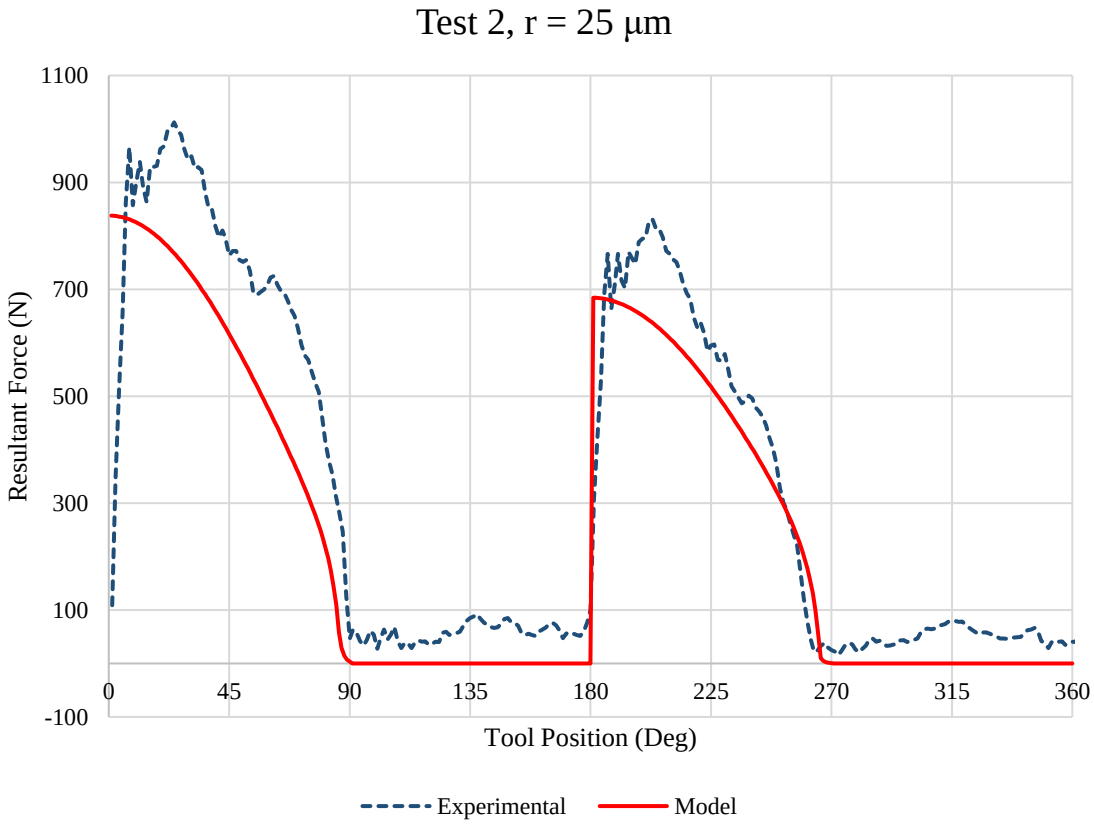
Test 2, r = 25 μm
Resultant Force (N)
1100
900
700
500
300
100
-100
0
45
90
135
180
225
270
315
360
Tool Position (Deg)
Experimental
Model

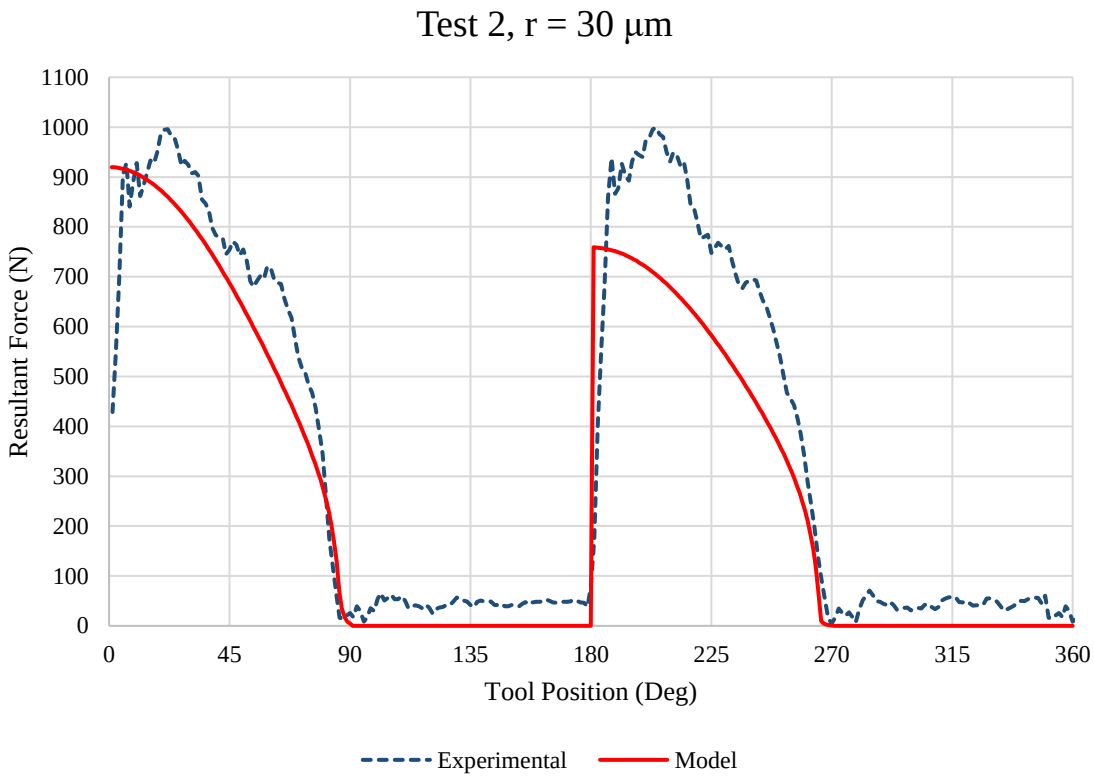
Test 2, r = 30 μm
Resultant Force (N)
1100
1000
900
800
700
600
500
400
300
200
100
0
0
45
90
135
180
225
270
315
360
Tool Position (Deg)
Experimental
Model

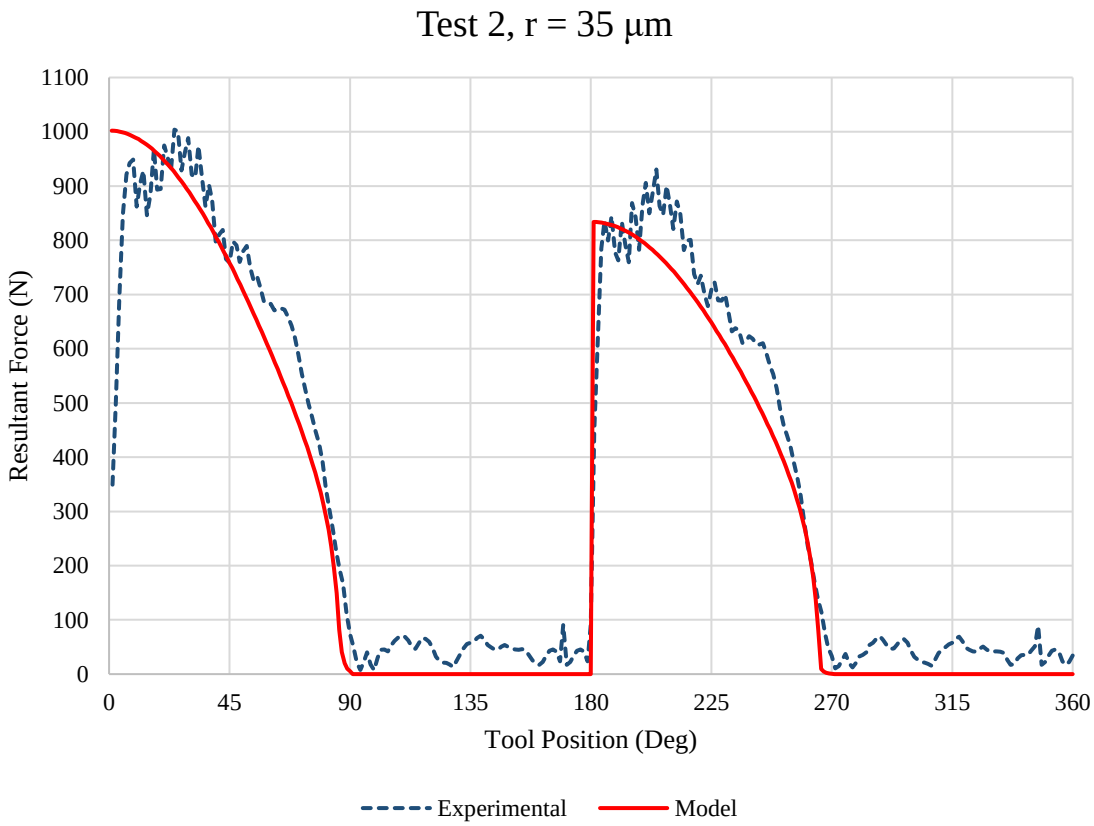
Test 2, r = 35 μm
Resultant Force (N)
1100
1000
900
800
700
600
500
400
300
200
100
0
0
45
90
135
180
225
270
315
360
Tool Position (Deg)
Experimental
Model

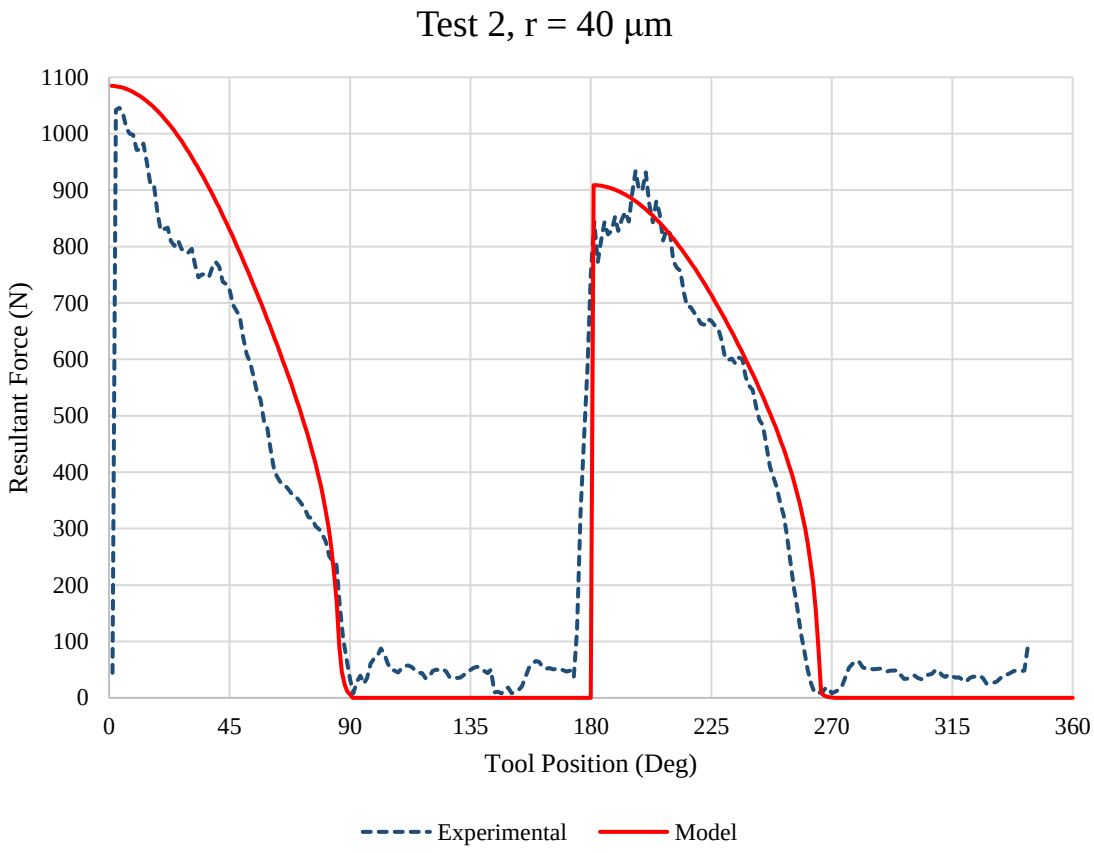
Test 2, r = 40 µm
Resultant Force (N)
1100
1000
900
800
700
600
500
400
300
200
100
0
0
45
90
135
180
225
270
315
360
Tool Position (Deg)
Experimental
Model

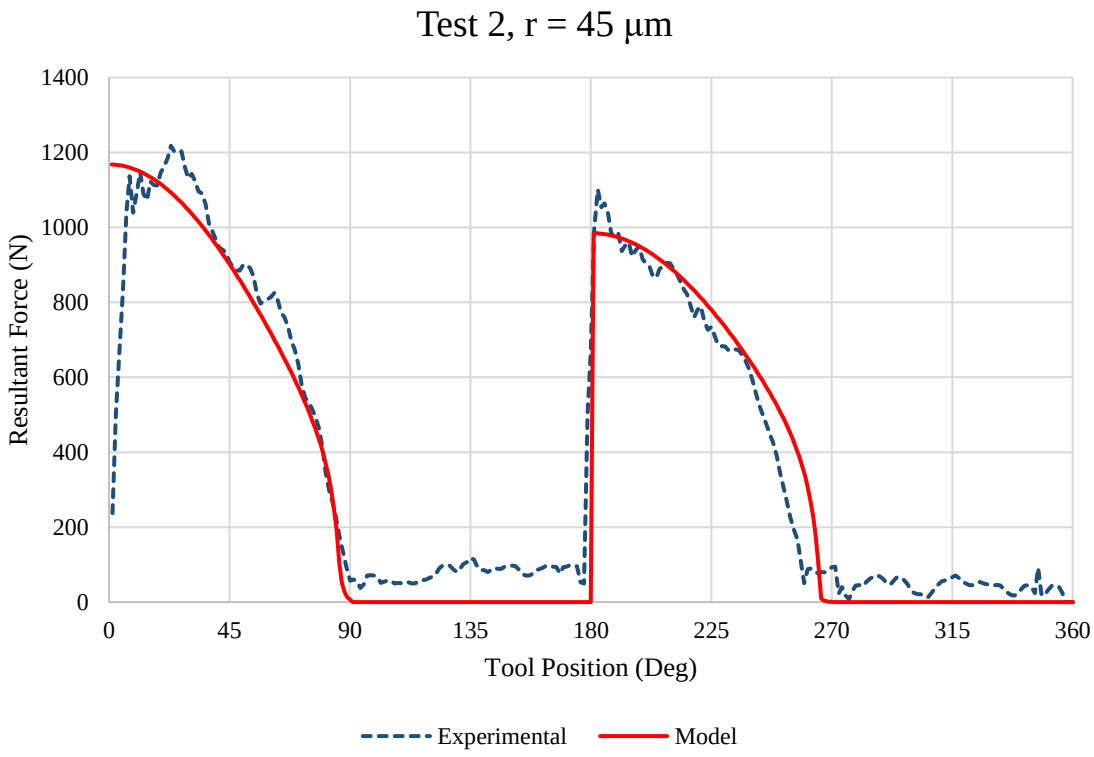
Test 2, r = 45 µm
Resultant Force (N)
1400
1200
1000
800
600
400
200
0
0
45
90
135
180
225
270
315
360
Tool Position (Deg)
Experimental
Model

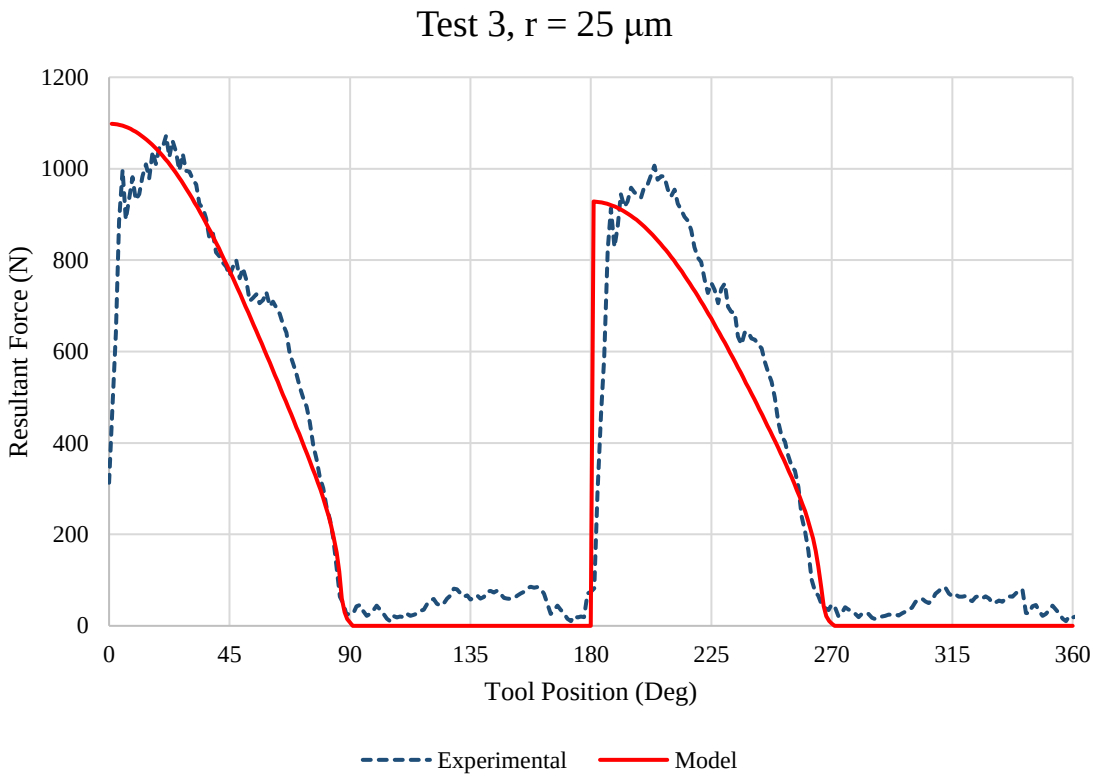
Test 3, r = 25 μm
Resultant Force (N)
1200
1000
800
600
400
200
0
0
45
90
135
180
225
270
315
360
Tool Position (Deg)
Experimental
Model

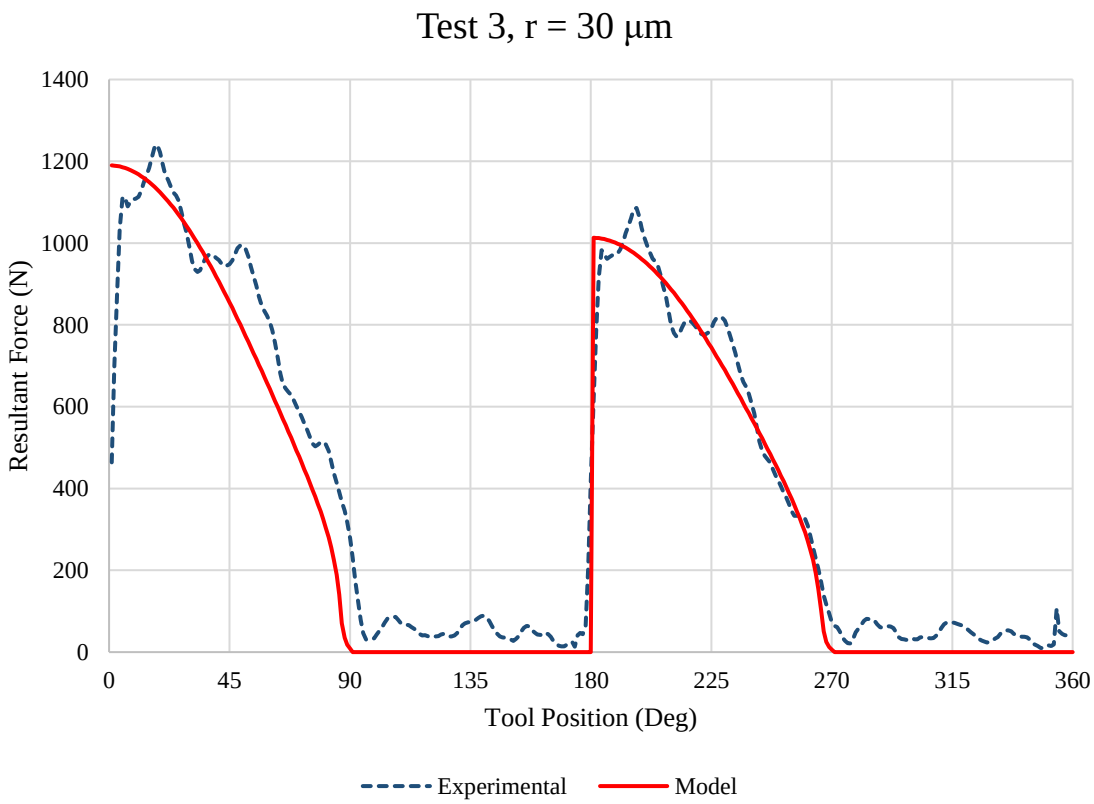
Test 3, r = 30 μm
Resultant Force (N)
1400
1200
1000
800
600
400
200
0
0
45
90
135
180
225
270
315
360
Tool Position (Deg)
Experimental
Model

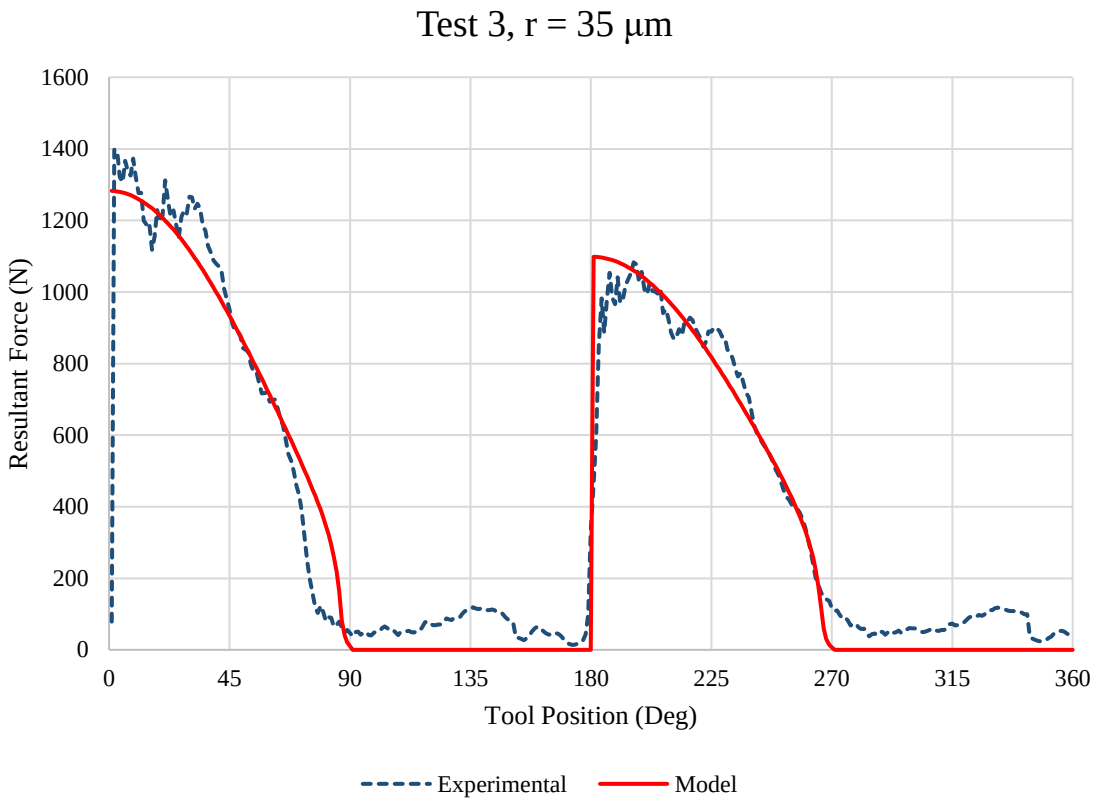
Test 3, r = 35 μm
Resultant Force (N)
1600
1400
1200
1000
800
600
400
200
0
0
45
90
135
180
225
270
315
360
Tool Position (Deg)
Experimental
Model

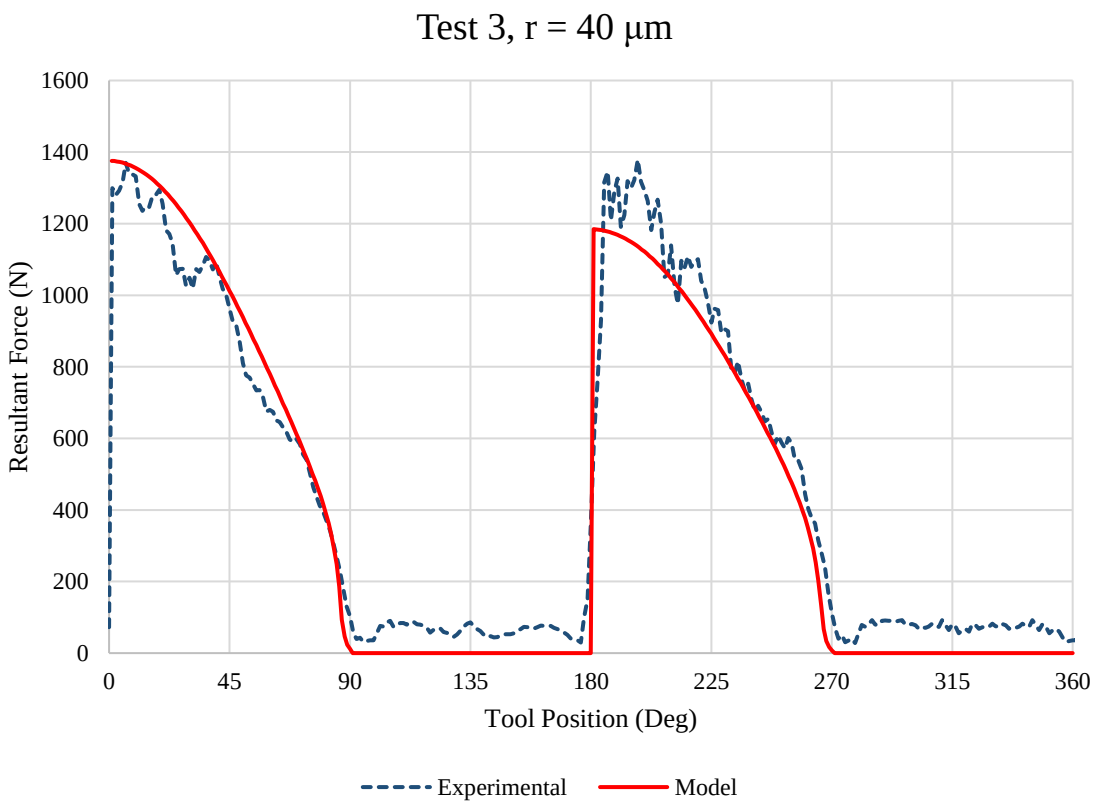
Test 3, r = 40 μm
Resultant Force (N)
1600
1400
1200
1000
800
600
400
200
0
0
45
90
135
180
225
270
315
360
Tool Position (Deg)
Experimental
Model

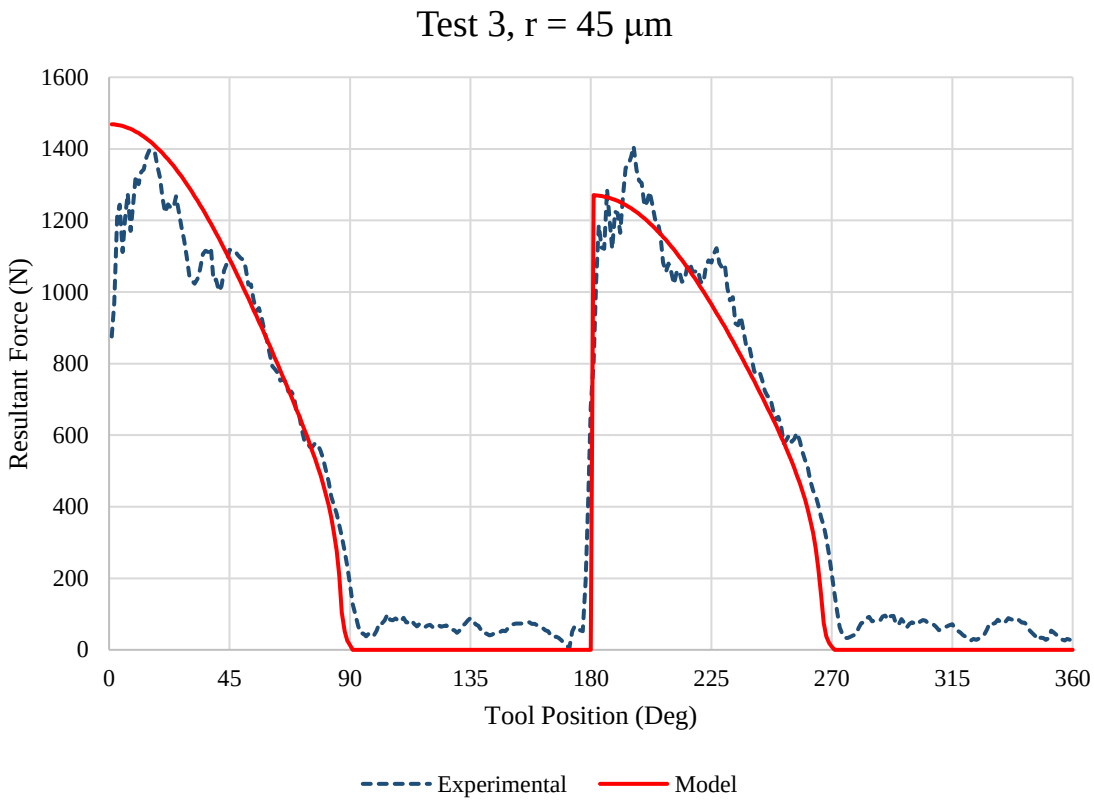
Test 3, r = 45 μm
Resultant Force (N)
1600
1400
1200
1000
800
600
400
200
0
0
45
90
135
180
225
270
315
360
Tool Position (Deg)
Experimental
Model

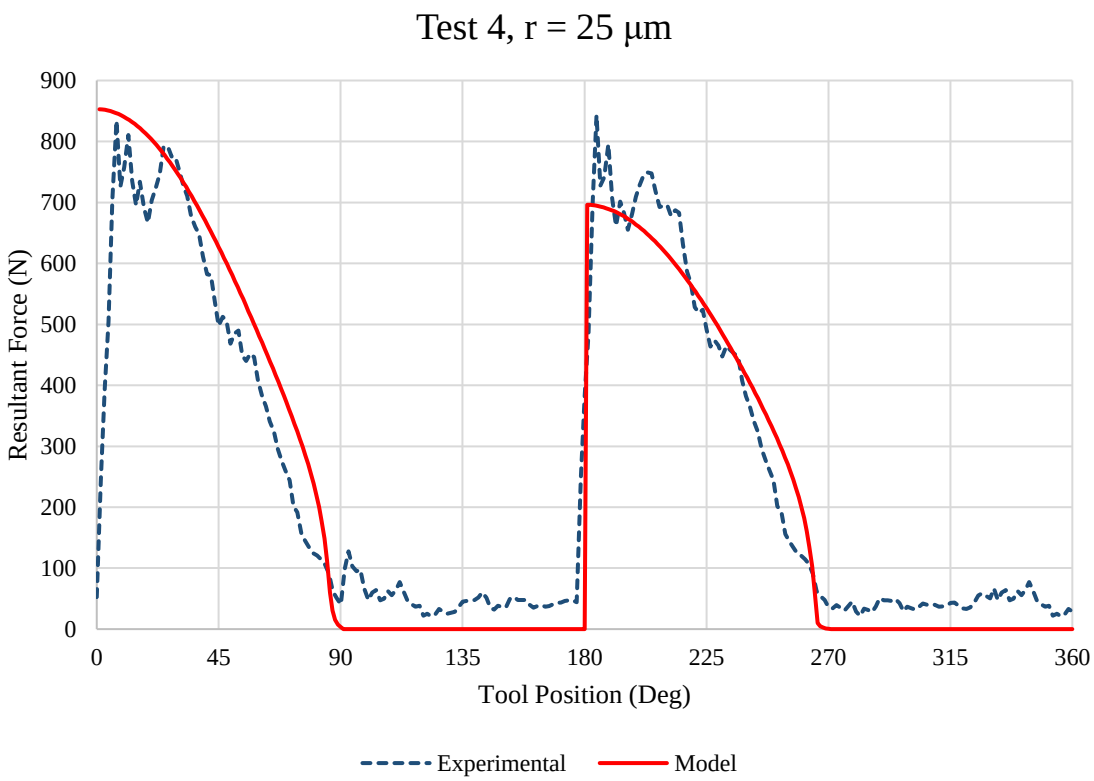
Test 4, r = 25 μm
Resultant Force (N)
900
800
700
600
500
400
300
200
100
0
0
45
90
135
180
225
270
315
360
Tool Position (Deg)
Experimental
Model

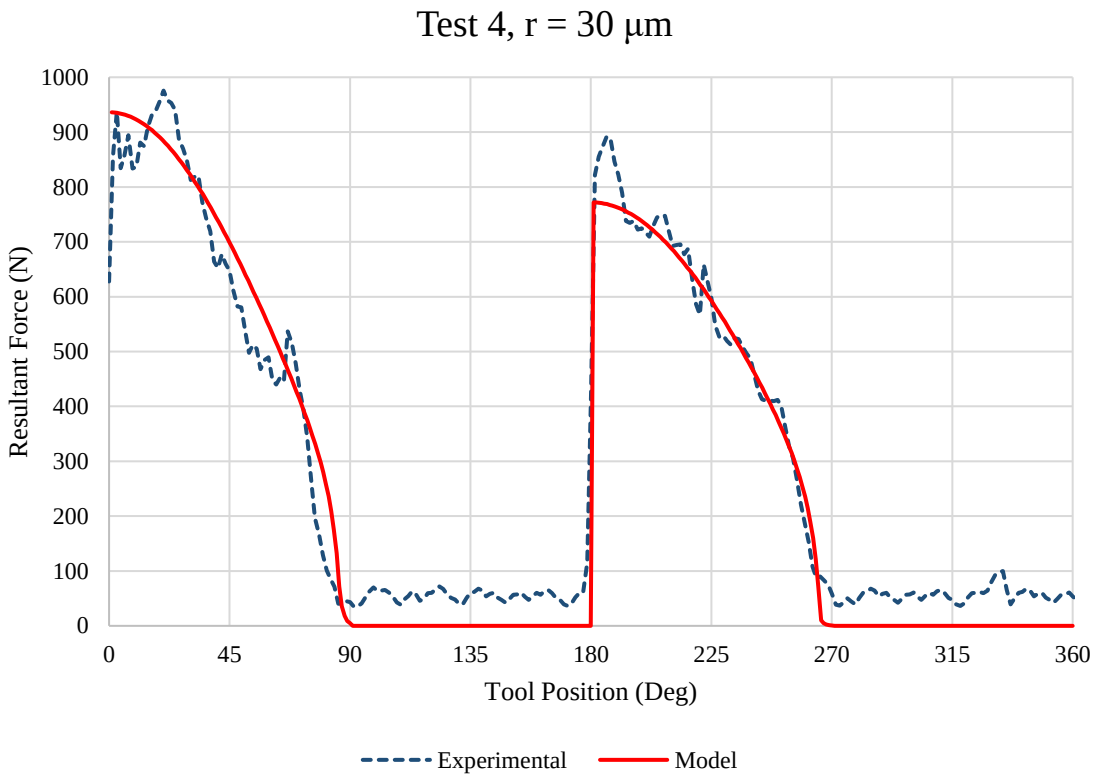
Test 4, r = 30 μm
Resultant Force (N)
1000
900
800
700
600
500
400
300
200
100
0
0
45
90
135
180
225
270
315
360
Tool Position (Deg)
Experimental
Model

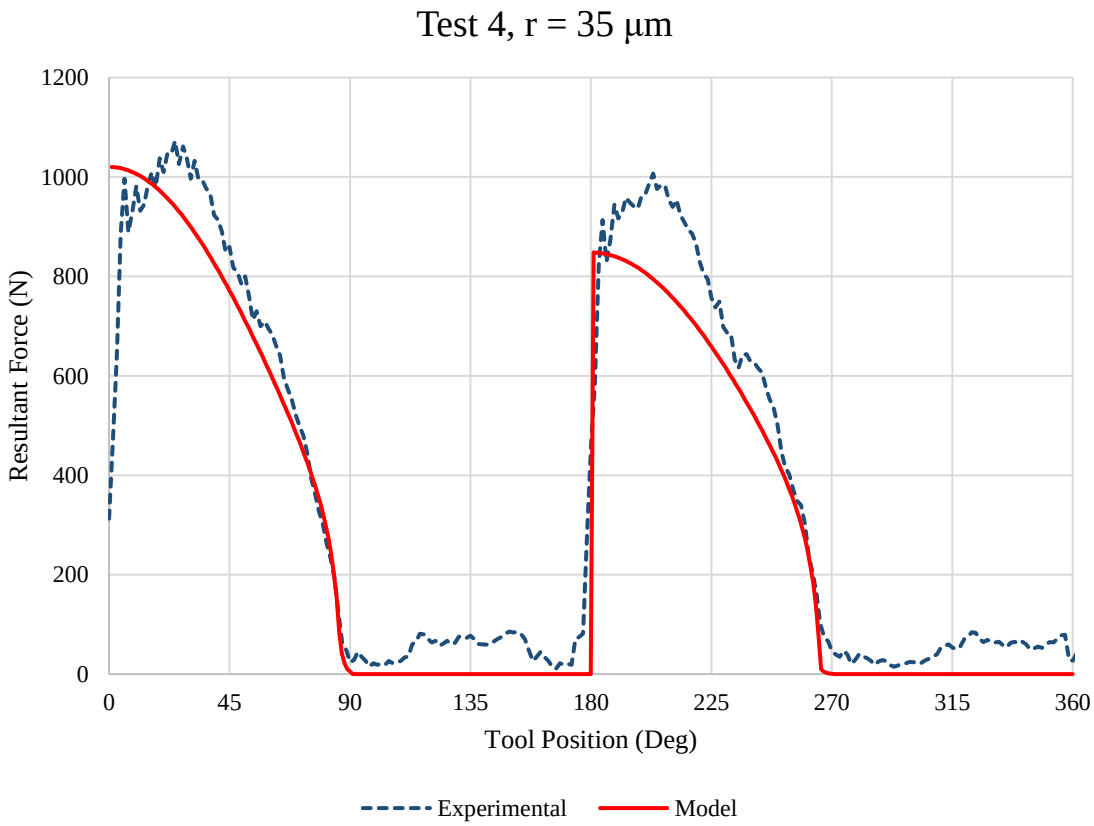
Test 4, r = 35 μm
Resultant Force (N)
1200
1000
800
600
400
200
0
0
45
90
135
180
225
270
315
360
Tool Position (Deg)
Experimental
Model

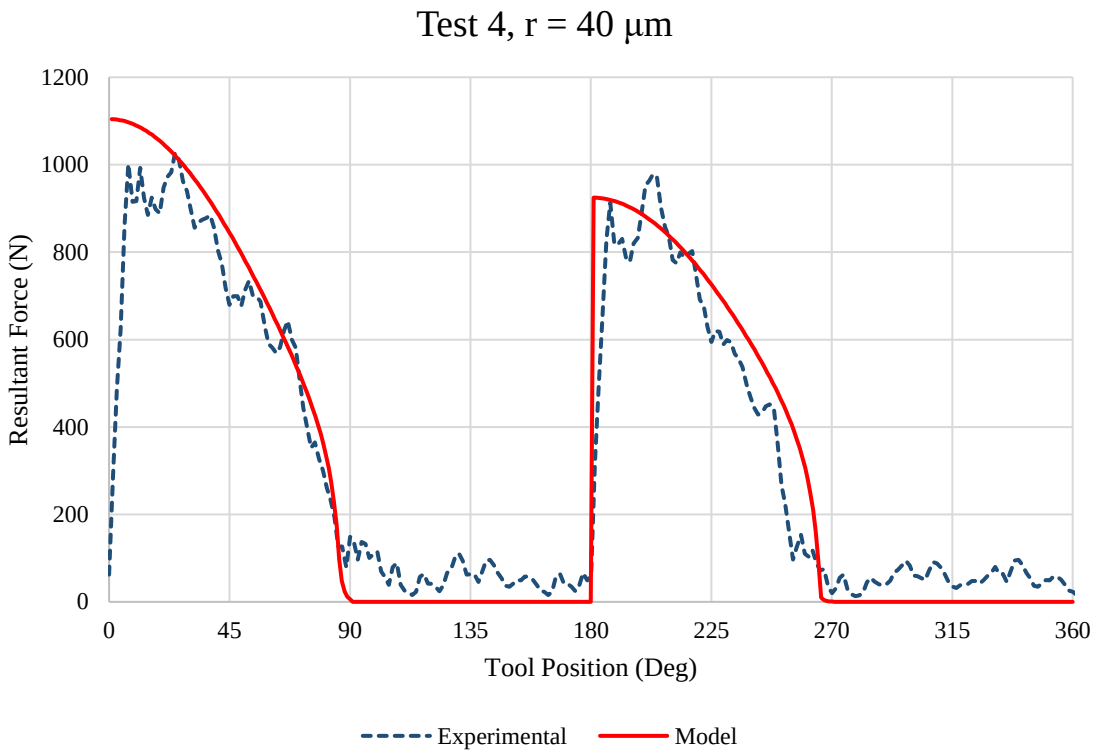
Test 4, r = 40 μm
Resultant Force (N)
1200
1000
800
600
400
200
0
0
45
90
135
180
225
270
315
360
Tool Position (Deg)
Experimental
Model

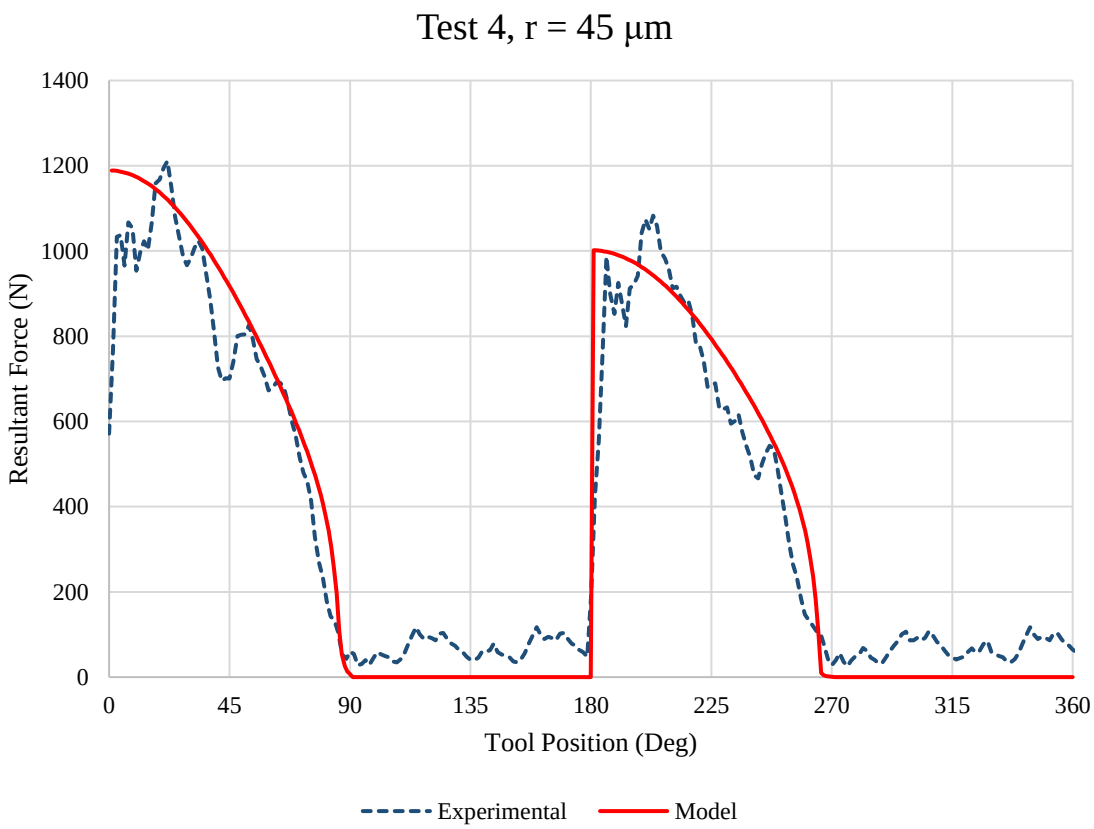
Test 4, r = 45 μm
Resultant Force (N)
1400
1200
1000
800
600
400
200
0
0
45
90
135
180
225
270
315
360
Tool Position (Deg)
Experimental
Model

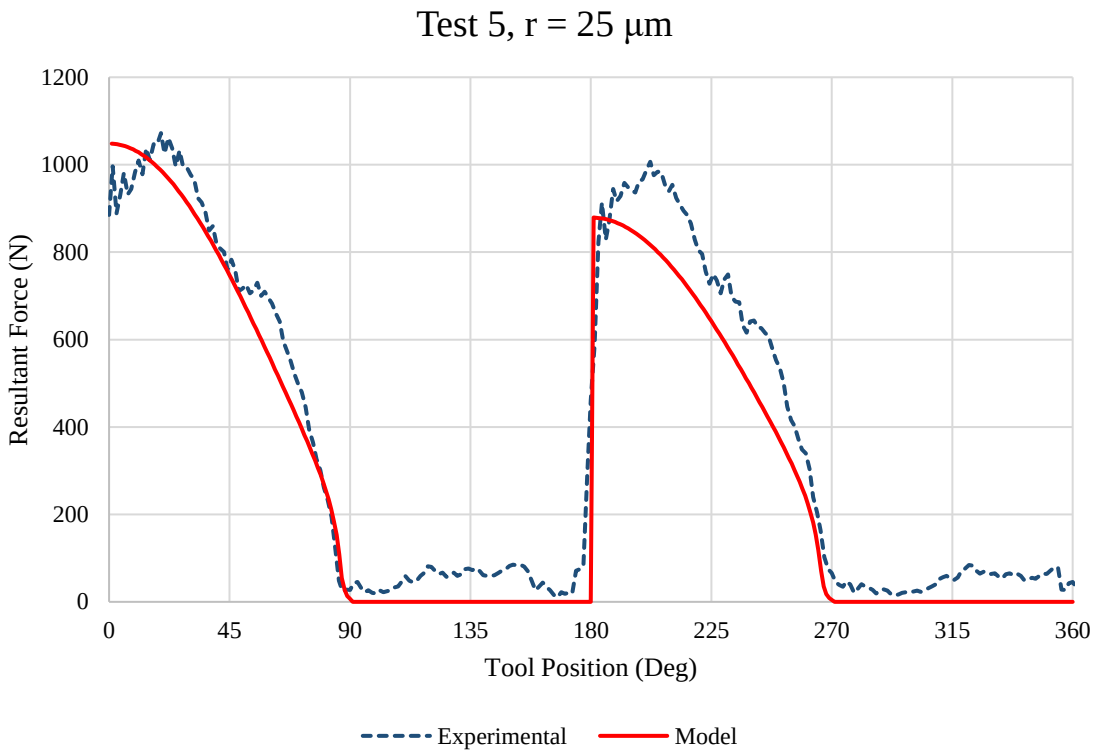
Test 5, r = 25 μm
Resultant Force (N)
1200
1000
800
600
400
200
0
0
45
90
135
180
225
270
315
360
Tool Position (Deg)
Experimental
Model

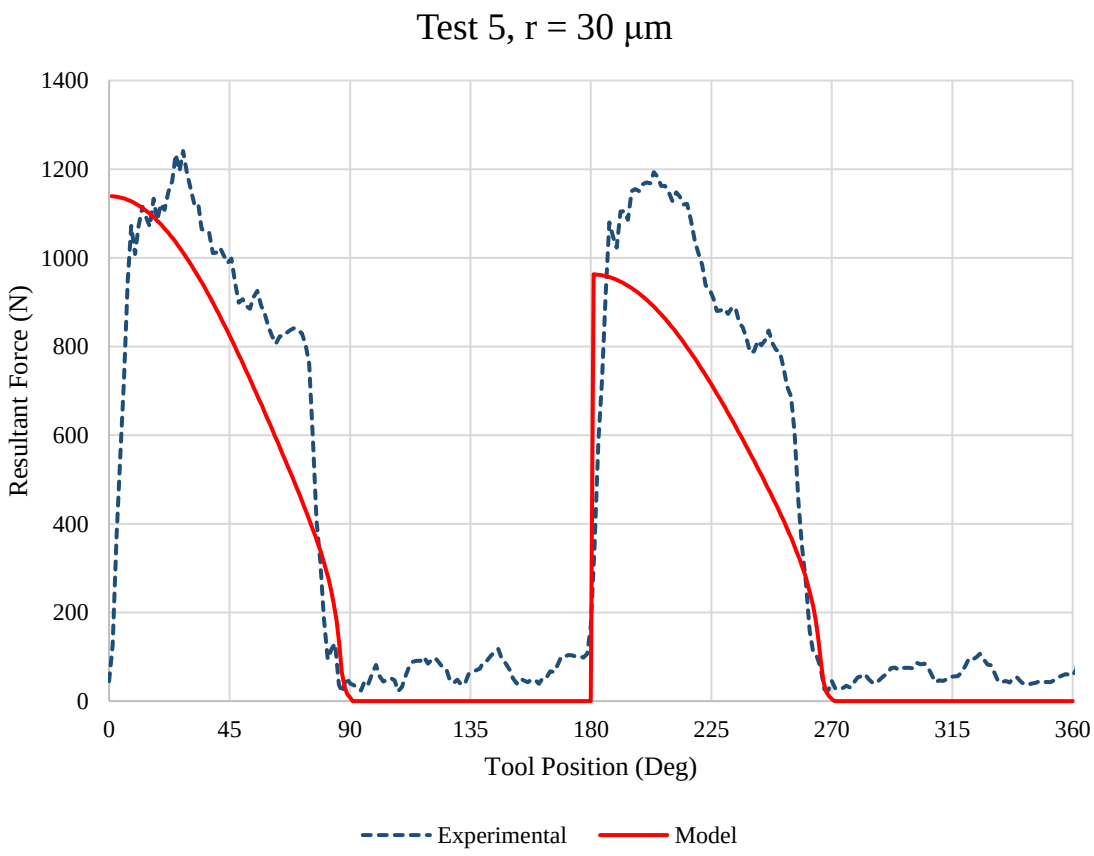
Test 5, r = 30 μm
Resultant Force (N)
1400
1200
1000
800
600
400
200
0
0
45
90
135
180
225
270
315
360
Tool Position (Deg)
Experimental
Model

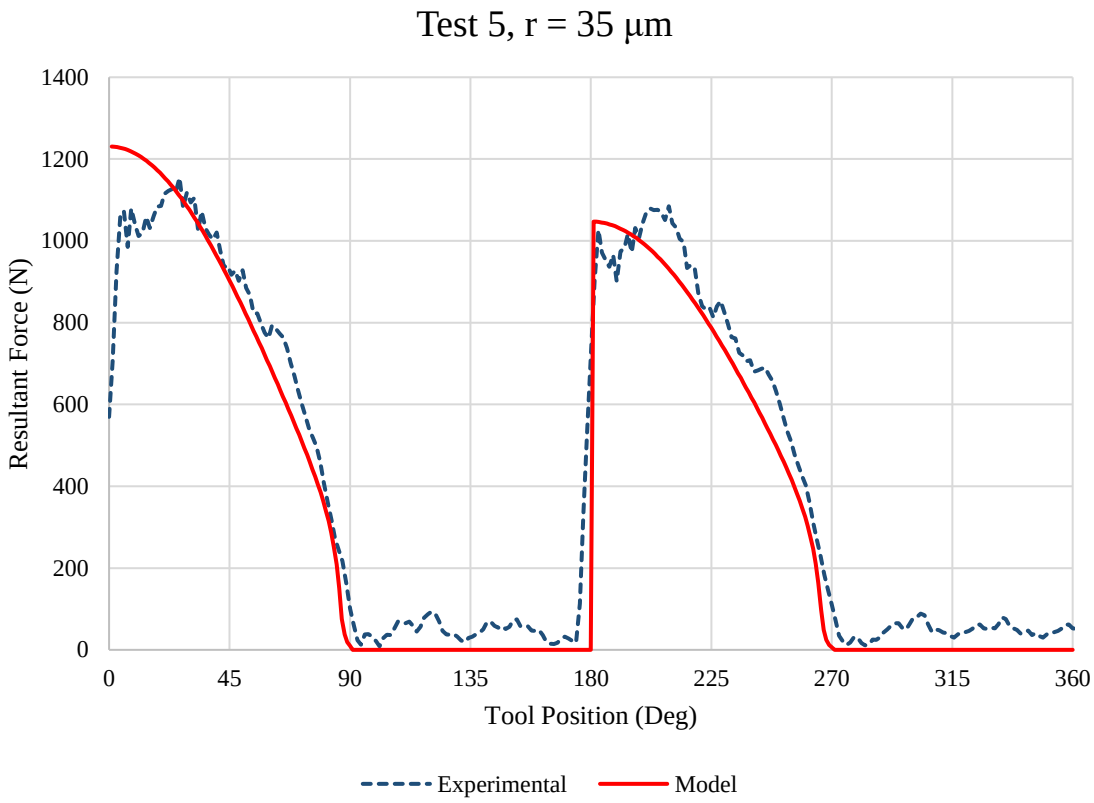
Test 5, r = 35 μm
Resultant Force (N)
1400
1200
1000
800
600
400
200
0
0
45
90
135
180
225
270
315
360
Tool Position (Deg)
Experimental
Model

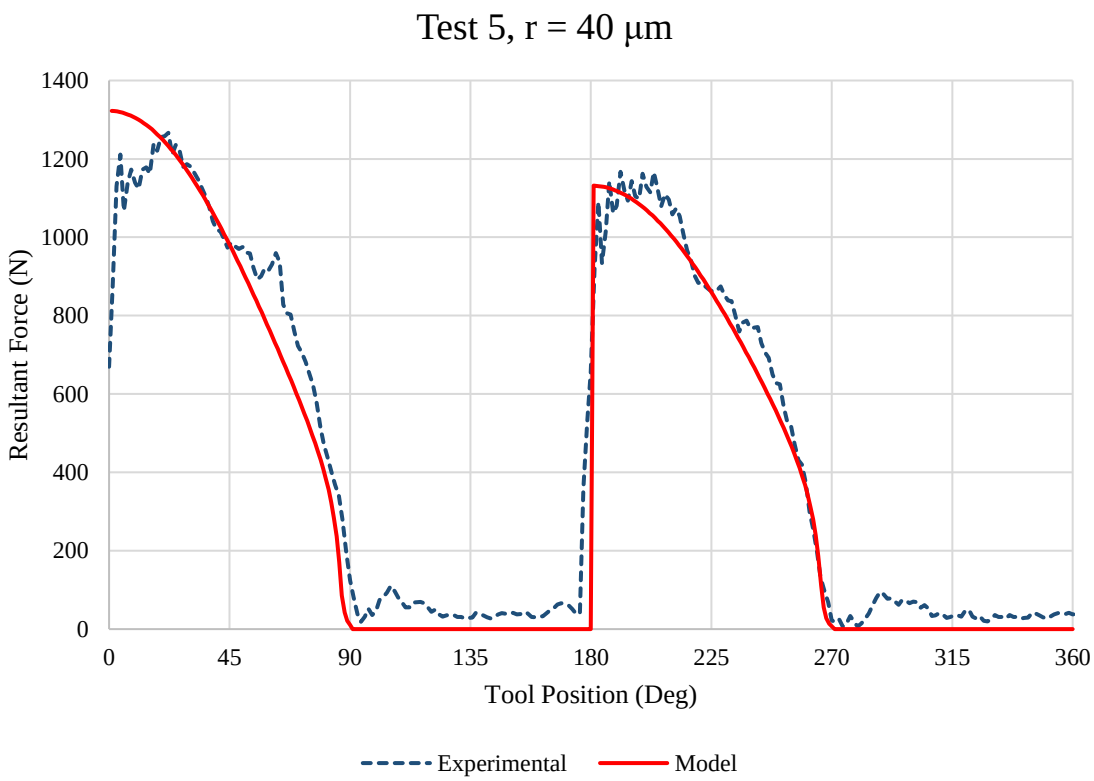
Test 5, r = 40 μm
Resultant Force (N)
1400
1200
1000
800
600
400
200
0
0
45
90
135
180
225
270
315
360
Tool Position (Deg)
Experimental
Model

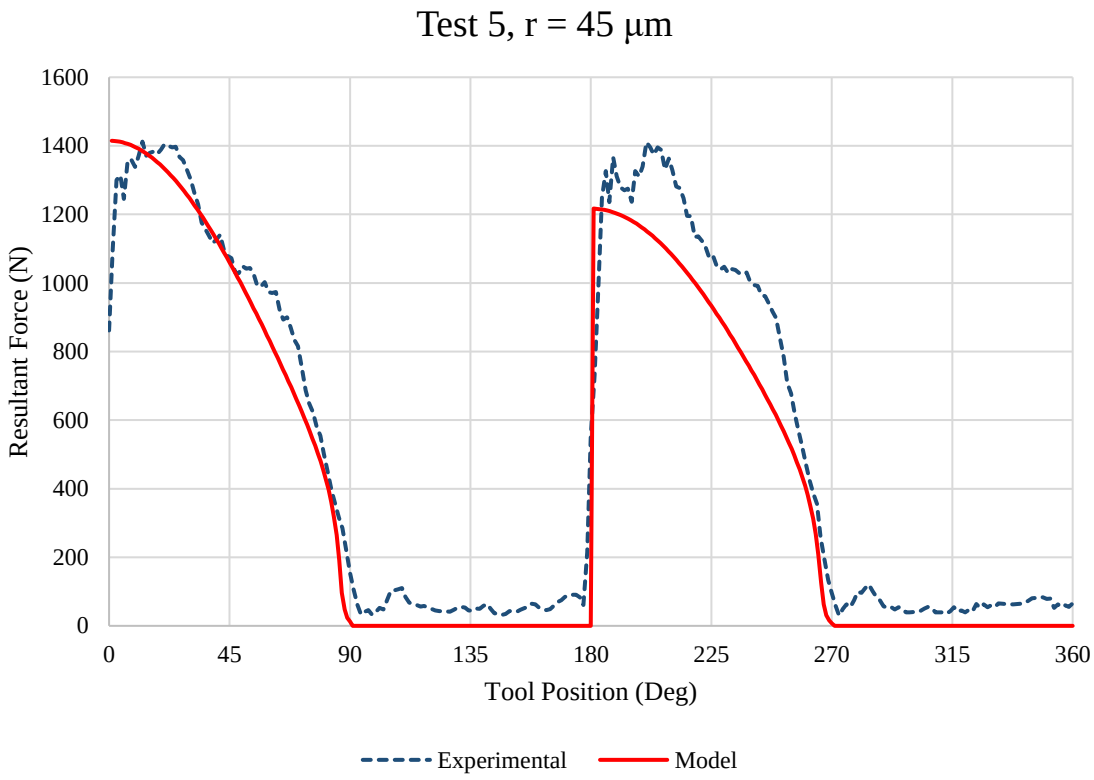
Test 5, r = 45 μm
Resultant Force (N)
1600
1400
1200
1000
800
600
400
200
0
0
45
90
135
180
225
270
315
360
Tool Position (Deg)
Experimental
Model

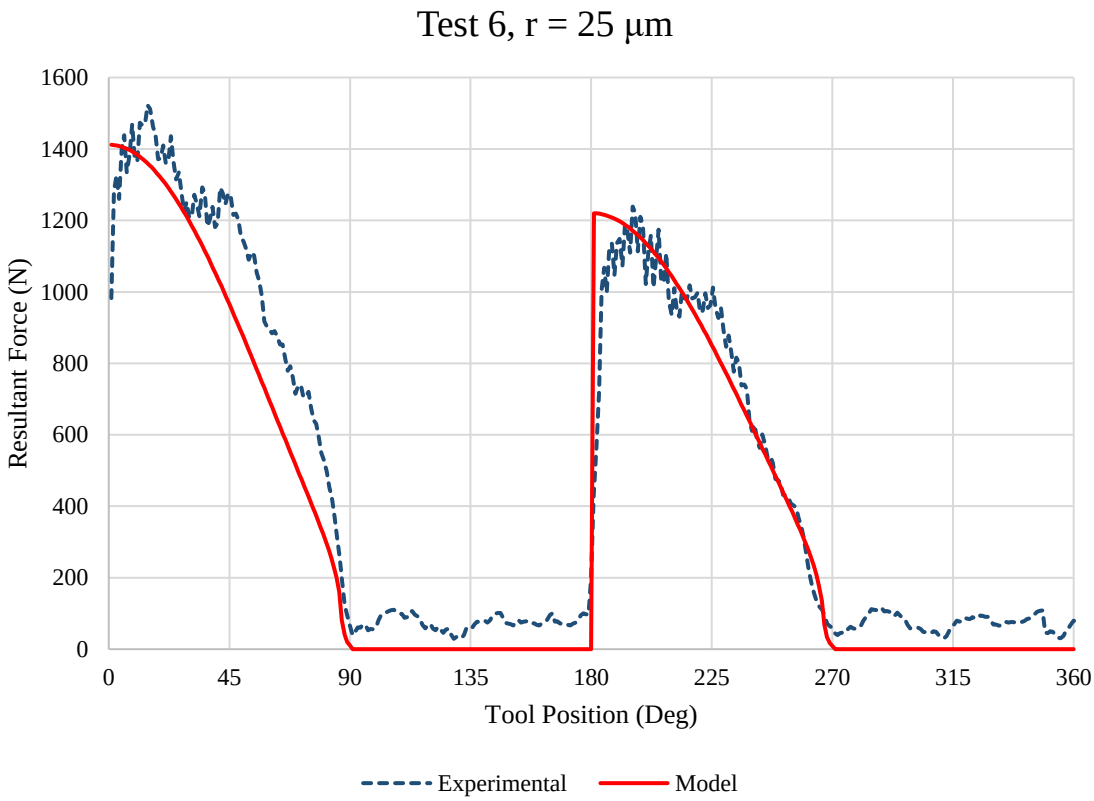
Test 6, r = 25 μm
Resultant Force (N)
1600
1400
1200
1000
800
600
400
200
0
0
45
90
135
180
225
270
315
360
Tool Position (Deg)
Experimental
Model

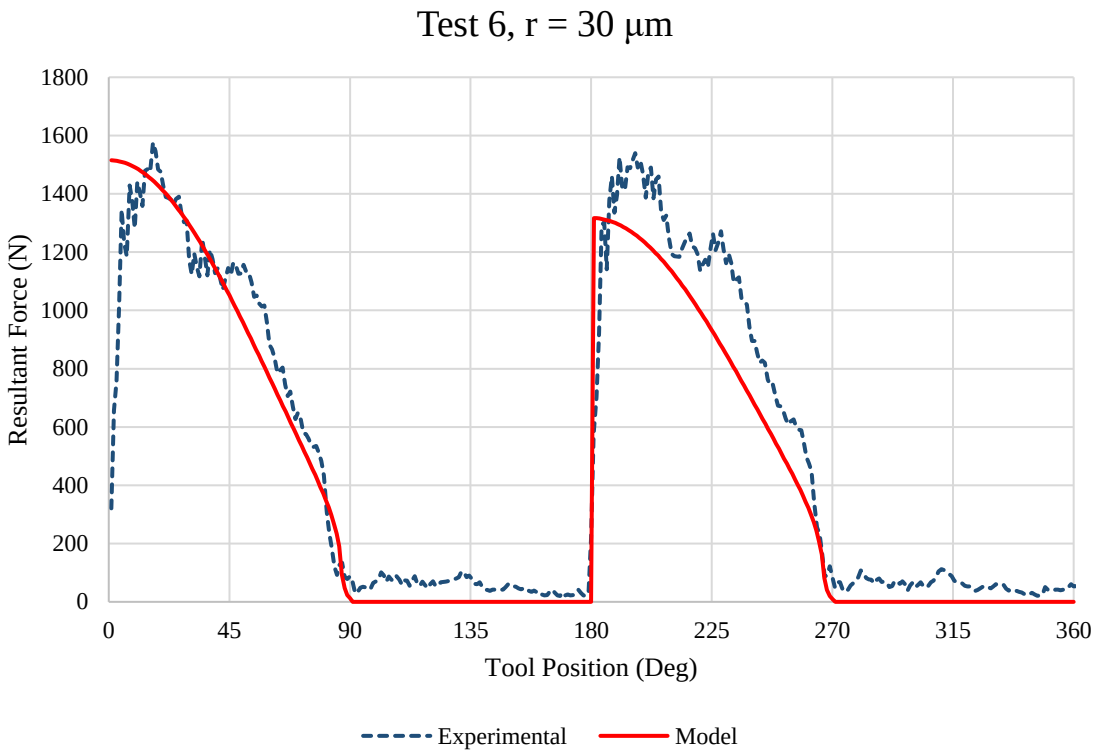
Test 6, r = 30 μm
Resultant Force (N)
1800
1600
1400
1200
1000
800
600
400
200
0
0
45
90
135
180
225
270
315
360
Tool Position (Deg)
Experimental
Model

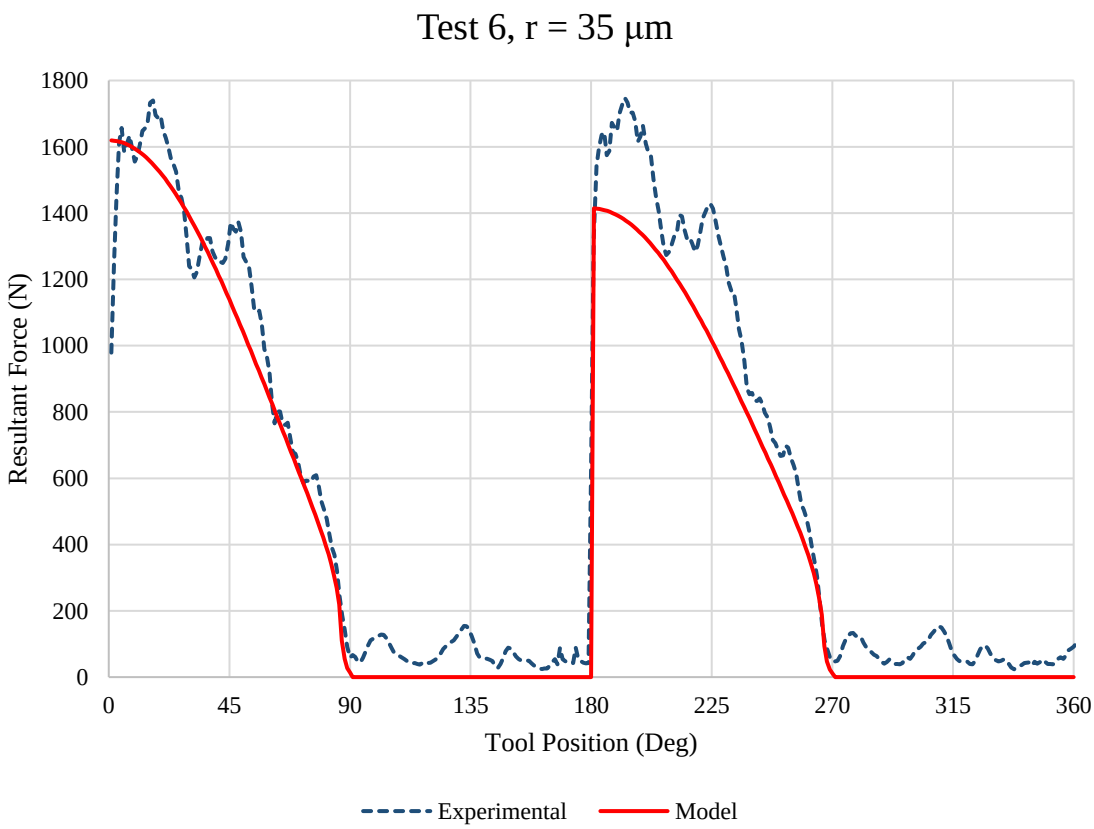
Test 6, r = 35 μm
Resultant Force (N)
1800
1600
1400
1200
1000
800
600
400
200
0
0
45
90
135
180
225
270
315
360
Tool Position (Deg)
Experimental
Model

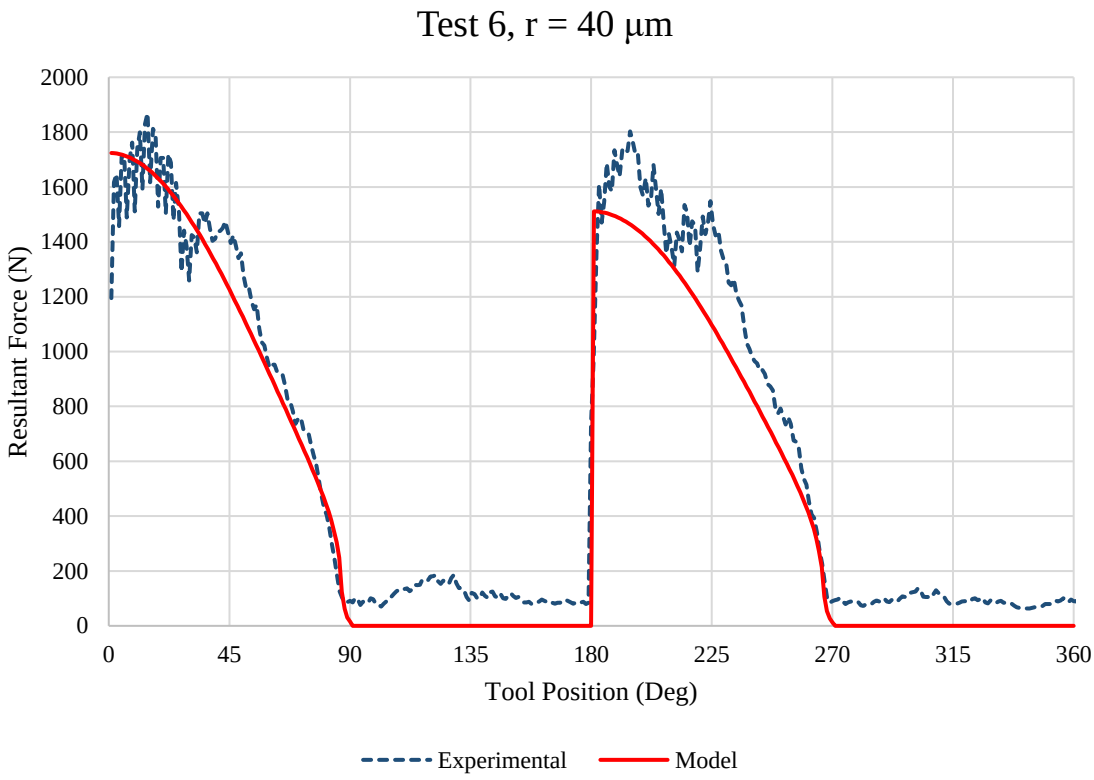
Test 6, r = 40 µm
Resultant Force (N)
2000
1800
1600
1400
1200
1000
800
600
400
200
0
0
45
90
135
180
225
270
315
360
Tool Position (Deg)
Experimental
Model

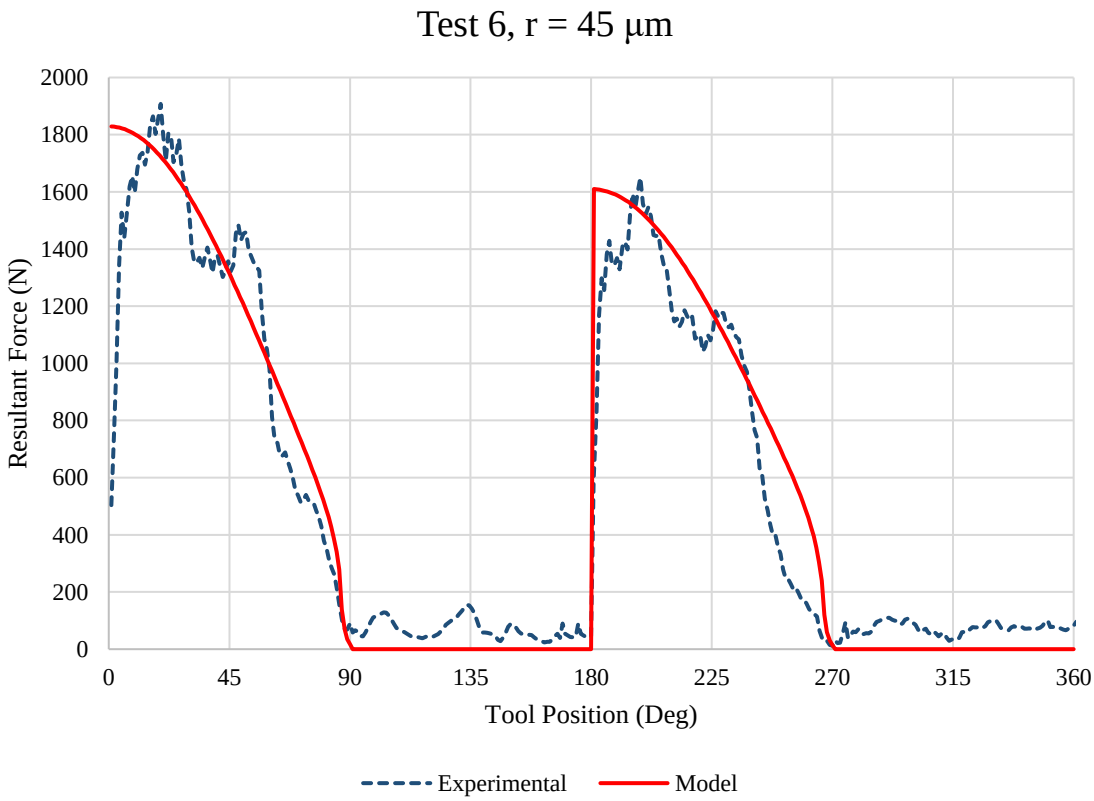
Test 6, r = 45 µm
Resultant Force (N)
2000
1800
1600
1400
1200
1000
800
600
400
200
0
0
45
90
135
180
225
270
315
360
Tool Position (Deg)
Experimental
Model